Vegard Mikkelsen Bjerkeli

Computational Fluid Dynamics of airflows inside buildings: a comprehensive review of the cavity flow benchmark

Master's thesis in Mechanical Engineering
Supervisor: Laurent Georges
December 2020

Master's thesis

NTNU
Norwegian University of Science and Technology
Faculty of Engineering
Department of Energy and Process Engineering

NTNU
Norwegian University of
Science and Technology

Vegard Mikkelsen Bjerkeli

Computational Fluid Dynamics of airflows inside buildings: a comprehensive review of the cavity flow benchmark

NTNU

Norwegian University of
Science and Technology

NTNU

Master`s Agreement

Faculty	IV - Fakultet for ingeniørvitenskap
Institute	Institutt for energi- og prosessteknikk
Programme code	MTPROD
Course code	194_TEP4925_1

Personal information

Family name, first name	Bjerkeli, Vegard Mikkelsen
Date of birth	23.02.1995
Email address	vegardmb@stud.ntnu.no

The Master`s thesis

Starting date	19.08.2020
Submission deadline	09.01.2021
Thesis working title	Computational Fluid Dynamics of airflows inside buildings: case of ventilation in a cavity
Thematic description	The knowledge of building airflows is widely used to design high-performance buildings. In this respect, Computational Fluid Dynamics (CFD) is a powerful tool to study and predict airflows. Nowadays, CFD in buildings is mostly performed using Reynolds-Averaged Navier Stokes (RANS) modelling, typically using industrial flow solvers such as Openfoam. Recent research has shown that results obtained on a benchmark cavity flow (representative for real applications of mixing ventilation in buildings) were strongly dependenent on users. Benchmark flows with available experimental data can be used to validate CFD simulations of similar flow problems, and be used to gain insigt in what models and input to the CFD simulation give a physically correct result. The objective of this master thesis is to investigate the influence of different input parameters on the CFD results for several benchmarks representative for airflows inside buildings. Both from looking at what have been done in the literature and by doing own simulations. Research done in the project assignment (a precursor to the master thesis) on a cavity benchmark showed that the choice of turbulence model is the most important parameter so this will be emphasised, however parameters such as the mesh, numerical discretization, boundary conditons etc. will also be investigated. The objective is to establish a best practice for the use of CFD in buildings and to better understand the limitations of industrial CFD tools for this application.

Abstract

This master thesis presents an extensive review of the cavity flow benchmark, with the purpose of validating RANS turbulence models for mixing ventilation applications. CFD is used more and more in indoor airflows applications. It can be a powerful tool to optimize ventilation systems, and the last decades increase in the availability of computational power has made CFD simulations less time consuming. Two recent studies have, however, questioned the accuracy of CFD for indoor airflow applications. In these studies, several teams of researchers were asked to simulate two benchmark cases, representative for mixing ventilation applications. A concerning spread was seen in the results, indicating that the result from a CFD simulation is very dependent on the choices made by the user. To overcome this issue, these studies emphasized the need to validate CFD against representative benchmark cases with available experimental data. To address this, this thesis gives a comprehensive review of the available cavity flow benchmarks – representative for mixing ventilation applications – with the overall goal to establish a best practice use of RANS turbulence models for mixing ventilation applications.

Seven benchmarks are presented in the thesis. The benchmark's geometry, flow regime, experimental setup and type of experimental data are first introduced, before simulations of the seven benchmarks done by other researchers are presented in the literature review. The focus is on how well two-equation RANS turbulence models produce results that are in agreement with the experimental data. This is because the results from the preceding project assignment indicated that the choice of turbulence model is the single input parameter with the largest impact on the results, and RANS turbulence models are widely used in the industry. How well the turbulence models have performed in the literature is summarized, before the results from CFD simulations of the benchmarks from this thesis are presented. The turbulence model performance varies significantly from benchmark to benchmark, which was expected since the benchmarks represent different challenges. None of the tested turbulence models are capable of producing good results for all seven benchmarks, underlining the importance of selecting a suitable turbulence model for a given case.

The results indicate that the k-ϵ models perform best for the benchmarks with fully turbulent flow, in particular the standard k-ϵ model. Furthermore, the SST k-ω model gives poorer agreement with experiments for the fully turbulent benchmarks and seems to overpredict the maximum velocity in a fully turbulent wall jet. For a benchmark in the transitional regime, however, the SST k-ω model gives the best agreement with the experimental data and the standard k-ϵ model the worst. However, it is not always clear what causes the change in turbulence model performance since several features of the flow – geometry, flow regime and magnitude of the adverse pressure gradient in the wall jet – change from benchmark to benchmark. The results also indicate that the inlet values for k and ϵ/ω have a bigger impact on the result for low Reynolds number flows, than high Reynolds number flows. The majority of the results from this thesis are consistent with the results from the literature, however, the SST k-ω model gives results that are inconsistent with literature for two of the benchmarks.

From the discoveries in this thesis some best practice guidelines are given, but further work is also needed to conclude on what causes the variations seen in turbulence model performance. In particular, there is a need for additional benchmarks that systematically changes one feature at a time. This will give the opportunity to say with more certainty what features of the cavity flow the different RANS turbulence models are capable and incapable to model correctly.

Norsk sammendrag

Denne masteroppgaven presenterer en omfattende gjennomgang av «cavity flow» benchmarket, med den hensikt å validere RANS turbulensmodeller for mikseventilasjonsformål. CFD brukes mer og mer for luftstrømmer inne i bygninger. Det kan være et kraftig verktøy for å optimalisere ventilasjonssystemer, og de siste tiårenes økning i tilgjengeligheten av datakraft har gjort CFD simuleringer mindre tidkrevende. To nylige studier har imidlertid stilt spørsmål ved nøyaktigheten av CFD simuleringer anvendt for innendørs luftstrømmer. I disse studiene har flere forskergrupper blitt spurt om å simulere to benchmarker, representative for mikseventilasjonsformål. En bekymringsfull spredning ble sett i resultatene, som indikerer at resultatet fra en CFD simulering er veldig avhengig av hvilke valg som blir gjort av brukeren. Disse studiene understreker nødvendigheten av å validere CFD opp mot representative benchmarker med tilgjengelige eksperimentelle data. For å adresse dette gir denne masteroppgaven en omfattende gjennomgang av de tilgjengelige «cavity flow» benchmarkene – representative for mikseventilasjon – med det overordnede målet å etablere en beste bruksmåte av RANS turbulensmodeller for mikseventilasjonsformål.

Syv benchmarker presenteres i denne oppgaven. Deres geometri, strømningsregime, eksperimentelle oppsett og typen eksperimentelle data som er tilgjengelig introduseres først, før simuleringer av benchmarkene gjort av andre forskere presenteres i litteraturstudiet. Fokuset er på hvor bra to-liknings RANS turbulensmodeller greier å produsere resultater som gir samsvar med de eksperimentelle dataene. Dette er fordi resultatene fra den foregående prosjektoppgaven indikerte at valget av turbulensmodell er den enkelt input parameteren med størst påvirkning på resultatet, og RANS turbulensmodeller er mye brukt i industrien. Hvor godt turbulensmodellene har prestert i litteraturen oppsummeres før CFD simuleringer fra denne oppgaven presenteres. Ytelsen til turbulensmodellene varier betydelig fra benchmark til benchmark, noe som var forventet siden de representerer ulike utfordringer. Ingen av de testede turbulensmodellene greier å produsere tilfredsstillende resultater for alle benchmarkene, noe som understreker viktigheten av å velge en passende turbulensmodell for et spesifikt tilfelle.

Resultatene indikerer at k-ϵ modellene gir best resultat for benchmarkene med fullt turbulent strømning, spesielt standard k-ϵ modellen. SST k-ω modellen gir dårligere samsvar med eksperimentene for de fullt turbulente benchmarkene og virker å overpredikere makshastigheten i en fullt turbulent vegg jet. For et benchmark i overgangsregime derimot, gir SST k-ω modellen best samsvar med de eksperimentelle dataene og standard k-ϵ modellen det verste. Det er dog ikke alltid helt klart hva som forårsaker endringen i ytelsen til turbulensmodellene fordi flere karakteristikker – geometri, strømningsregime og effekten av motstående trykkgradient – endres fra benchmark til benchmark. Resultatene indikerer også at innløpsverdiene for k og ϵ/ω har større påvirkning på resultatet for strømninger med lavt Reynoldstall enn høyt. Majoriteten av resultatene fra denne oppgaven stemmer overens med resultatene fra litteraturen, men SST k-ω modellen gir resultater som ikke stemmer med de fra litteraturen for to av tilfellene.

Fra oppdagelsene i denne oppgaven gis det noen beste bruksmåte anbefalinger, men det trengs også videre arbeid for å konkludere på hva som forårsaker variasjoner sett i ytelsen til turbulensmodellene. Spesielt er det et behov for flere benchmarks som systematisk endrer en og en karakteristikk av gangen. Dette vil gi muligheten til å si med mer sikkerhet hvilke karakteristikker av «cavity flow» strømningen de forskjellige RANS modellene er kapable til å modellere korrekt.

Preface

I would like to thank my supervisor Prof. Laurent Georges and my co-supervisor Elyas Lark-ermani for their guidance throughout the work with this master thesis. I would also like to express my gratitude to friends and family who have been willing to read and give feedback on parts of the thesis.

This thesis is an extension of the project assignment written by the same author in the spring 2020. The project assignment focused on the same thesis question, but presented only four benchmarks and a lot less simulations. Some of the text from this assignment have been reused in the introduction, theory and literature review of this thesis, but is significantly extended and refined in this thesis.

Contents

List of Figures

List of Tables

List of Symbols and Abbreviations

β	Thermal expansion coefficient	L	Length of cavity
δ_{ij}	Kronecker-delta	l	Length of the inlet
ℓ	Length scale	LDV	Laser doppler velocimetry
ϵ	Turbulent dissipation rate	LES	Large eddy simulation
κ	Thermal conductivity	P	Pressure
μ	Dynamic viscosity	PIV	Particle Image Velocimetry
μ_t	Dynamic turbulent (eddy) viscosity	$RANS$	Reynolds Averaged Navier-Stokes
ν	Kinematic viscosity	Re	Reynolds number
ν_t	Kinematic turbulent (eddy) viscosity	Ri	Richardson number
ω	Turbulent frequency	RNG	Re-Normalization Group
ϕ	Dissipation function	s'_{ij}	Fluctuating rate of deformation
ρ	Density	S_e	Energy source term
τ_{ij}	Reynolds stress	S_M	Momentum source term
u'	Fluctuating velocity vector	S_{ij}	Mean rate of deformation
U	Mean velocity vector	s_{ij}	Rate of deformation
u	Velocity vector	SS	Steady State
Ar	Archimedes number	SST	Shear Stress Transport
b	Length of the outlet	T	Temperature °C
Bn	Benchmark n (e.g. B1)	t	height of outlet
C_v	Specific heat capacity	T_i	Turbulent intensity
CFD	Computational Fluid Dynamics	T_{in}	Bulk inlet temperature °C
D_h	Hydraulic diameter	U	Mean velocity in x-direction
DNS	Direct numerical simulation	u	Velocity component in x-direction
e	Internal energy	U_{in}	Bulk inlet velocity
H	Height of cavity	W	Width of cavity
h	Height of inlet	x_{re}	Reattachment length
k	Turbulent kinetic energy	K	von Karman constant

1 Introduction

Computational Fluid Dynamics (CFD) was first introduced in the ventilation industry in the 70s and have been used increasingly since then [36]. One of the reasons for this increased use of CFD is that the last 50 years have seen a huge increase in the availability – and decrease in cost – of computational power. There has also been a substantial development in numerical schemes, turbulence models and the user-friendliness of CFD software and mesh generators. In total, this results in CFD being far more efficient today than 50 years ago, and it has gone from being a pure research tool to be used in the industry when designing large and complicated ventilation systems. It can also complement, and in some cases replace the "old" techniques such as wind tunnel experiments, and full or small scale mock-up experiments. These techniques are still in use and are essential to validate CFD simulations, but due to cost implications CFD, is used more and more.

Nielsen et al. [37] categorize today's applications of CFD in buildings in the following groups:

1. Prediction of air jet diffusion

2. Room air movement analysis

3. Prediction of contaminant dispersal

4. Modelling emissions from materials and equipment in buildings

5. Indoor air quality prediction

6. Thermal comfort assessment

7. Mean age of air and ventilation effectiveness predictions

8. Prediction of fire and smoke spread

9. Wind flow around buildings

Many of the categories listed above can easily involve simulation of complex flow patterns and acquisition of accurate results is in general no simple task. The accuracy of CFD simulations for indoor airflows was questioned after a study by Peng et al. [39], related to the ISHVAC-COBEE July 2015 Tianjin Workshop. Here an isothermal backward facing step flow, for a range of different Reynolds numbers, was modelled by 19 different teams from the ventilation research community and industry. No experimental data were provided for validation. The results from this workshop were very diverse, with the largest relative difference in the predicted reattachment length of the flow being more than 150%. The largest spread in the results was seen in the believed transitional flow regime, at Reynolds numbers from 80 to 500 approximately. This was expected, as accurate modelling of transitional flows is one of the most challenging aspects of CFD. The authors of this study argued that the difference between users might be the most contributing factor to the difference in the results, as different results were observed even when teams used the same models. In other words, possible errors in multiple user decisions, from convergence criteria to wall treatment, is one of the most contributing factors to the final result. However, the single parameter with the biggest impact seemed to be the choice of turbulence model. The spread in computed reattachment length for different turbulence models is seen in figure 1.1

A follow-up study by van Hoff et al. [22] from the Indoor Air Conference in Ghent in 2016, when a similar, but this time non-isothermal flow simulation was undertaken by 32 teams of CFD users.
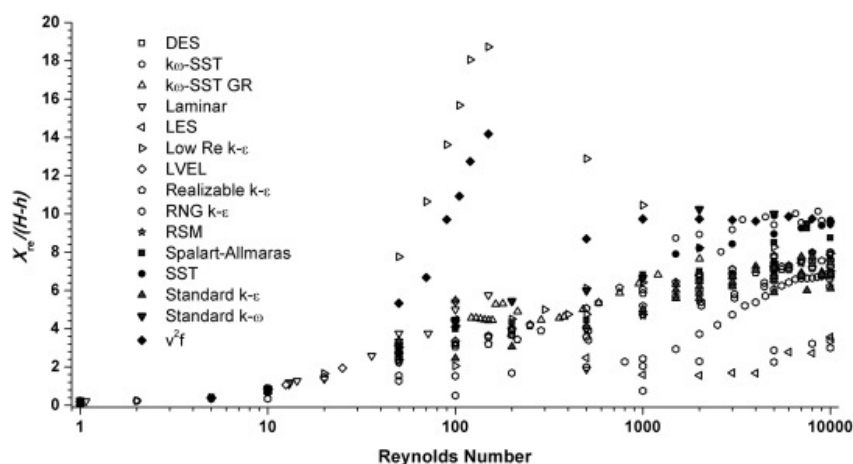
Figure 1.1: The spread in the computed reattachment length for different turbulence models plotted with Reynolds number on the x-axis (figure from Peng et al. [39] p. 135).

The teams in this study were also told to evaluate the reattachment length, as well as the maximum velocity in the lower part of the recirculation zone and its location. The results from this study showed also a very large spread in the results, as well as a clear dependence on the turbulence model and the turbulence model family.

The authors of both these studies argued that despite the concerning spread in the results from the teams, this spread would most likely have been a lot smaller if experimental data from a benchmark case was available. The results from the two studies show that validation against experimental data is essential to ensure accuracy in CFD simulations. The authors of these two studies deliberately picked cases without benchmark tests, in order to test how the results depended on the user. However, there is a consensus in the CFD community that one should always validate a simulation against some experimental data. If no experiment matches a simulation exactly – which is rarely the case – then there is the possibility to find a benchmark from a similar flow problem, preferably in the same flow regime. This is sometimes referred to as subconfiguration validation, and van Hoff et al. [22] argue that in such a study the most important is that the turbulence model is validated with experimental data, before moving to the actual simulation.

Although CFD has come a long way in improving accuracy, efficiency and user friendliness over the last four decades, the two studies [39] and [22] stress the need for benchmarks to validate CFD simulations of indoor airflows. They also argue that these benchmarks should be used to build competence in simulating indoor airflows, getting direct experience in what models and settings give good results for particular flow problems. To address this issue, this project gives an overview of seven benchmarks available for validation of indoor airflows. Benchmarks 2-5 are cavity flows with one inlet and one outlet, suitable for validation of mixing ventilation problems. These cavity flows consist of a wall jet that is discharged along the ceiling of a cavity before it impinges and turns 90 degrees when hitting the opposing wall. Typically a large recirculation vortex is created in the cavity. To look particularly at these two important features of the cavity flow – the wall jet and the impinging jet – Benchmark 6 is a pure impinging jet and Benchmark 7 is a pure wall jet. This gives the opportunity to decompose the flow features and investigate exactly which part of the flow a turbulence model struggle to model correctly. Figure 1.2 gives a graphical explanation of the different features of the cavity flow. Benchmark 1 is the backward facing step flow from the ISHVAC-COBEE July 2015 Tianjin Workshop

[39]. This was not simulated in the thesis as it was considered the least comparable with a real scenario due to its high supply opening and absence of an impingement region.
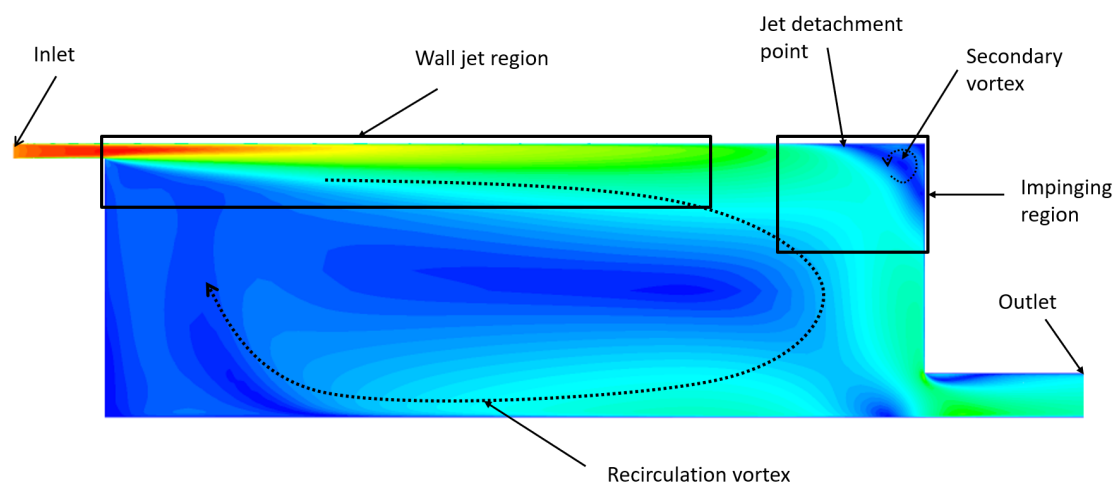
Figure 1.2: Features of the cavity flow.

A real mixing ventilation system consists of similar flow features. One or several wall jets are typically discharged along the ceiling. Because of the high velocity in the jet, it is desirable to keep it outside the occupied zone to avoid draught. It therefore important to know when the jet detaches from the ceiling, and this is why the spread in reattachment length seen in figure 1.1 is concerning. This spread is although for a jet without an opposing wall. Typically, the jet is designed to reach the opposing wall before it detaches and an impinging region is formed. The jets form a recirculation pattern in the room, and it is desirable to create a pattern that supplies fresh air to all parts of the room.

In addition to present the benchmarks themselves, this thesis presents CFD simulations of the seven benchmarks done by other researchers. Addressing what are the state of the art CFD simulations today, and as well as possible accounting for what settings and models are used, such that the simulation can be reproduced for validation or training purposes. Additionally, the results from simulations done in this thesis are presented for six of the seven benchmarks. The impact of different input parameters that are necessary for a CFD simulation has been investigated. Here, input parameters refer to all models, settings and numerical values that have to be selected by the user. The focus has been on two-equation Reynolds Averaged Navier-Stokes (RANS) turbulence models, and more precisely establish the most suitable RANS turbulence models for each of the various benchmarks. This is because the results from the preceding project assignment indicated that the choice of turbulence model is the single parameter with the biggest impact on the result. How the turbulence models perform, and how other input parameters affect the result, is shown by comparing the results form the simulations with the experimental data from the benchmarks. The results are also compared with the results from literature to see if there is agreement, and if so strengthen the conclusions that can be drawn. To the knowledge of the author, it does not exist any similar comprehensive review of the cavity flow benchmark, and this thesis is addressing this by systematically present the available benchmarks and associated simulations. By doing this, the ultimate goal of the thesis is to establish a best practice use RANS turbulence models for mixing ventilation applications.

2 Theory

2.1 Governing equations

The flow of air in a room is governed by the continuity equation (2.1), the Navier-Stokes equations (2.2-2.4) and the energy equation (2.5). Accounting for conservation of mass, momentum and energy, respectively. Here they are written as in the textbook by Versteeg [44].

$$\frac{\partial \rho}{\partial t} + \boldsymbol{\nabla} \cdot (\rho \mathbf{u}) = 0 \tag{2.1}$$

$$\frac{\partial (\rho u)}{\partial t} + \boldsymbol{\nabla} \cdot (\rho u \mathbf{u}) = -\frac{\partial p}{\partial x} + \boldsymbol{\nabla} \cdot (\mu \boldsymbol{\nabla} u) + S_{Mx} \tag{2.2}$$

$$\frac{\partial (\rho v)}{\partial t} + \boldsymbol{\nabla} \cdot (\rho v \mathbf{u}) = -\frac{\partial p}{\partial y} + \boldsymbol{\nabla} \cdot (\mu \boldsymbol{\nabla} v) + S_{My} \tag{2.3}$$

$$\frac{\partial (\rho w)}{\partial t} + \boldsymbol{\nabla} \cdot (\rho w \mathbf{u}) = -\frac{\partial p}{\partial z} + \boldsymbol{\nabla} \cdot (\mu \boldsymbol{\nabla} w) + S_{Mz} \tag{2.4}$$

$$\frac{\partial (\rho e)}{\partial t} + \boldsymbol{\nabla} \cdot (\rho e \mathbf{u}) = -p \boldsymbol{\nabla} \cdot (\mathbf{u}) + \boldsymbol{\nabla} \cdot (\kappa \boldsymbol{\nabla} T) + \phi + S_e \tag{2.5}$$

S_{Mi} are the momentum source terms, S_e is the energy source term, e = C_vT is internal energy and ϕ is the dissipation function defined in (2.6)

$$\phi = \mu \left\{ 2 \left((\frac{\partial u}{\partial x})^2 + (\frac{\partial v}{\partial y})^2 + (\frac{\partial w}{\partial z})^2 \right) + (\frac{\partial u}{\partial y} + \frac{\partial v}{\partial x})^2 + (\frac{\partial u}{\partial z} + \frac{\partial w}{\partial x})^2 + (\frac{\partial v}{\partial z} + \frac{\partial w}{\partial y})^2 \right\} + \lambda (\boldsymbol{\nabla} \cdot \mathbf{u})^2 \tag{2.6}$$

λ is known as the second viscosity. The effect from this term is small in practice and usually neglected [44].

When the Mach number is less than 0.3, which is always the case for air flows in buildings, changes in the density due to pressure can be neglected. The continuity and the Navier-Stokes equations can be simplified into equation (2.7) and (2.8), written in compact form. Furthermore, the kinetic energy's contribution to the energy equation is negligible, and the total energy equation (2.5) simplify into the internal energy equation (2.9).

$$\boldsymbol{\nabla} \cdot \mathbf{u} = 0 \tag{2.7}$$

$$\frac{\partial \mathbf{u}}{\partial t} + (\mathbf{u} \cdot \boldsymbol{\nabla})\mathbf{u} = -\frac{1}{\rho}\boldsymbol{\nabla}p + \nu\nabla^2\mathbf{u} + \mathbf{f} \qquad (2.8)$$

$$\frac{\partial \rho e}{\partial t} + \boldsymbol{\nabla} \cdot (\rho\mathbf{u}e) = \boldsymbol{\nabla} \cdot (\kappa\boldsymbol{\nabla}T) + S_e \qquad (2.9)$$

Together the continuity, Navier-Stokes and energy equation are five coupled, non-linear, partial differential equations (PDEs) and must for almost all practical purposes be solved numerically, as exact solutions exist only for very simplified geometries and boundary conditions.

Problems with solving these equations arise when the flow in question is turbulent. The Reynolds number (2.10) is a dimensionless number expressing the ratio of inertia forces to viscous forces. A high Reynolds number indicates turbulent flow, and a low Reynolds number indicates laminar flow.

$$Re = \frac{\rho u L}{\mu} \qquad (2.10)$$

For some geometries like the flow over a flat plate or the flow around a cylinder, experiments have determined what is the critical Reynolds number where transition from laminar to turbulent flow occurs. This does not mean that transition occurs exactly at this number – since transition occurs over a range of Reynolds number – but it's a clear indicator of which flow regime, or regimes, that are present in the flow. The cavity flow, however, is not as well documented and there is no well established critical Reynolds number. Van Hooff et al. [21] did experiments of a cavity flow with Reynolds numbers of 1000 and 2500, and verified that the flow was transitional for both cases. This was done by injecting fluorescent dye into the flow and observe the formation of vortices typical for the transitional regime. Nielsen [35] specifies his cavity experiment as fully turbulent at a Reynolds number of 5000 thus it is reasonable to assume transition occurs in the range 2500-5000. This will however most likely depend on the geometry of the specific cavity in question. Turbulent fluctuations are dampened near solid walls, thus the distance between the walls in the cavity can affect the level of turbulence.

2.2   Turbulence modelling

It is hard to define turbulence, but essentially if a flow is turbulent the velocity and other flow properties vary in a stochastic and chaotic way. Turbulence is from nature a three-dimensional and transient phenomenon. The motion is intrinsically unsteady and turbulent eddies are formed in the flow. Energy is transferred from larger to smaller eddies, all the way down to the smallest Kolmogorov microscale where it is dissipated due to viscosity [44].

It is possible to capture the turbulent motion simply by solving the governing equations if the grid is fine enough to capture even the Kolmogorov length scales. This is called Direct Numerical Simulation (DNS). It is solely used as a research tool, as the requirement for computational power is very large and proportional to $Re^{9/4}$ [44].

The more common approach is to decompose the velocity into one mean component **U**, and one fluctuating component **u'** like in equation (2.11), insert the decomposed velocity into the governing

equations, and then take the time average of the governing equations [44]. This procedure results in the Reynolds-Averaged Navier-Stokes (RANS) equations, where six new unknown stresses called Reynolds stresses (2.12) are added to the equations, three normal stresses and three shear stresses. They are called stresses and are usually placed on the right hand side of the equations together with the viscous stresses, but in reality they are convective transport of momentum caused by the turbulent eddies. Equation (2.13) shows the x-component of the RANS equations for incompressible flow, with Reynolds stresses added to the right hand side in the square bracket. Similarly, extra turbulent transport terms are added for transport of scalar quantities (e.g. internal energy).

$$\mathbf{u} = \mathbf{U} + \mathbf{u'} \tag{2.11}$$

$$\tau_{ij} = -\rho \, \overline{u'_i u'_j} \tag{2.12}$$

$$\frac{\partial U}{\partial t} + \boldsymbol{\nabla} \cdot (U\mathbf{U}) = -\frac{1}{\rho}\frac{\partial P}{\partial x} + \nu \, \boldsymbol{\nabla}^2 U + \frac{1}{\rho}\left[-\frac{\partial \rho \overline{u'^2}}{\partial x} - \frac{\partial \rho \overline{u'v'}}{\partial y} - \frac{\partial \rho \overline{u'w'}}{\partial z} \right] \tag{2.13}$$

Different RANS turbulence models are then categorized after how many additional transport equations that are solved to compute the six Reynolds stresses. The most common turbulence models are in the k-ϵ family and k-ω family. All these models solve two additional transport equations to calculate the Reynolds stresses, one for the turbulent kinetic energy k and one for either turbulent dissipation rate ϵ or specific turbulent dissipation rate ω (also referred to as turbulent frequency). k is defined by Versteeg [44] from the fluctuating velocities (2.14), and ϵ from the fluctuating rates of deformation (2.15). The specific dissipation rate ω – used in the k-ω models – is defined as ϵ divided by k (2.16). The decomposition of the rates of deformation is defined in equation (2.17).

$$k = \frac{1}{2}(u'^2 + v'^2 + w'^2) \tag{2.14}$$

$$\epsilon = 2\nu \overline{s'_{ij} \cdot s'_{ij}} \tag{2.15}$$

$$\omega = \epsilon/k \tag{2.16}$$

,

$$s_{ij} = S_{ij} + s'_{ij} = \frac{1}{2}\left(\frac{\partial U_j}{\partial x_i} + \frac{\partial U_i}{\partial x_j} \right) + \frac{1}{2}\left(\frac{\partial u'_j}{\partial x_i} + \frac{\partial u'_i}{\partial x_j} \right) \tag{2.17}$$

The most widely used and validated two equation turbulence model is the standard k-ϵ model [44]. It's transport equation for k and ϵ are shown in equations (2.18) and (2.19), respectively. The two transport equations contain five constants C_μ, σ_k, σ_ϵ, $C_{1\epsilon}$ and $C_{2\epsilon}$ which values have been determined by comprehensive data fitting to a wide range of turbulent flows [44].

$$\frac{\partial \rho k}{\partial t} + \boldsymbol{\nabla} \cdot (\rho k \mathbf{U}) = \boldsymbol{\nabla} \cdot \left(\frac{\mu_t}{\sigma_k} \boldsymbol{\nabla} k \right) + 2\mu_t S_{ij} \cdot S_{ij} - \rho\epsilon \tag{2.18}$$

$$\frac{\partial \rho \epsilon}{\partial t} + \boldsymbol{\nabla} \cdot (\rho \epsilon \mathbf{U}) = \boldsymbol{\nabla} \cdot \left(\frac{\mu_t}{\sigma_\epsilon} \boldsymbol{\nabla} \epsilon \right) + C_{1\epsilon} \frac{\epsilon}{k} 2 S_{ij} \cdot S_{ij} - C_{2\epsilon} \rho \frac{\epsilon^2}{k} \tag{2.19}$$

The values for k and ϵ or ω are used to calculate the turbulent eddy viscosity μ_t. In the standard k-ϵ model, equation (2.20) is used. Then from this the Reynolds stresses are calculated with the Boussinesq relationship (2.21).

$$\mu_t = \rho C_\mu \frac{k^2}{\epsilon} \tag{2.20}$$

$$- \rho \overline{u_i' u_j'} = \mu_t \left(\frac{\partial U_i}{\partial x_j} + \frac{\partial U_j}{\partial x_i} \right) - \frac{2}{3} \rho k \delta_{ij} \tag{2.21}$$

The popularity of the standard k-ϵ model is explained by its good performance for confined flows where the Renyolds shear stresses are most important, which includes a wide range of engineering flow applications. However, the standard k-ϵ model also has known shortcomings, among others an overestimated spread of axisymmetric jets and an incapability to model secondary flows in non-circular ducts due to the treatment of normal Reynolds stresses [44]. Two popular models overcome some of the deficiencies of the standard k-ϵ model: the RNG k-ϵ model and the realizable k-ϵ model.

The RNG k-ϵ model was derived from a statistical technique called Re-Normalization Group (RNG) theory. It is similar in form to the standard model, but has different constants and additional terms in the transport equations for k and ϵ. Compared to the standard model this gives the following refinements according to the ANSYS Fluent theory guide [3], that make the RNG k-ϵ model more accurate and reliable for a wider range of flows:

- An additional term in the ϵ equation that improves the accuracy for rapidly strained flows.

- The effect of swirl on turbulence, enhancing accuracy for swirling flows.

- An analytical formula for the turbulent Prandtl numbers.

- While the standard model is a high-Reynolds number model, the RNG theory provides an analytically derived differential formula for effective viscosity that accounts for low-Reynolds number effects. Effective use of this feature does, however, depend on appropriate treatment of the near-wall region.

The realizable k-ϵ model differs from the standard model in two ways [3]:

- An alternative formulation for the turbulent viscosity.

- A modified transport equation for ϵ, derived from an exact equation for the transport of the mean-square vorticity fluctuation.

The turbulent viscosity is still computed from equation (2.20) in the realizable model, but C_μ is a variable, something that was originally proposed by Reynolds, and this notion is justified by experimental evidence. Both the RNG k-ϵ model and the realizable k-ϵ models have shown substantial improvements over the standard model where the flow features include strong streamline curvature,

vortices and rotation. Since the realizable k-ϵ model is relatively new it is not clear in exactly which cases it consistently outperforms the RNG model [3].

In the k-ω models, a transport equation is solved for ω rather than ϵ. An advantage with this is that the ω transport equation can be integrated to the wall without wall damping functions, and as a consequence, the standard k-ω model is superior to the standard k-ϵ when it comes to modelling the flow near walls. The problem with the standard k-ω model is that it is sensitive to the free stream value for ω that is typically unknown. This issue was overcome with the SST k-ω model which combines the standard k-ϵ and standard k-ω model. The k-ϵ model is applied in the fully turbulent region far away from the wall, while the k-ω model is applied in the wall region. Blending functions are used to achieve a smooth transition between the two models.

In all the two equations models the turbulent eddy viscosity μ_t is assumed to be isotropic, i.e. the same in all directions. In some complex flows, there are non-negligible directional effects in the Reynolds stresses that cannot be captured by the two equation models. In other words, areas where the assumption of an isotropic eddy viscosity is invalid. The Reynolds Stress Model (RSM) solves one transport equation for each Reynolds stress and is capable of capturing these effects at the price of higher computational cost. The model also solves one equation for ϵ or ω so a total of seven additional equations must be solved. Because of this the RSM model is less used and validated than the two equation models, but it has the potential to describe all mean flow properties without case-by-case adjustment [44].

Another approach to turbulence modelling than RANS is that of Large Eddy Simulation (LES). LES uses a spatial filter to separate larger and smaller eddies. The large eddies are solved directly as in DNS, while the smaller eddies are modelled. LES is by definition transient and three-dimensional [44].

One of the problems with RANS is that one turbulence model must describe the behaviour of all turbulent eddies from largest to smallest. However, large eddies are more anisotropic, interact with the main flow and depend on the geometry, while the smaller eddies have a nearly universal behaviour. LES overcome this problem by using the spatial filtering, but at the price of a computational cost that is much greater than for a RANS simulation. For this reason, LES is mostly used in research, but is slowly becoming more popular in the industry as well, as it gives a higher accuracy and a more detailed solution than RANS simulations.

2.3   Boundary conditions

All CFD problems must have well defined boundary conditions that represent the real physics of the flow in the best possible way. Boundary conditions must be defined for all flow parameters: velocity, pressure, temperature and turbulence parameters. In the cavity flow, the three different boundaries are the inlet, outlet and the walls.

2.3.1   Inlet & Outlet

There are several different ways to set up the boundary conditions for inlet and outlet and all possibilities are not reviewed here. Typically the velocity profile is specified at the inlet, as well as the inlet temperature. At the outlet, the pressure is usually set to zero if the flow is incompressible and gauge pressure can be used, while the velocity and temperature are set to having a zero gradient.

The most problematic part is often to determine the turbulence parameters at the inlet. The turbulent kinetic energy k is usually determined from a guessed value of the inlet turbulent intensity T_i and the inlet velocity U_{in} [44].

$$k = \frac{3}{2}(U_{in} T_i)^2 \tag{2.22}$$

While ϵ and ω, can be determined from a defining length scale ℓ, k and the model constant C_μ.

$$\epsilon = C_\mu^{3/4} \frac{k^{3/2}}{\ell} \tag{2.23}$$

$$\omega = C_\mu^{3/4} \frac{k^{1/2}}{\ell} \tag{2.24}$$

Versteeg [44] suggests $\ell = 0.07L$ where L is the diameter if the inlet is a pipe and the hydraulic diameter, D_h,if it is of non-circular geometry. For ventilation applications in particular Nielsen et al. [37] suggest ℓ as a ratio of the height of the supply opening (e.g. ℓ = 0.1h) or as 0.005 times the height of the cavity (e.g. ℓ = 0.005H). In the latter approach the constant C_μ is omitted from the formula.

It should be noted that using these or other equations to compute the inlet values for k, ϵ or ω are estimates. The sensitivity of these input values can be determined from a sensitivity analysis.

2.3.2 Wall treatment

How one should calculate the velocity in the grid point closest to a wall will depend on whether or not that point is within the viscous sub layer, the buffer layer or the log-law region. To determine this location the value of the dimensionless number y^+ must be determined. y^+ and u^+ are defined from the friction velocity u_τ (2.25). Some papers report the value of y^* rather than y^+, which is defined from k rather than the friction velocity. The values for y^+ and y^* are very similar for most flows, and serve the same purpose, but can give slight variations in complex flows.

$$y^+ = \frac{y u_\tau}{\nu} \quad u^+ = \frac{u}{u_\tau} \quad u_\tau = \sqrt{\frac{\tau_w}{\rho}} \tag{2.25}$$

The relationship between y^+ and u^+ will be linear (2.26) in the viscous sub layer and logarithmic (2.27) in the log-law region. K is the von Karman constant and C^+ is an integration constant that depends on the wall roughness.

$$u^+ = y^+ \quad y^+ < 5 \tag{2.26}$$

$$u^+ = \frac{1}{K} ln(y^+) + C^+ \quad 30 < y^+ < 200 \tag{2.27}$$

The expression in equation (2.27) is commonly referred to as the standard wall function. Plotting these expressions against DNS data like in figure 2.1, the fit is – as one would expect – very good in the valid range of y^+ for each expression. In the buffer layer, however, neither the linear-law nor the log-law fits the data. There are different ways to improve the accuracy in the buffer layer. One way is to use the Spalding wall function, which is a wall function created to fit the DNS data in all the three layers. Another way is to use a blending of the linear-law and log-law based on the y^+ value in each cell, and this is what most modern CFD codes do today.

It should be noted that the log-law is derived from assuming a 1D Couette flow along a wall, thus it is not valid in the presence of significant adverse pressure gradients, flow separation and curvature. This is one of the reasons why this approach is rarely used in e.g. external aerodynamics simulations.
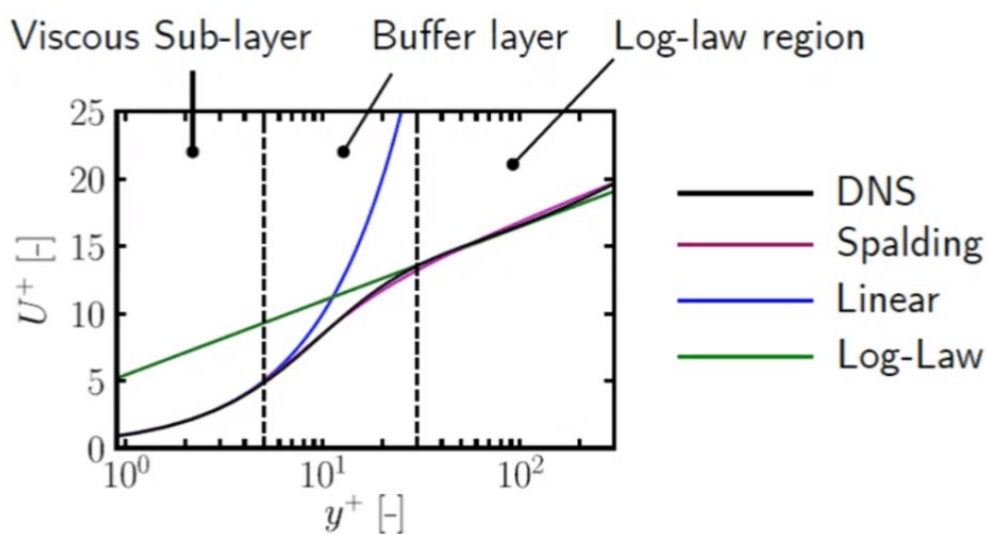
Figure 2.1: Viscous sub layer, buffer layer and log-law region.

There is however a consensus in the CFD community that one should avoid placing a large number of cells in the buffer layer, as the blending of the two laws is known to be inaccurate. This has lead to the use of meshes that either resolve the boundary layer and have $y^+ < 5$ for all the wall adjacent cells, or meshes have $y^+ > 30$ for all the wall adjacent cells and use wall functions. In general, resolving the boundary layer gives a better prediction of wall shear stress and heat transfer, at the cost of longer computational times and potentially stability issues, since the cells have to be long and thin to resolve the boundary layer, leading to high aspect ratios and high skewness if the wall is curved.

It should be noted that although mainly velocity is discussed here all flow variables, temperature, k, ϵ etc. need a form of wall treatment. A more thorough description of wall functions is given by Bredberg [7]. For temperature, the approach is essentially the same as for velocity only that the molecular Prandtl number and the turbulent Prandtl number is involved in the linear-law and the log-law, respectively.

Furthermore, different turbulence models have different options for near wall modelling. The standard k-ϵ model was originally created to be used only in the log-law region, as it does not capture the damping of turbulent eddies caused by the wall in the viscous sub layers. This problem has been overcome by using damping functions which reduce the dissipation of ϵ and the turbulent viscosity μ_t

close to the wall. k-ϵ models with damping functions are usually referred to as low-Re k-ϵ models. These models give improved performance for some flows, but are more unstable than the standard model.

In recent years, y^+ insensitive wall treatment methods have been developed for most industrial CFD codes. The ANSYS Fluent theory guide [3] recommends using "Enhanced Wall Treatment" or "Menter-Lechner" wall treatment for the k-ϵ models. Enhanced wall treatment uses a two-layer model for ϵ, where in the near wall region ϵ is not calculated by its transport equation, but instead the one-equation model by Wolfstein is used [45]. Furthermore, enhanced wall functions are used to blend equations (2.26) and (2.27) in the buffer region. The blending function is of the following form [3]:

$$u^+ = e^\Gamma u^+_{lam} + e^{1/\Gamma} u^+_{turb} \tag{2.28}$$

Where Γ is given by (a = 0.01 and b=5):

$$\Gamma = -\frac{a(y^+)^4}{1 + by^+} \tag{2.29}$$

This gives an improved fit to the DNS-data in the buffer region, and give reasonable accuracy also here, hence this wall-treatment is referred to as y^+ insensitive. It should however be noted that the fit in the buffer region is not perfect and placing a large number of cells here is still not recommended.

Menter-Lechner wall treatment uses another approach to give a y^+ insensitive wall treatment. Here source terms are added to the transport equation for k to account for the near-wall effects. [3]

Despite all the improvements in the near wall modelling for the k-ϵ models, the k-ω models are usually said to be superior for near wall modelling, since the transport equation for ω can be integrated to the wall. In ANSYS Fluent, this feature is utilized to create a y^+ insensitive wall treatment where the viscous sub-layer formulation is blended with the log-law formulation. This is the default setting for all ω based models in Fluent [3].

2.4   Discretization schemes

The textbook by Versteeg [44] gives a thorough description of different numerical schemes. Essentially the discretization (or numerical) schemes determine how the partial differential equations are discretized into algebraic equations that can be solved by a computer. When discretization schemes are discussed in a CFD context it is usually the schemes applied to the convection term of the Navier-Stokes equations that are discussed.

There are numerous schemes available, but the three most common ones are the central differencing scheme (or linear scheme), the upwind scheme and the second order upwind scheme (or linear upwind).

- The central scheme is second order accurate, but unbounded which often causes stability issues when applied to the convection term.

- The upwind scheme is bounded, but is only first order accurate and can cause numerical diffusion − an artificial increase in viscosity. This again leads to wrong and possibly nonphysical results.

- The second order upwind scheme is second order accurate, it is unbounded, but much less so than the central scheme. Thus it usually comes with fewer stability issues than the central scheme.

It is recommended to never use the upwind scheme for the final solution of a simulation, but it is often used to calculate an approximate solution before switching to higher order schemes for the final iterations. The central scheme is rarely used for the convection term, but is very common for the diffusion term of the Navier-Stokes equations. Furthermore, more advanced schemes often use a blending of the central scheme and the upwind scheme, such as the vanLeer scheme and OpenFOAM's limitedLinear scheme.

2.5   Pressure-velocity coupling

The Navier Stokes equations are as mentioned coupled, meaning that each velocity component appears in each equation, as well as in the continuity equation. However, the pressure gradient is present in all components of the Navier-Stokes equations, but there is no transport equation for pressure when the flow is incompressible. If the pressure gradient is unknown and does not appear in any equation, there is no way of solving the velocity field, so the equations cannot be solved without further ado [44].

This issue was overcome with the SIMPLE algorithm by Patankar and Spalding from 1972 [44]. Very simplified, this algorithm uses a guessed pressure field to solve the Navier-Stokes equations, and then uses the continuity equation to compute a pressure correction, which in turn is used to update the velocity field. The iterative procedure stops at convergence for both pressure and velocity.

Later additional pressure-velocity coupling (PV coupling) algorithms have been proposed, some of which are the SIMPLER, SIMPLEC and PISO algorithms. They can all be seen as extensions of the SIMPLE algorithm [44], but can introduce savings in computational time by improved convergence and stability. Which algorithm is best will depend on the particular flow problem.

2.6   Buoyancy and the Boussinesq approximation

If a flow is non-isothermal, density changes will occur although the Mach number is below 0.3 due to changes in temperature. In other words, the incompressible Navier-Stokes equations (2.8) are not valid. This means that either the compressible Navier Stokes equations must be solved by computing the density from the ideal gas law, or one can use the Boussinesq approximation.

A good description of the Boussinesq approximation is given by Ferziger and Peric [17]. It is derived from decomposing the density into one reference density and a deviation from this, and then say that the deviation is only relevant in the buoyancy force term of the Navier-Stokes equations. This allows the incompressible Navier-Stokes equations to be used, with an additional buoyancy term (2.30) on the right hand side.

$$[1 - \beta(T - T_0)]\mathbf{g} \tag{2.30}$$

Where β is the thermal expansion coefficient (2.31) and ρ_0 and T_0 are the reference density and temperature, respectively.

$$\beta = -\frac{1}{\rho_0}\left(\frac{\partial \rho}{\partial T}\right)_p \tag{2.31}$$

The Boussinesq approximation allows for faster computations by avoiding to solve the more non-linear compressible Navier- Stokes equation. It also removes the need to store the density as

a variable, since the buoyancy force is a function of the temperature only. For air the Boussinesq approximation introduces an error in the order of 1% if the maximum temperature difference is within $15°C$ [17], in other words it, is usually applicable for airflows inside buildings.

A measure on how dominant the buoyancy forces are in a particular flow can be given by the Richardson number (2.32), which is the ratio of buoyancy forces to viscous forces.

$$Ri = \frac{\beta g L \Delta T_0}{U_{in}^2} \tag{2.32}$$

Where L is a length scale, ΔT_0 is the temperature minus a reference temperature and U_{in} is the inlet supply velocity. Some of the papers in the literature review use the Archimedes number instead of the Richardson number, but essentially with a formulation that is similar to equation (2.32).

2.7   Mixing ventilation and the cavity flow

Generally speaking a "cavity flow" is just a flow inside a cavity. A cavity flow can be driven by several different mechanisms: by having one or more inlets supplying the cavity with momentum, by one of the walls moving and this motion propagates into the flow from the action of viscosity or by having one or more heat sources that drive the flow through buoyancy forces. For replicating the flow structures encountered in ventilated spaces both inlets supplying momentum and heat sources are highly relevant. To replicate mixing ventilation one usually looks at cavities with velocity inlets, creating a jet that mixes fresh air with old and polluted air and causes the air in the cavity to recirculate. To replicate displacement ventilation heat sources have to be included, as the concept of displacement ventilation is to utilize these in order to convect the polluted air away into exhausts mounted above the occupied zone. In this thesis, the focus is on cavity flows with no or limited heat sources, suitable for validation of mixing ventilation systems.

A guide on how to design mixing ventilation systems is given in the REHVA guidebook by Muller et al. [32]. In a typical mixing ventilation system, the air inlets generate a wall jet in the upper part of the room, outside of the occupied zone. To achieve good mixing the air is supplied with high initial velocity to have high velocity gradients and high turbulent intensity. Care must be taken when designing a mixing ventilation system to avoid having too high velocities in the occupied zone, typically below 0.15 m/s. An important parameter to judge this is the throw length, defined as the distance from the inlet to where the maximum jet velocity is equal to a reference velocity, typically 0.2 m/s. Experience shows that the throw length should be equal to the room length, or when several diffusers are used, equal to half of the distance between two opposing diffusers. If the throw length is too long the jet will impinge in the opposing wall and can then be deflected into the occupied zone with too high velocity. If the throw length is to short the jet can detach from the wall and enter the occupied zone before it reaches the opposite wall. It can also create zones with insufficient mixing. In the design of a mixing ventilation system, a CFD simulation can be used to predict the flow pattern and parameters like the maximum velocity in the occupied zone and the point of wall jet detachment can be determined from the simulation.

To validate CFD for mixing ventilation applications one usually undertakes a cavity flow with one inlet and one outlet. This was the approach used by Nielsen [34] when he began his early work in the 70s, and has been used by several other researchers up until today. The inlet is typically located in the upper left corner of the cavity and the outlet in the lower right. This creates a wall jet that entrains the room air and generates turbulence from the velocity gradients, much like a real mixing ventilation

system. Furthermore, the jet drives a recirculating flow pattern much like what is desired in mixing ventilation. The idea behind validating CFD for mixing ventilation applications is that if the CFD code is capable of solving the benchmark cavity cases, it is likely to be able to solve real cases as well. This is because the flow phenomena the CFD code has to able to model in the real and benchmark cases are similar.

The cavity flow is not simple and straightforward to model with CFD. Up until now the RANS approach has been widely used to simulate ventilated spaces. However, van Hooff et al. [21] list three challenges with using RANS turbulence models to model indoor airflows. Transitional flow, turbulence anisotropy and adverse pressure gradients. Transitional flows are challenging because of their transient nature and the fact that many RANS turbulence models, including the popular standard k-ϵ model, were developed for fully turbulent flows. Turbulent anisotropy can be present in regions of high shear, and most first order RANS model based on the assumption of an isotropic eddy viscosity does not capture such an effect. An adverse pressure gradient will be present in the impinging region. The increased pressure can induce the separation of the boundary layer along the ceiling. Boundary layer separation is not easily predicted with some steady RANS turbulence models – specially the standard k-ϵ model – as they underpredict the turbulent dissipation rate, ϵ, [21] close to the wall. This again leads to an incorrect eddy viscosity, increased shear stress near the wall and delayed detachment. The k-ω and RSM model are known to be more accurate for modelling separating flows [21]. The magnitude of the adverse pressure gradient will depend on the distance from the inlet to the opposing wall, the inlet height and inlet momentum. For some benchmarks, this distance can be so long that the pressure is not significantly increased in the corner opposite to the inlet and the flow detachment is not caused by an adverse pressure gradient. Thus, different cavity benchmarks will represent different challenges.

In his Phd. thesis from 1996 Karimipanah [28] investigates turbulent jets in confined spaces both experimentally and numerically. Part of the motivation for this thesis was that in the industry, mixing ventilation systems are usually designed using the throw length supplied by the manufacturer. When determining the throw length ,however, Karimipanah claims manufacturers use experiments in large surroundings, thus the jet is not in a confined space as it will be in a real scenario. Among other things, Karimipanah investigates the difference between different jets in confined and open rooms. He finds that there are significant differences between the two cases. When a jet hits an opposing wall a negative pressure gradient is present, and this increases the spreading rate of the jet and the decay of the maximum velocity. The air movement in the room can influence the assumption of momentum being conserved in a jet as air might enter the jet at angles not equal to 90 degrees. In general, Karimipanah concludes that jets in confined spaces are even more complex to model than just pure wall jets. In particular, in the corners of a room the jet has to turn, and secondary vortex flows emerge in the corners. In this area the assumption of an isotropic eddy viscosity is not valid according to Karimipanah, thus a first order RANS turbulence model is not suitable to simulate such a flow.

The discoveries of Karimipanah is a concern for RANS turbulence modelling of indoor airflows, as the flow includes areas of non-isotropic eddy viscosity. On the other hand, Karimipanah also questions the traditional way of designing mixing ventilation systems, and insinuates that using the traditional methods based on the throw length might lead to unintended flow patterns. Thus, CFD is the only way – besides a full scale experiment – to determine the correct flow pattern in a room.

3 Literature review

The following section presents seven different benchmark flows which can be used to validate CFD simulations of indoor airflows. Later the success of CFD to simulate these flows is addressed. Benchmark 1 is a backward facing step flow, i.e. the jet does not impinge on any opposing wall and there are as a consequence no adverse pressure gradient. Benchmarks 2-5 are cavity flows with one inlet and one outlet. Benchmark 6 is an impinging jet flow and benchmark 7 is a pure wall jet. All benchmarks except B3 and B4 are isothermal, and these two have limited buoyancy effects.

3.1 Benchmarks

For the purpose of systematising the different geometries and make comparisons easier, every value for x, y and z used in this paper is based on an origin in the corner straight below the inlet as shown in figure 3.1. Here the names used for the different benchmarks walls are described as well. The geometry of each benchmark is specified using the following notation: L is the length in the x-direction, H is the height in the z-direction, W is the width in the y-direction, h is the inlet height, t is the outlet height and l and b is the inlet and outlet length in the x-direction where it is applicable. This is explained graphically in figure 3.2.

Note that the figures describing the geometry of each benchmark is taken from the paper describing it. Therefore the origin used in figures can be different from what is used in this text, however, all captions and text in this paper use the origin and axis in figure 3.1. For all benchmarks the inlet and outlet span the entire width. Only benchmark 1 specifies an inlet length l. For the other benchmarks it is a choice of the CFD user to include an inlet length l or not. None of the benchmarks specifies an outlet length b, but it is used in some of the simulations.
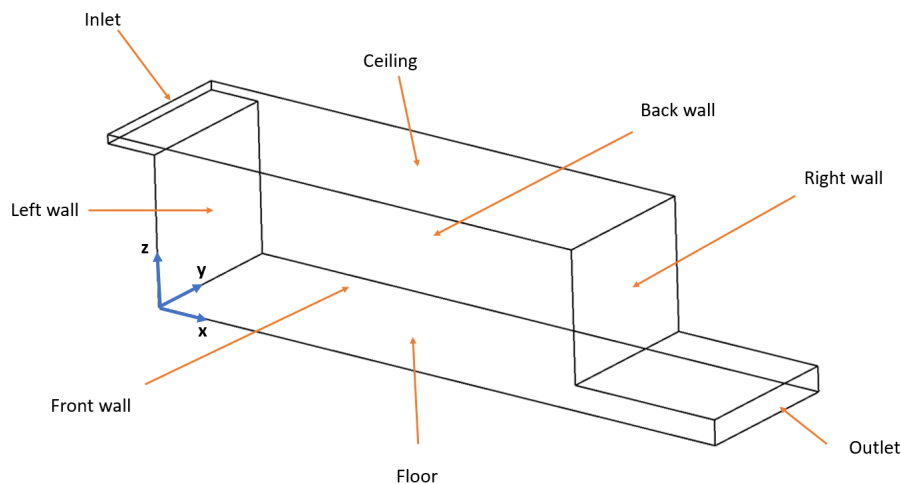
Figure 3.1: Origin and wall names used for benchmarks 1-5.
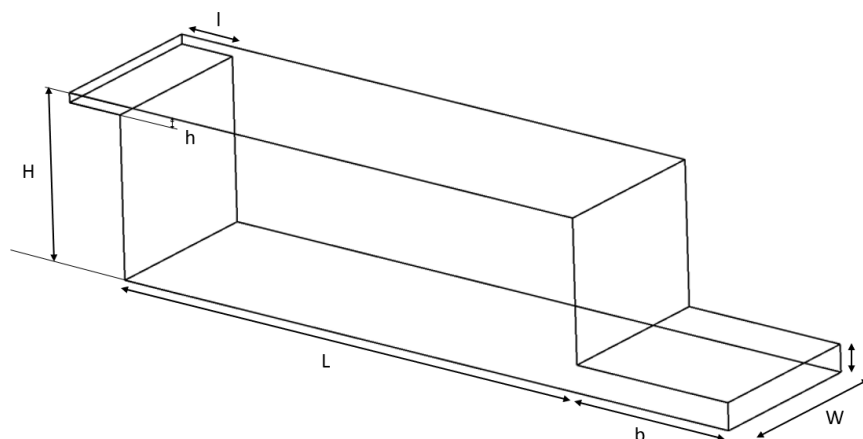
Figure 3.2: Benchmarks 1-5 notation.

3.1.1   Benchmark 1

Benchmark 1 is a simple backward facing step flow. The experiment was done by Nielsen et al. [33] and the measurements as well as the experiment report can be found in the webpage www.cfd-benchmarks.com [1]. The experimental data are available as .xls files. The layout is shown in figure 3.3. The flow is isothermal and the geometry is similar to that one used in the workshop study by Peng et al. [39] for the ISHVAC-COBEE conference, however, the measurements were made available for the teams after the conference workshop.
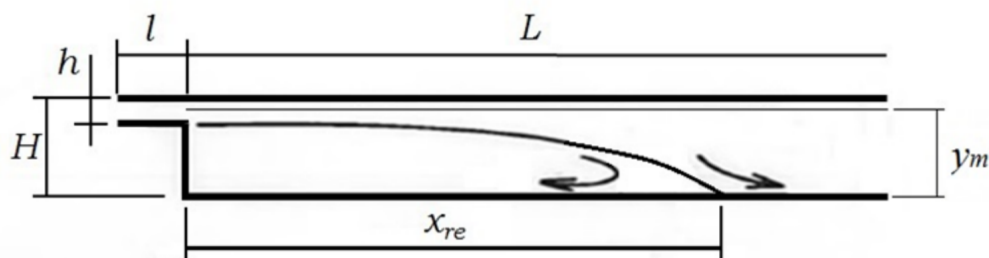
Figure 3.3: B1 geometry (figure from Nielsen et al. [33] p. 2).

The geometry of the experimental model are as follows: h/H = 0.2, L/H = 25, W/H = 2 and l/H = 4. The model had the following size: H = 0.2 m.

Experiments were carried out for Reynolds numbers ranging from 0 to 10 000 and velocity measurements were done with a Particle Image Velocimetry (PIV) system. x_{re} as shown in the figure is the reattachment length measured from the vertical wall to the point where the flow separates into a flow going towards the outlet and a flow going back to the left wall. This point can be located as the point with zero shear stress on the lower wall or a point of zero velocity a very small vertical distance above the floor.

Measured data are available for a Reynolds number of 500 and 4000 representing transitional flow and fully turbulent flow according to Nielsen et al. [33]. These data do not contain the reattachment length as this was not possible to determine from the measurements. This sadly impedes the possibility

to compare the reattachment length reported in the ISHVAC-COBEE workshop with experimental data. However, velocity data along a horizontal line at a height z/H = 0.952, is available for validation of future simulations.

3.1.2   Benchmark 2

The layout of the second benchmark is shown in figure 3.4. The experiment was done by Nielsen [35] and the experiments report and measurement can be found at www.cfd-benchmarks.com [1]. The experimental data are available as .xls files. The benchmark is often cited by the name "IEA Annex 20 two dimensional benchmark test" or "IEA Annex 20 test room" and there are numerous papers from researchers who have done CFD simulations on this geometry. This makes it a good benchmark test, as comparisons can be made both against experimental data and multiple simulations of other researchers.
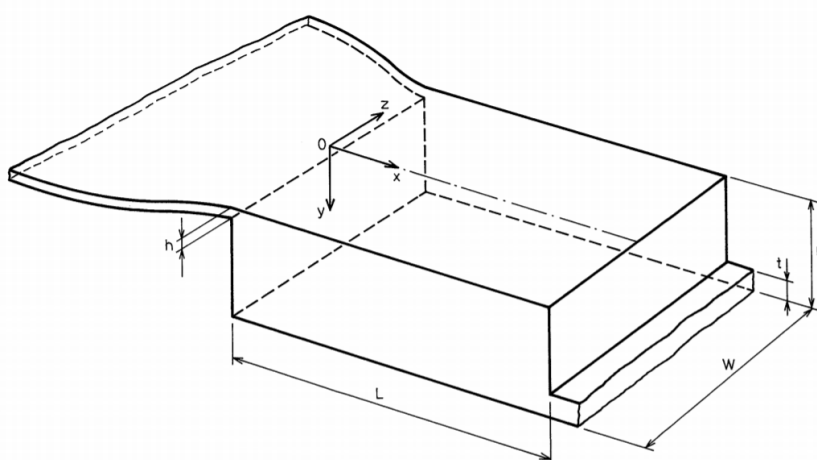
Figure 3.4: B2 geometry (figure taken from Nielsen [35] p. 1).

The geometry of the experimental model have the following dimensions: L/H = 3, h/H = 0.056, t/H= 0.16, W/H = 1 and a model size H = 0.0893 m. No inlet length l or outlet length b is specified.

The velocity is measured with Laser Doppler Velocimetry (LDV). Measurements are only done for a Reynolds number of 5000, representing fully turbulent flow. The mean velocity in the x-direction, U and the root mean square of the velocity $\sqrt{\overline{u'^2}}$ is measured at four different lines. Two vertical at x = H and x = 2H, and two horizontal at z = h/2 and z = H-h/2. The measurements of the root mean square makes it possible to evaluate the turbulent intensity of the flow.

Note that the size of the model is different than in the test case defined in the experiment report [35] for the Annex 20 test room where H = 3m, however, the inlet velocity is also scaled such that the Reynolds number remains equal at 5000 and similarity is achieved.

3.1.3   Benchmark 3

The third benchmark has the same geometry as the second benchmark, the only difference being the dimension W/H which is here W/H = 4.7 and the size of the model with H = 0.127 m in this case. The experimental data are only available in plots from the report, and must be read manually or with some

digitizer software.

The experiment was done by Nielsen in he's PhD thesis [34] and measurements were done for a flow that is both non-isothermal and isothermal. For the non-isothermal flow only temperature measurements were performed. However, Nielsen [34] claims that the non-isothermal flow has an Archimedes number so low (order of 10^{-6}) that it does not affect the velocity profile. In other words can the isothermal velocity profile also be used in the non-isothermal case for the same Reynolds numbers. The isothermal flow has Reynolds numbers of 4700 and 7100, while the non isothermal has Reynolds numbers of 2400, 4700 and 7100 and measurements at three different Archimedes numbers for each Reynolds number. The isothermal flow is measured with hot wire anemometry, and measurements were done only at a line x = 2H. The non-isothermal flow had temperature measurements done at 10 locations with thermocouples. It should be noted that Nielsen also did various experiments varying the width and length of the model in the same paper, but here only the width used for the non-isothermal flow is undertaken.

3.1.4 Benchmark 4

The fourth benchmark has the geometry shown in figure 3.5 the experiment was done by Blay et al. [5] in 1992. The experiment report [5] is not openly available, but must be requested, and the data must be read from plots.

This has a slightly different geometrical configuration than benchmark 2 and 3 in the sense that the width is considerably smaller compared to the length and height, and the inlet and outlet openings are smaller. The setup has two guard cavities to make the side walls adiabatic, thus eliminating thermal effects to make the flow as two dimensional as possible. The floor is kept at a constant temperature of $35.5°C$. The remaining three walls have a temperature equal to the inlet temperature of $15°C$, thus the flow is non-isothermal. The walls were made of aluminium and kept at a constant temperature by the use of temperature controlled water. The wall temperature had a precision of $0.25°C$.
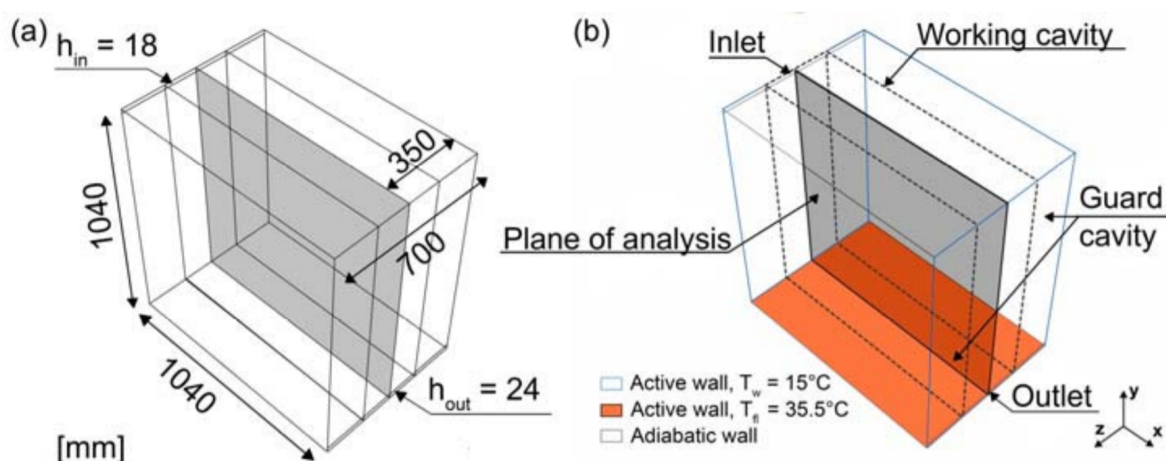
Figure 3.5: B4 geometry (figure from Kosutova et al. [29] p. 3).

The dimensions of the model are: h/H = 0.0173, t/H = 0.0231, W/H = 0.288, L/H = 1, with H = 1.04m. No inlet or outlet length is specified. Supply velocity was 0.57 m/s making the Reynolds number 684 based on the inlet height. Velocity measurements were done with a LDV system and temperature measurements with Cr-Al thermocouples. Values for the turbulent kinetic energy were also measured and are available in the report. The inlet turbulent intensity was measured by the LDV to be 6%. To

check whether the flow was in fact 2D the u velocity was measured along the width of the cavity at two different lines, the difference was found to be less than 4%.

In addition to measuring the velocity, temperature and k, it was investigated for which Froude number (3.1) the flow changed the way it rotated. The Froude number is essentially the inverse and squared Richardson number. For low values of the Froude number, the buoyancy effects are more dominant and the flow starts to rotate counter clockwise as the cold inlet air "sinks" rather than being discharged into the room as a jet. For high values of the Froude number, it is the momentum from the jet that drives the flow thus, it rotates clockwise.

$$Fr = \frac{U_{in}}{g\beta h(T_{floor} - T_{in})} \tag{3.1}$$

This effect was investigated for two different floor temperatures, $35°C$ and $54.3°C$. The values of the critical Froude number is found in table 3.1. The value for Fr_c depended on both the floor temperature and for whether the value of Fr was increasing or decreasing when the change in rotation occurred. The Froude number was 5.31 when the measurements of velocity and temperature were performed, thus the flow was well within the range of clockwise rotation.

Table 3.1: Values for critical Froude number (Fr_c) for benchmark 4 reported by Blay et al. [5]

Floor temp [$°C$]	Decreasing or increasing Fr	Value
35	Decreasing	$1.93 < Fr_c < 2.06$
35	Increasing	$3.12 < Fr_c < 3.31$
54.3	Decreasing	$1.92 < Fr_c < 2.45$
54.3	Increasing	$2.89 < Fr_c < 3.41$

If one scales benchmark 4 up to a slightly more realistic room size – e.g. multiply all the dimensions with 3 to get a room that is approximately 3x3x1 cubic meters – one can get an idea of for what level of floor heating B4 is representative. If the Reynolds and Froude numbers are to be kept constant at 684 and 5.31, respectively, the inlet velocity reduces to 0.19 m/s as the inlet height is now 0.054 m. To keep the Froude number constant the floor temperature is then only $15.7°C$, that is only $0.7°C$ more than the air inlet temperature. In a realistic scenario a heated floor temperature can be as high as $26°C$. Keeping all the other parameters constant this would mean a Froude number of 1.3, thus the flow would rotate in the opposite directions according to the values in table 3.1, and the experimental data are not representative for the flow in question. Thus, Benchmark 4 is not suitable to validate CFD simulations of rooms with high floor temperature, but should be seen as another benchmark for mixing ventilation. Nonetheless, by comparing the experimental and simulated temperatures, B4 can be used to estimate the accuracy of the modelling of the heat transfer from the floor.

3.1.5   Benchmark 5

The layout of benchmark 5 is shown in figure 3.6. A general description of the benchmark and the data files can be found at the webpage kbwiki.ercoftac.org [15] – there referred to as UFR 4-20 – as well as the results from some CFD simulations of this benchmark. The experiment was done by van Hoff et al. [20] in 2012 and the report is publicly available for a more thorough description of the experimental setup.

(a) B5 geometry   (b) B5 experimental setup
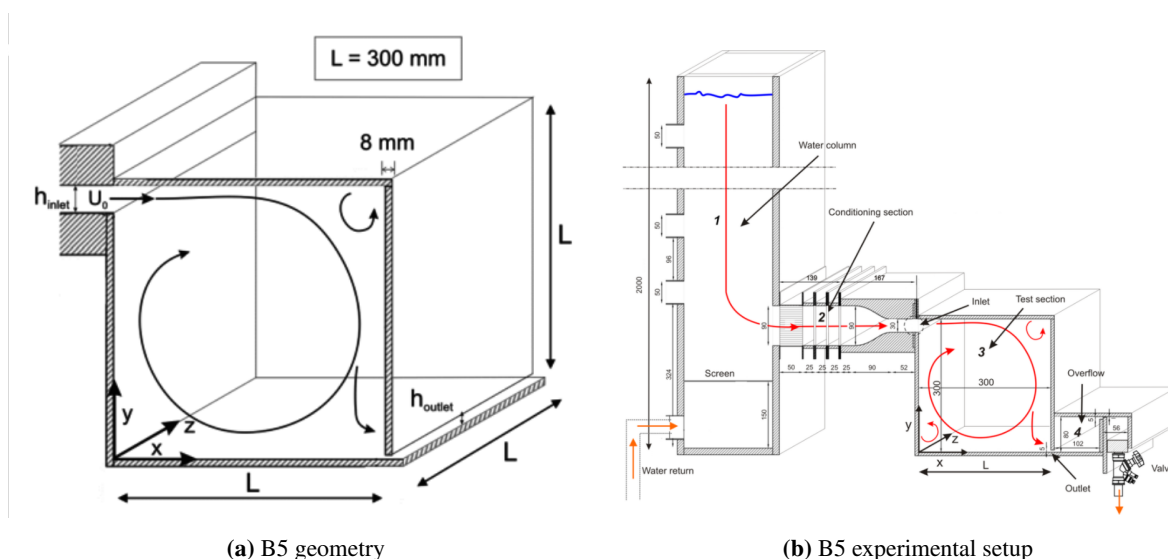
Figure 3.6: B5 geometry and experimental setup (figures from kbwiki.ercoftac.org [15]).

This benchmark has a cubical geometry, where H = L = W = 0.3 m in the experiment. The dimensions of the inlet and outlet are h/H = 0.1 and t/H = 0.0167, respectively. The values of l and b from the experimental setup are also reported, with l/H = 0.173 and b/H = 0.34. As can be seen from figure 3.6b there is a conditioning section upstream of the inlet with a contraction to accelerate the flow and reduce the velocity gradients and turbulent intensities [15]. Measurements were done at two different Reynolds numbers 1000 and 2500, representing transitional flow. It was checked that the flow was in fact transitional by injecting dye into the flow, where the flow was first laminar before vortical structures started to develop downstream. The flow is isothermal i.e. no buoyancy effects are present.

The measurements were done with a 2D PIV system, measuring the horizontal u and vertical w components of the velocity. The working fluid was water. Two sets of measurements were performed, one for the entire vertical cross section and one focusing on the inlet region, both in the midplane at z/H = 0.5. The uncertainty in the measurements was investigated using the central limit theorem and found to be around 2-4 % in the majority of the test section, but slightly higher in areas with locally higher turbulence levels [15].

The data files at the website contain time averaged values of the x-velocity at three vertical lines x/L = 0.2, x/L = 0.5 and x/L = 0.8 spanning the entire cross section. For the measurements done at the inlet region both time averaged values of the x-velocity and turbulent kinetic energy values are available at vertical lines x/L = 0.2 and x/L = 0.5.

3.1.6   Benchmark 6 – Impinging jet

The sixth benchmark presented in this thesis has a completely different geometrical configuration than the ones presented so far. This benchmark is an impinging jet. That is a jet that is oriented normal to a surface, collides with the surface and this then spread out across the surface as a wall jet. This can be used a ventilation strategy and a way to distribute the air throughout a confined space, but it is also of further interest because this enables a more detailed study of a jet colliding with a wall. The wall jets in the previously presented benchmarks do also to some extent collide with the opposite wall (except B1), and this is the hardest part of the flow to model for RANS turbulence models as it is an area of turbulent anisotropy ([28], [21]).

The impinging jet presented is the experimental work by Chen et al. [10]. The geometry of the benchmark is shown in figure 3.7. The jet impinges on to the floor and spread out. There are three rather large openings from the cavity, two along the sidewalls and at the left side of the wall opposing the inlet. The openings are so large the authors describe the cavity as semi-confined. The experiment is isothermal.
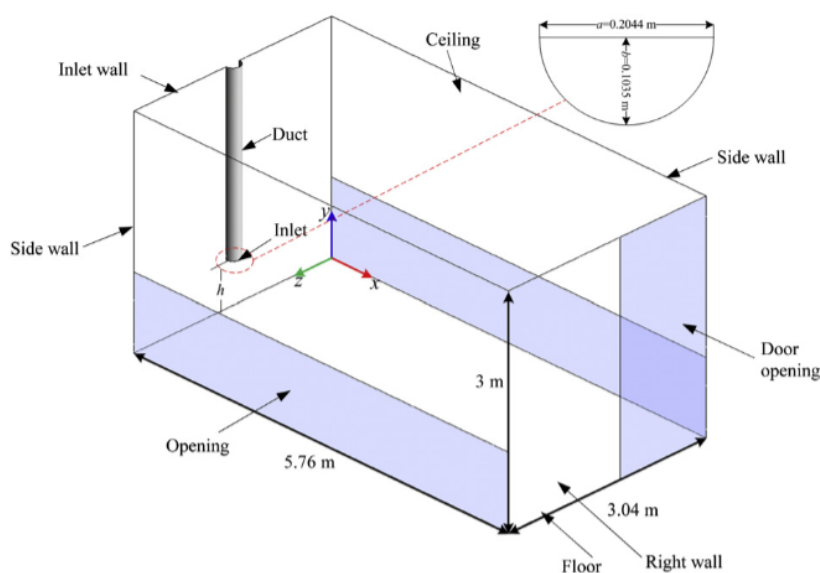
Figure 3.7: B6 geometry (figure from Chen et al. [10] p. 156).

The dimensions of the model are as follows: L = 5.76 m, H = 3 m, W = 3.04 m. The jet is discharged into the room from a 1.51 m long semi-elliptic pipe that ends 0.6 m above the floor. The height of the openings along the side is 1 m, while the third opening spans the full height and half width of the room, as seen in figure 3.7.

The experiments were carried out with hot wire anemometry and done in the midplane of the cavity. The measurements were performed at different horizontal lines z = 0.065 m, z = 0.125 m, z = 0.225 m, z = 0.545 m and different vertical lines x = 0.3 m, x = 0.5 m, x = 0.7 m, x = 1 m. The location of these lines relative to the inlet can be seen in figure 3.8. The accuracy of the velocity data were determined to be ± 5 % or ± 0.03 m/s, whichever is greatest. The air temperature was 20 °C at the time of measurements, with a difference of less than 1 °C between the inlet and outlet of the cavity.
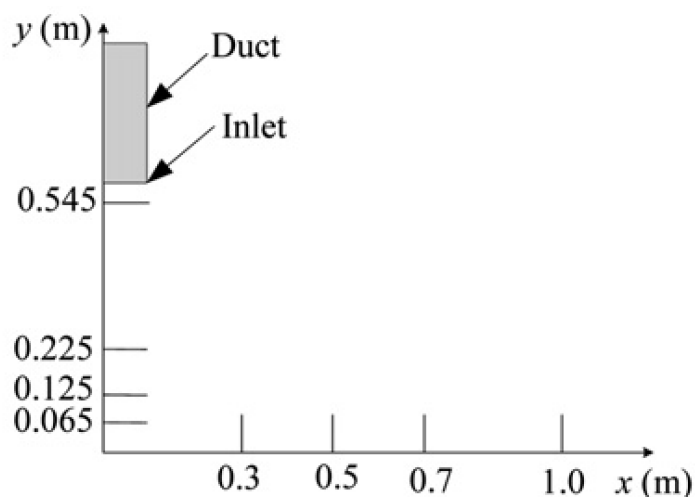
Figure 3.8: B6 measurement lines (figure from Chen et al. [10] page 158).

3.1.7 Benchmark 7 – Wall jet

The final benchmark presented in this thesis – Benchmark 7 – is simply a 2D wall jet. The idea behind including this benchmark is that the wall jet is the main flow element of all the other benchmarks, thus a CFD code unable to reproduce this flow will most likely fail to reproduce the other benchmark flows as well. It also gives an opportunity to say with more certainty what parts of the flow a turbulence model is unable to model correctly. If it is successful in simulating this benchmark, the "problematic" flow structures are most likely something else than the wall jet itself.

The experimental procedure and setup are described by Eriksson et al. [16]. Figure 3.9 shows the experimental setup. Water is used as the working fluid and two weirs are used to create a constant difference in height between the upstream and downstream free surfaces. This height difference was about 1.4 m, giving an inlet velocity of 1 m/s. The inlet slot height was 9.6 mm and thus the Reynolds number was approximately 9600 for water at room temperature. The tank itself was 7 meters long and 1.45 meters wide. There is a solid wall above the inlet, resembling the conditions in the other benchmarks. This does however cause some inevitable recirculation in the flow and creates some challenges in imposing the correct boundary conditions.
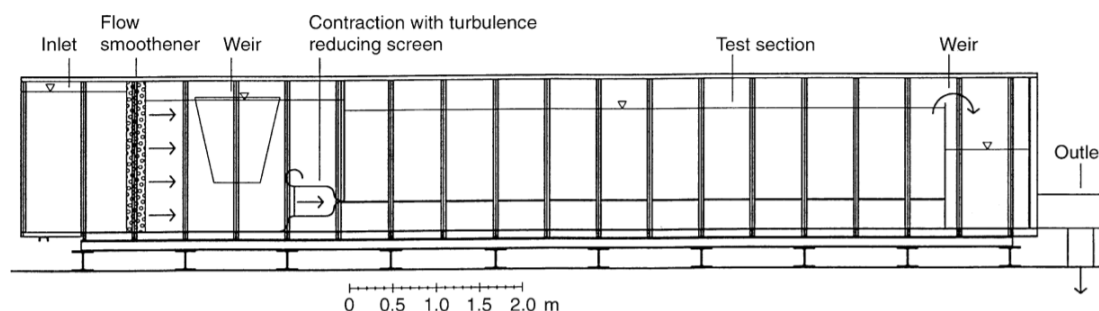
Figure 3.9: Experimental setup of Benchmark 7 (figure from Eriksson et al. [16] p. 51).

The measurements were done with LDV and the main measurement series were done in the middle of the tank. Measurements were done at several streamwise locations, x = 50, 100, 200, 400, 700, 1000,

1500, 2000 mm. The measurements were stopped at 2000 mm because after this the flow was losing its wall jet character. Momentum was conserved up until x/b = 150, after this the momentum in the jet was influenced by the return flow. Measurements were done of both the mean and fluctuating velocity. The inlet conditions were determined using pitot tube and LDV measurements and both mean velocity and turbulent intensity profiles are available.

3.2 CFD simulations of benchmark cases

This sections presents CFD simulations of the benchmarks from literature and accounts for the settings and models that were used in the best way possible. For some of the simulations the figure comparing simulations and experimental data is shown to make a comparison with the results from this thesis easier. These figures are copied into this master thesis. No figure presented in this section is created by the author of this master thesis, and the original paper for each figure is referenced in the figure caption.

3.2.1 Benchmark 1

Several simulations have been done on the geometry of benchmark 1 as this was the geometry used in the workshop study by Peng et al. [39]. However, the teams in the workshop were told to report back the reattachment length, but the reattachment length was not possible to determine in the experiment. Instead, the velocity was measured along a horizontal line at location z/H = 0.952 that spans from inlet to outlet. This makes a comparison between the results from the workshop and the experimental data a hard task, as no velocity profiles at all are available in the workshop paper [39]. However, Nielsen et al. [33] – the researchers behind the experiment – conducted some CFD simulations for comparison, found in the experiment report [33], using several different turbulence models. The comparison between their CFD simulations and the experimental data is shown in figure 3.10 and figure 3.11 for a Reynolds number of 500 and 4000, respectively. The figures are copied from Nielsen et al. [33].
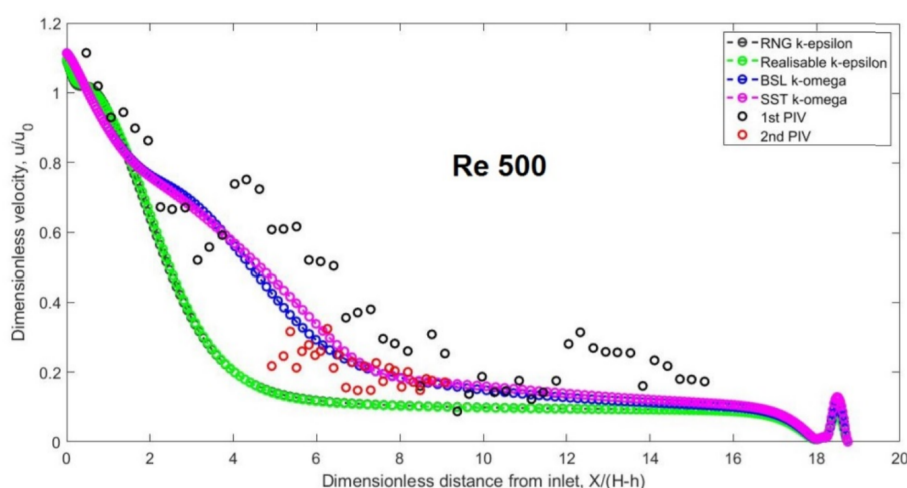
Figure 3.10: Comparison between CFD and experiment for benchmark 1 at Re=500. Velocity along a horizontal line at z/H = 0.952 (figure from Nielsen et al. [33] p. 9).
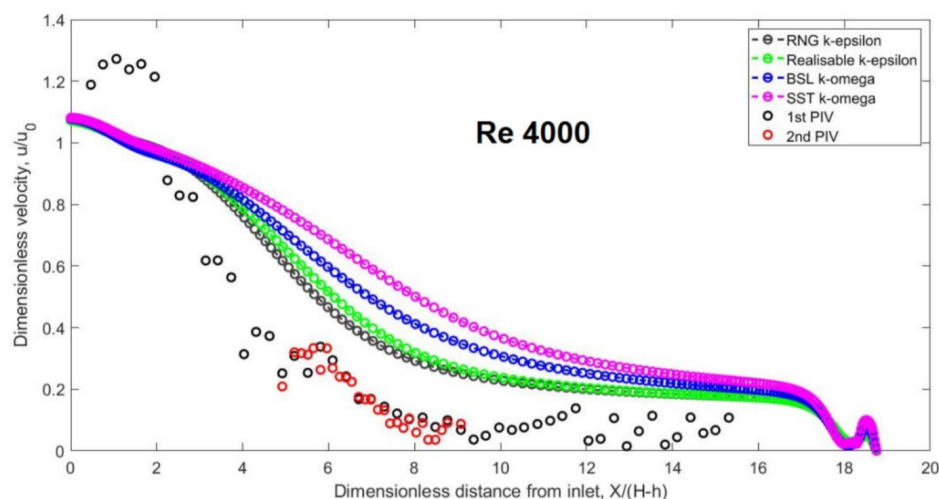
Figure 3.11: Comparison between CFD and experiment for benchmark 1 at
Re=4000. Velocity along a horizontal line at z/H = 0.952 (figure from Nielsen et al.
[33] p. 9).

As can be observed by the reader, the fit is rather good for the Re=500 case while a larger deviation can be seen for Re=4000. This is surprising as the believed transitional regime at Re = 500 should be more challenging for the RANS turbulence models. Four different turbulence models were used in the simulations: RNG k-ϵ, Realizable k-ϵ, BSL k-ω and SST k-ω. The k-ϵ models seem to perform better for Re=500 while the opposite is true for Re=4000. The authors [33] argue this implies that the k-ω models might be a better option for low turbulence flow and k-ϵ models better for fully turbulent. No comment is made on why the overall performance is better for Re = 500.

The settings used in the CFD simulations are slightly underreported in the report [33]. The solver is not mentioned, but is assumed to be ANSYS Fluent based on the use of "Enhanced wall treatment" that is an option in this solver. y^+ values are reported to be below 5 near the floor, while the other walls are unreported. Numerical schemes, boundary conditions, convergence criteria, mesh type and number of cells is not mentioned, making it impossible to reproduce the simulation. It is however reported that the same setup was used for all turbulence models, except the wall treatment which has different options for the k-ϵ and k-ω models.

3.2.2   Benchmark 2

Simulation by Dréau et al.
The simulation by Dréau et al. [14] was done in 2013 using Star CCM+ and good agreement between experiments and simulations were obtained for some turbulence models. They tested six different turbulence models: Standard k-ϵ, standard k-ϵ Low Re, AKN k-ϵ Low Re, realizable k-ϵ, standard k-ω and SST k-ω. It is a bit unclear exactly which model the standard low-Re k-ϵ model is, this probably refers to which one is standard in the Star CCM+ software. The AKN low-Re k-ϵ model is the one developed by Abe et al. [2]. They also tested three different meshes, one coarse and structured with 4100 cells, and two different unstructured meshes with 4800 and 16700 cells. For the k-ϵ models the fine unstructured mesh is used, while for the k-ω models the authors use the course unstructured mesh – this can affect the comparison between the two model families. All simulations were done in 2D, and steady state was assumed.

The wall functions used are reported as "High y^+ wall treatment" for the k-ϵ and realizable k-ϵ, for the remaining models it is reported a use of "All y^+ wall treatment", however no values for y^+ are reported for any of the simulations, thus one can only assume the use of wall functions is correct. Use of numerical schemes is also unreported. The turbulent intensity is set to 4% at the inlet and the turbulent dissipation rate ϵ is calculated based on this and a length scale $\ell = h/10$.

Convergence for the different grids are reported as plots of the residuals and stable, but oscillatory, values around 10^{-6} are reached for all parameters. The best agreement with experiments was obtained with the k-ϵ models, in particular the standard k-ϵ and AKN low-Re k-ϵ. The k-ω models and the realizable k-ϵ gives a poorer fit with experiments, in particular close to the floor.

Simulation by Ito et al.

Another simulation was performed by Ito et al. in 2015 [25] and they used ANSYS Fluent to test four different turbulence models: standard k-ϵ, k-ϵ low Re, standard k-ω and SST k-ω. Several structured meshes were used, in 2D one with 4208 cells was used for the standard k-ϵ model and one with 70 296 cells was used by all the other models. 3D meshes were also created, with 126 240 and 4 428 648 cells for the course and fine version, respectively.

A summary of the settings used for these simulations can be found in figure 3.12. The QUICK scheme was used for the advection terms which have third order accuracy. For some reason, the turbulent intensity was set to 10% rather than 4% which was measured in the experiment. This can be seen in the table from the calculation of turbulent kinetic energy, however, it could just be a typo.

Geometry	H=3.0 m, L=9.0 m, W=3.0 m, h=0.168 m, t=0.48 m
Inflow Condition of Experiment	U_{in} =0.455 m/s and TI= 4 %, (Corresponds to Re=$U_{in}h/\nu$=5000)
Mesh	Structured grid
Algorithm	SIMPLE
Scheme	QUICK for advection term
Inflow boundary	U_{in} =0.455 m/s, k_{in}=3/2× $(U_{in}×0.1)^2$, ε_{in} =$C_\mu^{3/4}$×$k_{in}^{3/2}/l_{in}$, C_μ=0.09, l_{in} =(1/10)h
Outflow boundary	U_{out} = free slip, k_{out}= free slip, ε_{out} = free slip
Wall treatment	Wall function (Generalized log law) for Standard k–ε fine near wall mesh for Low Re k–ε

Figure 3.12: The settings used in the experiment by Ito et al. (figure from Ito et al [25] p. 10).

For the 2D simulations there was good agreement between simulations and experiments for the k-ϵ models, while the k-ω models had the same unsteady trend for the velocity along the floor, similar to what was observed in the simulations by Dréau et al. [14]. Results are shown in figure 3.13.

(a) z = H - h/2   **(b)** z = h/2
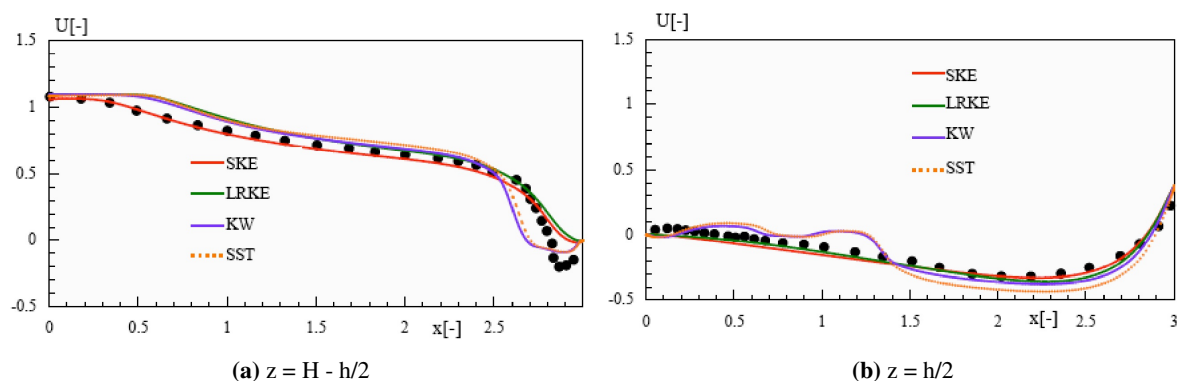
Figure 3.13: Results for four different turbulence models by Ito et al. in 2D.
Standard k-ϵ (SKE), Low Re k-ϵ (LRKE), standard k-ω (KW) and SST k-ω (SST)
(figure from Ito et al. [25] p. 11).

However, when three of the models were used in a 3D simulation – values were taken at the mid-plane y = W/2 – the performance of the SST k-ω model changed considerably, while the k-ϵ models gave the same result as for the 2D simulation. In the 3D simulation there is less difference between the turbulence models, and this shows that the impact of changing from 2D to 3D depends on the chosen turbulence model. Results are shown in figure 3.14.

(a) z = H - h/2   **(b)** z = h/2
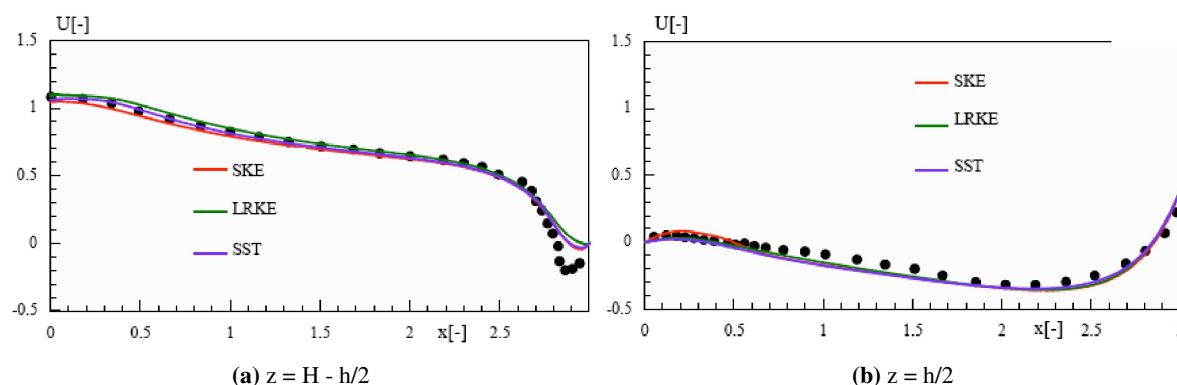
Figure 3.14: Results for three different turbulence models by Ito et al. in 3D.
Standard k-ϵ (SKE), Low Re k-ϵ (LRKE) and SST k-ω (SST) (figure from Ito et al.
[25] p. 12).

Simulations by Olmedo and Nielsen

More simulations done on Benchmark 2 were done in 2010 by Olmedo and Nielsen [38] who investigated the different results obtained by simulating in 2D, 3D and 3D transient. At the time, some recent works by Susin et al. [42] had suggested the results varied from 2D to 3D, although the case was originally designed to be 2D.

Using Fluent 6.0 the standard k-ϵ model were used to simulate the flow. One 2D mesh and one 3D mesh were created. The 2D mesh had 3586 elements, while the 3D mesh consisted of 60 divisions of this mesh in the plane normal direction resulting in a 3D mesh of 215 160 cells. Further details about the simulations are not provided in the report [38].

The authors conclude that the results obtained from a 2D, 3D and 3D transient simulation are very similar, indicating that the flow is indeed 2D and that there are no transient effects in the flow.

Simulations by Rong and Nielsen

In 2008 Rong and Nielsen [41] used ANSYS CFX 11.0 to look at the impact of different turbulence models on the Annex 20 test room. Simulations were done in 2D. They used the standard k-ϵ model, standard k-ω, BSL k-ω and SST k-ω. Not many details about the settings used in the simulations are available, but a grid independence study is performed for each model with three mesh sizes ranging from 4736 to 28800. For all the models the results with the different meshes were quite similar.

The streamline patterns obtained with the four different turbulence models were compared, in additions to comparing each result with the experimental data. The four different streamline patterns are showed in figure 3.15.

(a) Standard k-ϵ

(b) Standard k-ω

(c) BSL k-ω

(d) SST k-ω
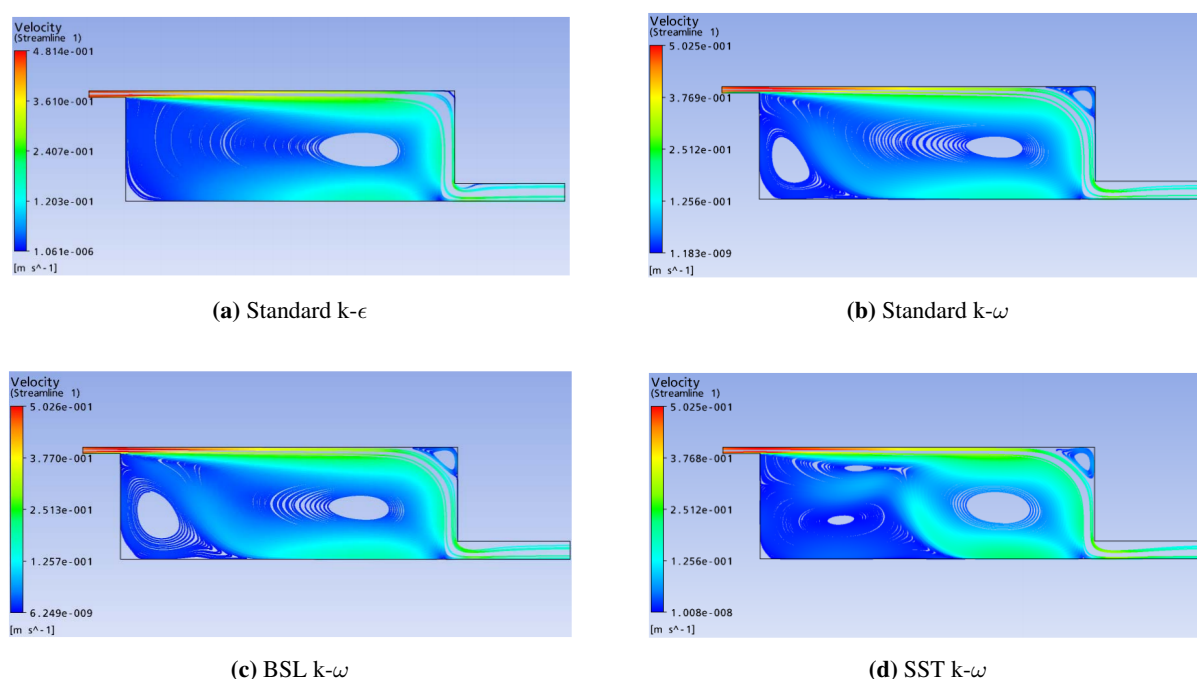
Figure 3.15: Streamlines obtained by using four different turbulence models on B2.
Simulations by Rong and Nielsen (figure from Rong and Nielsen [41] p. 5-6).

It can be observed from figure 3.15 that the streamlines obtained with the standard and BSL k-ω models are very similar. With the standard k-ϵ model the separation point from the floor when the floor jet turns upward occurs later, resulting in a much smaller recirculation zone in the lower left corner. With the SST k-ω model the entire flow field is different, with an additional recirculation zone appearing in the left part of the cavity.

Comparing the velocities from the simulations it is concluded by the authors that the standard k-ϵ, standard k-ω and BSL k-ω model all give satisfying results for the velocity profiles along the vertical lines at x=H and x=2H. However, for the horizontal line along the floor the standard k-ϵ model shows the best compliance with experiments. It is also concluded the SST k-ω model gives the largest deviations from the experimental values.

Simulation by Taghinia et al.

LES simulations of Benchmark 2 have been done by Taghinia et al. [43] in 2016. Two LES models

were tested the fairly common Dynamic Smagorinsky Model (DSM) and the Rahman-Agarwal-Siikonen-Taghinia (RAST) model, at the time recently developed by the authors. The motivation behind the study was to assess both these models performance for simulations of the indoor environment, and to compare the newly developed RAST model with the more tested DSM model.

(a) Vertical line: x = H

(b) Vertical line: x = 2H

(c) Horizontal line: z = h/2

(d) Horizontal line: z = H - h/2
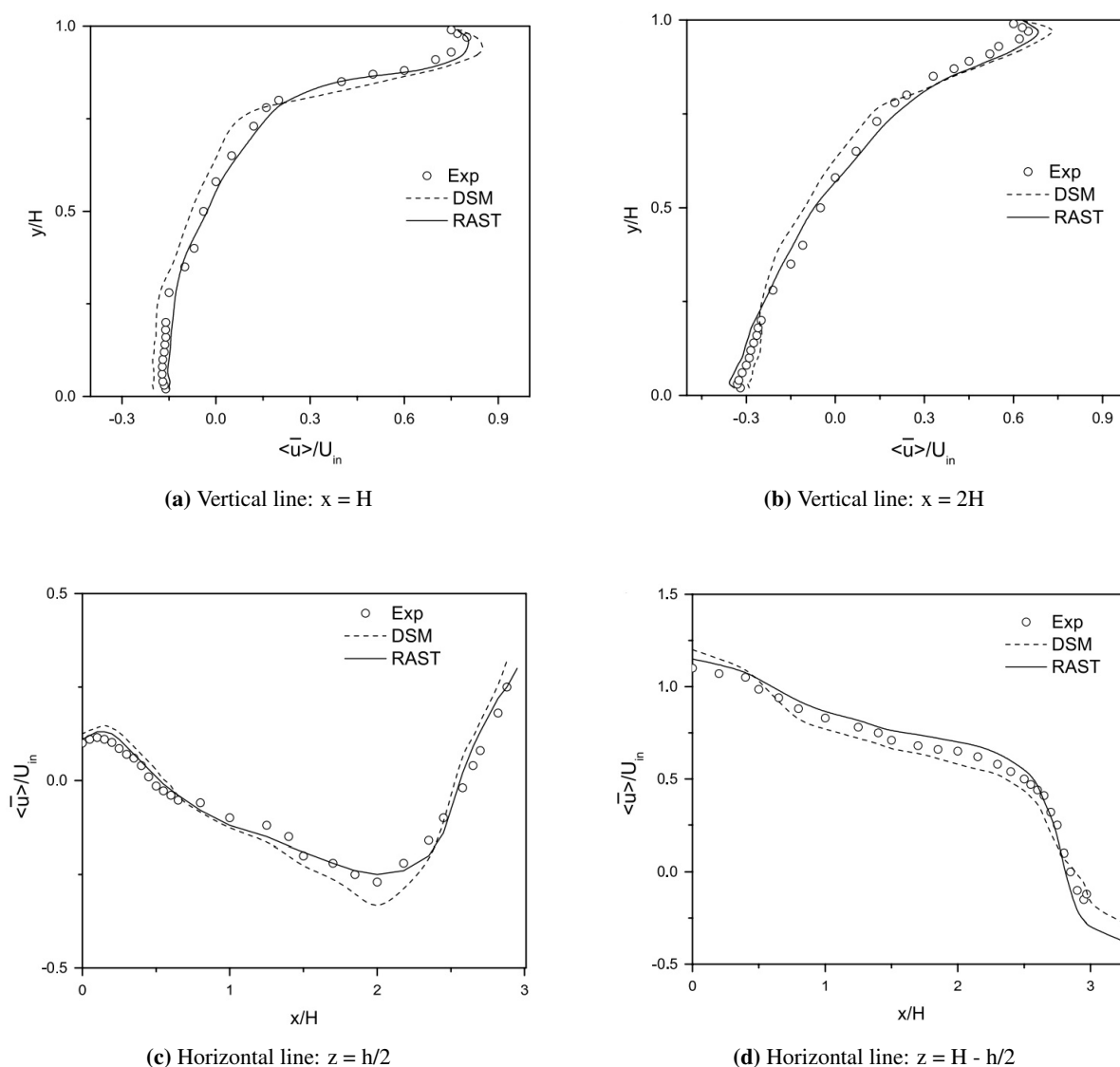
Figure 3.16: Comparison between experiments and LES simulation by Taghinia et al for B2.(figure from Taghinia et al. [43] p. 2785).

This paper bu Taghinia et al. [43] have done simulations of both B2, B4 and B6 and used the following setup for all Benchmarks. PV coupling was done with the SIMPLE algorithm. A modified Rhie-Chow interpolation is used for pressure gradients, second order upwind flux-difference splitting scheme is used for the convective terms and a central difference scheme for the diffusion terms. Crank-Nicholson second order scheme is used for time integration. y^+ values have been kept below 1 to properly resolve the viscous sublayer. For the inlet condition a separate LES simulation was performed in a rectangular channel of length 12h, with a grid identical to that of the inlet duct in the benchmark. The inlet condition was then set as the outflow of this simulation. The CFL condition was kept in the range 0.1-0.6 to enhance stability on the simulations. Flow statistics are obtained by

averaging over 800-1000 dimensionless time steps. To save CPU time the flow field was initialized from a RANS k-ϵ simulation, and then the LES simulations were started afterwards beginning from this result.

For B2 a mesh with 5 million cells was used, after this proved to give very similar results as a grid with 7 million cells. Overall the both LES models give very satisfying results, comparison with experiments for mean velocity is shown in figure 3.16. The LES simulations also show good agreement with the measured turbulent kinetic energy.

It can be observed from figure 3.16 that there is little difference between the two models, however, the authors conclude that the RAST model gives slightly better results than the DSM model. In particular, the DSM model overpredicts the jet velocity, which they claim is due to an underprediction of the sub-grid scale viscosity close to the top wall.

3.2.3   Benchmark 3

Simulations were done by Limane et al. [31] in 2014, using the experimental data from benchmark 3 to validate the simulation. OpenFOAM was used along with several turbulence models. A 3D, structured mesh was used with 415 104 cells. The mesh had a zero length of the inlet section, so the velocity profile flowing into the cavity is uniform.

Limane et al. [31] tested different solvers in OpenFOAM for this flow, with different combinations of transient vs steady state and Boussinesq approximation vs ideal gas law for buoyancy, resulting in four possible combinations. Which solver was used is shown in the legend in figure 3.17, BBPF is "buoyantBuossineqPimpleFoam", BBSF is "buoyantBuossineqSimpleFoam", BPF is "buoyantPimpleFoam" and BSF is "buoyantSimpleFoam".

As for many other papers the settings used in the simulation is slightly underreported, making it hard to reproduce the exact same simulation. There is no mentioning of the choice of neither numerical schemes nor wall treatment. However, the boundary conditions are reasonably well documented. A turbulent intensity of 5% is used with an inlet velocity of 15.2 m/s. All the walls are modelled as adiabatic except for the floor where a uniform heat flux of 563 W/m^2 is imposed. This heat flux is calculated from an Archimedes number of $1.8 * 10^{-6}$ which was one of many used by Nielsen. The air inlet temperature is 295.15 K.

The y^+ values are reported to be below 11.225 which is the point where the line for the log-law and linear law crosses in the buffer layer. For the transient simulation, the courant number was kept below 1. The convergence criteria used was constant residuals with values less than 10^{-6}.

In general Limane et al. [31] obtained good results that matched the experimental data. Results for the standard k-ϵ and SST k-ω model is shown in figure 3.17 where a comparison with the temperature measured in the experiment is made. The most difficult part seems to be the left side of the room, where, in particular, the k-ω model fails to predict the first temperature node at z=0.

(a) Standard k-ε: z = 0.25H, y = 0.67W

(b) Standard k-ε: z = 0, y = 0.67W

(c) SST k-ω: z = 0.25H, y = 0.67W

(d) SST k-ω: z = 0, y = 0.67W
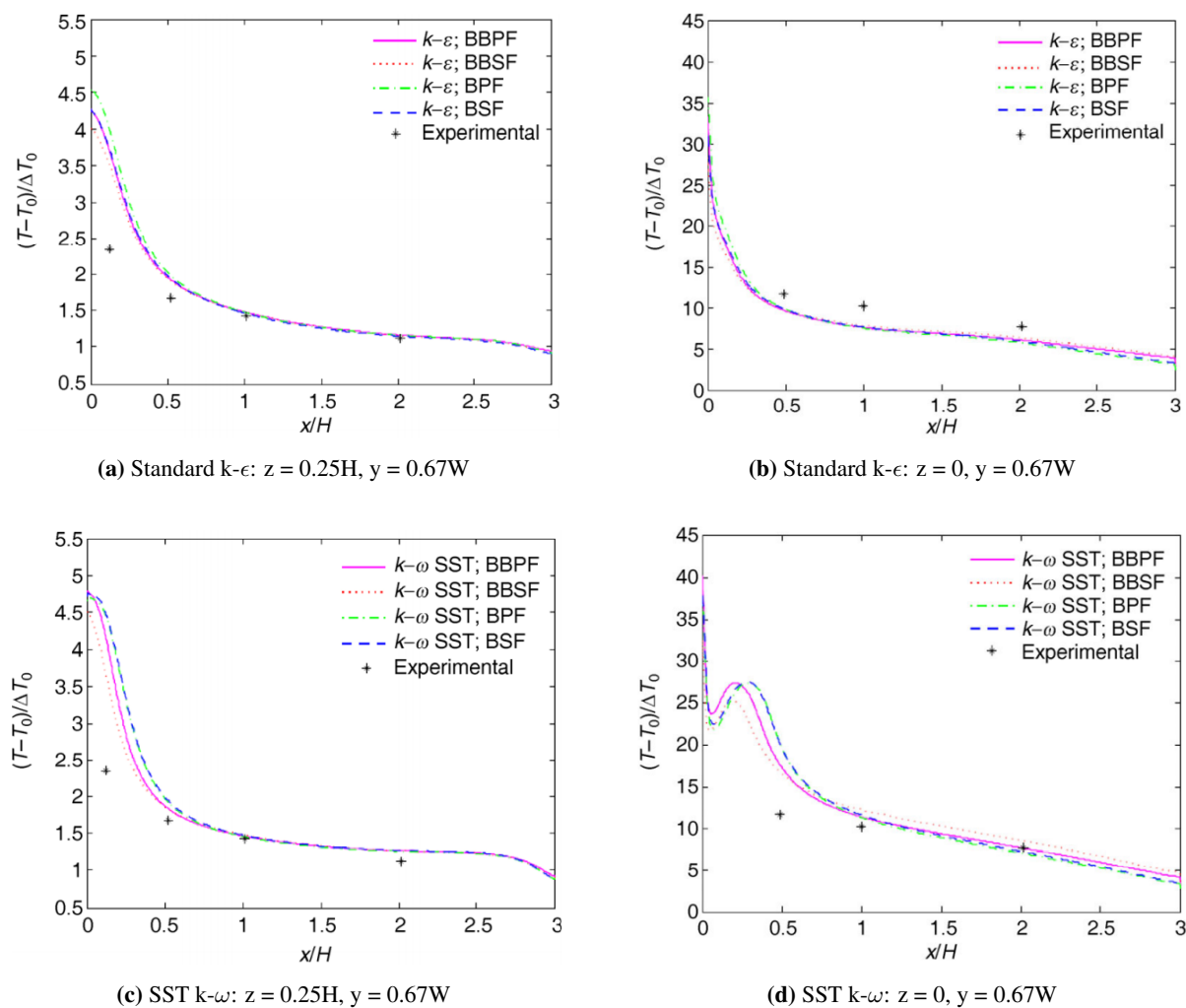
Figure 3.17: Temperature results from Limane et al. for the k-ε model and SST k-ω model for Benchmark 3. Four different solvers in OpenFOAM are used for each turbulence model (figures from Limane et al. [31] p. 5).

Limane et al. [31] also made comparisons with the velocity, however, the experimental data is for an isothermal case with the same Reynolds number. Nielsen [34] claimed that the velocity profile is the same for the isothermal and non-isothermal case due to the low Archimedes number, and the results from Limane et al. [31] seems to verify this. The velocity comparison is shown in figure 3.18. Both of the models give good agreement with the experimental data at x = 2H.

(a) k-ϵ: x = 2H, y = W/2   (b) SST k-ω: x = 2H, y = W/2
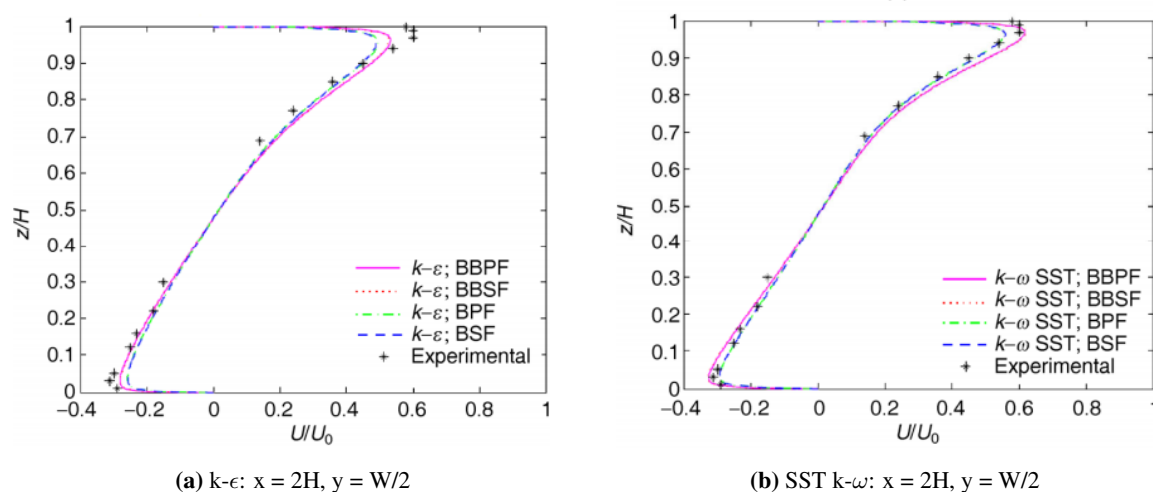
Figure 3.18: Velocity comparison with standard k-ϵ and SST k-ω model for Limane et al. Experimental data are from an isothermal experiment (figures from Limane et al. [31] p. 4).

3.2.4   Benchmark 4

Simulations by Kosutova et al.

Kosutova et al. [29] used benchmark 4 to validate their CFD simulation. A sensitivity study of different computational and physical parameters were undertaken, assessing each parameters impact on the result. Second order discretization schemes were used – exactly which is not mentioned – and the Boussinesq approximation was used for buoyancy. The simulation was done in 3D. The mesh was fully structured with 25 704 cells, and refined near the walls to keep y^+ below 5 to resolve the boundary layer. The authors argue this is important as the largest resistance to convective heat transfer is found in the viscous sub layer. No inlet section length is considered, so the inlet velocity profile is uniform when flowing into the cavity.

Boundary conditions were set as equal to the experiment as possible, setting the two side walls adiabatic, the floor to $35.5°C$ and the remaining walls to $15\,°C$. The inlet velocity was 0.57 m/s making the Reynolds number 684. The Froude and Richardson number is reported, with values Fr = 5.31 and Ri = 0.038 indicating limited buoyancy effects according to the authors. A turbulent intensity of 6% and the hydraulic diameter of the inlet was used to calculate the turbulent inlet properties. Near wall treatment is reported as low Reynolds number modelling (LRNM).

The comparison between simulation and experimental data is shown in figure 3.19. The simulation uses the RNG k-ϵ model which was used in the reference setup, but other turbulence models were also tested and results from these can be found in the report. The match is overall quite good, however, the temperature is slightly underpredicted both for the horizontal and vertical lines. Furthermore, the horizontal velocity is slightly underpredicted close to the floor and this could be an explanation for the low temperature as this limits the convective heat transfer along the floor.

(a) Velocity profile: z = H/2, y = W/2

(b) Velocity profile: x = L/2, y = W/2

(c) Temperature profile: z = H/2, y = W/2

(d) Temperature profile: x = L/2, y = W/2
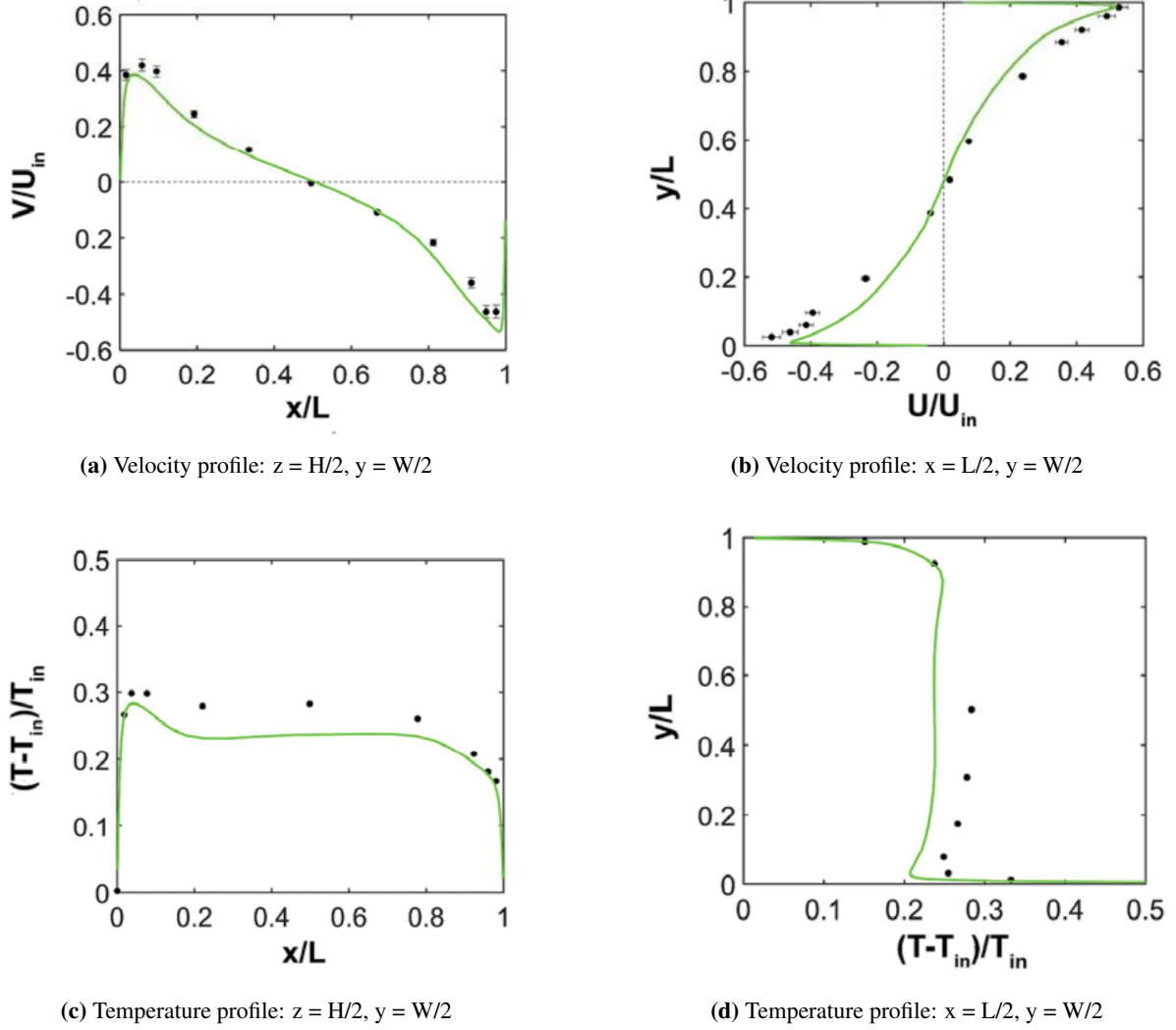
Figure 3.19: Comparison at vertical and horizontal centerlines, between experimental data and simulations with the RNG k-ϵ model done by Kosutova et al. (figures from Kosutova et al. [29] p. 351).

Kosutova et al. [29] also did a quantitative comparison of the simulation and experiment, calculating the fraction of data within a factor of 1.25 (FAC 1.25) for velocity and 1.05 (FAC 1.05) for temperature. Equation (3.2) and (3.3) shows the formulas used for calculating FAC 1.25 and FAC 1.05, respectively.

$$FAC1.25 = \frac{1}{N}\sum_{i=1}^{N} n_i \quad \text{with } n_i = \begin{cases} 1, & \text{if } 0.75 \leq \frac{P_i}{O_i} \leq 1.25 \\ 0, & \text{otherwise} \end{cases} \tag{3.2}$$

$$FAC1.05 = \frac{1}{N}\sum_{i=1}^{N} n_i \quad \text{with } n_i = \begin{cases} 1, & \text{if } 0.95 \leq \frac{P_i}{O_i} \leq 1.05 \\ 0, & \text{otherwise} \end{cases} \tag{3.3}$$

Kosutova et al. also calculated the fractional bias (FB) for the temperature, but say this is not suitable for parameters with both positive and negative values, e.g. velocity. Equation (3.4) shows the formula

$$FB = \frac{\bar{O} - \bar{P}}{0.5(\bar{O} + \bar{P})} \tag{3.4}$$

In all three equations P_i is the computed value from the CFD simulation and O_i is the measured value from the experiments. Figure 3.20 shows the values of FAC 1.25, FAC 1.05 and FB for velocity and temperature. Figure is copied from Kosutova et al. [29].

	Velocity		Temperature			
	FAC 1.25		**FAC 1.05**		**FB**	
	V/U$_{in}$	U/U$_{in}$	horizontal	vertical	horizontal	vertical
Aim	1		1		0	
Range	> 0.5		> 0.5		(-0.3;0.3)	
RNG k-ε	0.91	0.69	1	0.89	0.02	0.03

Figure 3.20: Values of FAC 1.25, FAC 1.05 and FB for velocity and temperature using the RNG k-ε model (figure from Kosutova et al. [29] p. 352).

The values in the figure confirms the good agreement between simulations and experiment according to the authors. Specially the values for temperature are very good, while the velocities show slightly lower values, in particular the horizontal component.

Simulations by Blay et al.

In the report describing the experiment [5], Blay et al. also present some results from CFD simulations of the same flow. Two Low-Re k-ε models were tested. The Jones and Launder model [26] and the Lam and Bremhorst model, later modified by Davidson [11]. The simulations were done in 2D on a mesh with 52x52 cells, this was chosen after a grid sensitivity analysis testing meshes up to 120x120 cells. The cell sizes were non-uniform, i.e. the mesh was refined near the walls. Other settings related to the simulations are unreported.

The results vary significantly between the two turbulence models. Using the Jones and Launder model the obtained flow field rotates counter clockwise, instead of clockwise as in the experiment. The reason according to the authors is that this model overestimates the heat transfer at the bottom wall, thus overpredicting the buoyancy effects in the flow.

The results with the Lam and Bremhorst model show much better agreement with the experiments. Plotting the simulation results against the experimental data, this model seems fairly capable of predicting both the velocity field, the temperature field and the correct value for k in this flow. The wall heat transfer with this model was 2.3 times less than for the Jones and Launder model. This result also shows that good results can be obtained for Benchmark 4 by simulating in 2D.

Simulations by Taghinia et al.

In the same paper that presents LES simulations of B2, Taghinia et al. also present LES simulations of B4. The same DSM and RAST models are used and the general settings such as numerical schemes are similar and described in section 3.2.2.

A mesh with 3.0 million cells is used as this gave very similar results to a mesh with 4.3 million cells in a grid sensitivity analysis. A uniform velocity profile of 0.57 m/s is imposed at the inlet. Both the velocity and temperature profiles are in very good agreement with the experimental data. The results are shown in figure 3.21.

(a) Velocity profile: z = H/2, y = W/2

(b) Velocity profile: x = L/2, y = W/2

(c) Temperature profile: z = H/2, y = W/2

(d) Temperature profile: x = L/2, y = W/2
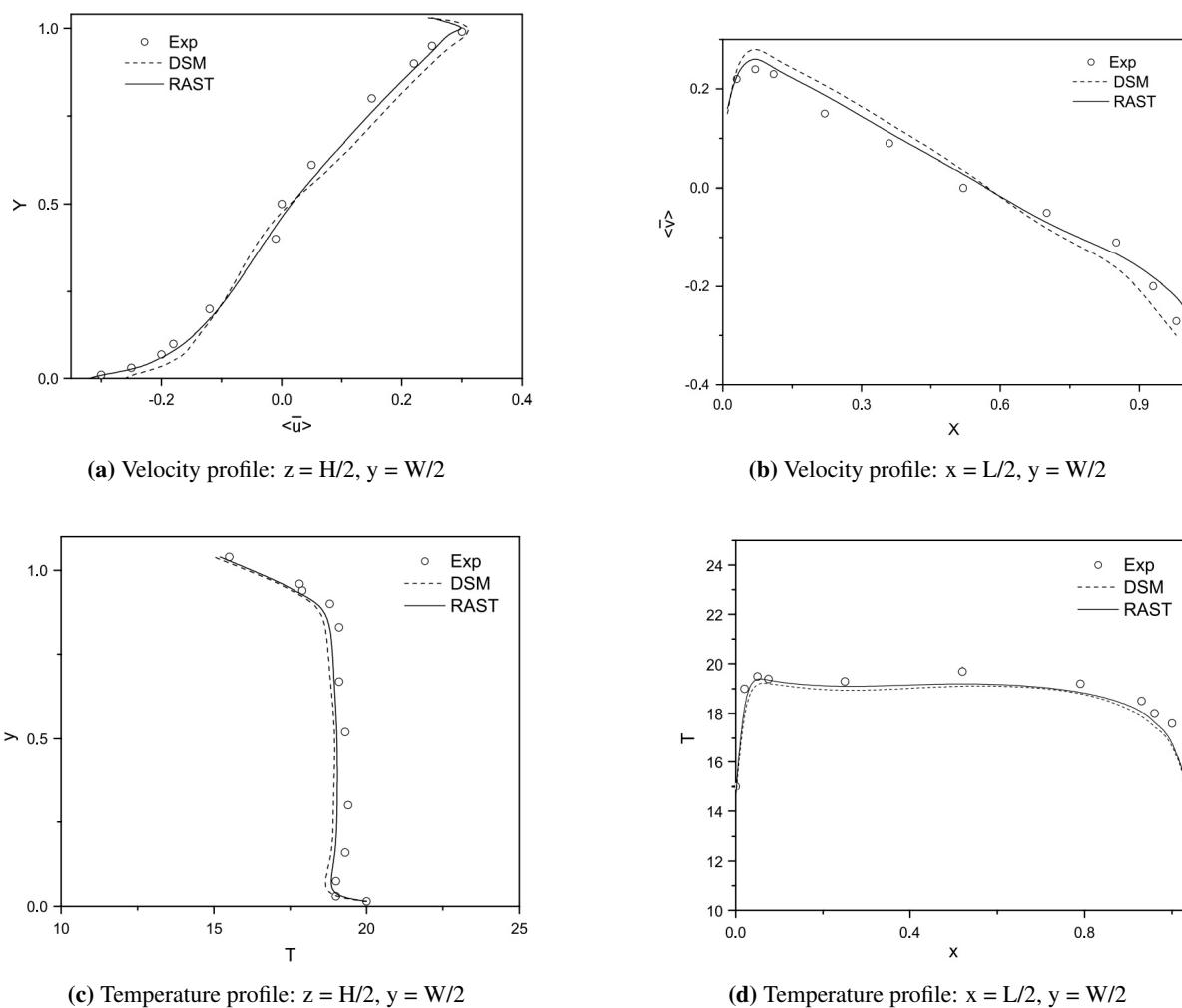
Figure 3.21: Comparison between experiments and LES simulation by Taghinia et al. for B4 (figure from Taghinia et al. [43] p. 2787).

Also for Benchmark 4 the authors conclude the RAST model shows slightly better performance than the DSM model. However, both models give better results than the RANS simulations by other researchers, in particular for temperature.

3.2.5 Benchmark 5

Several simulations have been done on Benchmark 5. This benchmark is particularly interesting since it has a transitional flow regime. Most RANS turbulence models are developed for the fully turbulent regime, so this benchmark can be used to check what turbulence models are most capable of modelling transitional flow.

Simulations by van Hooff et al. 2012

CFD simulations done by van Hooff et al. [21] in 2012 focused on the suitability of RANS turbulence models to model this transitional flow. Four different turbulence models were tested: the RNG k-ϵ model, the low-Reynolds k-ϵ by Chang et al. [9], the SST k-ω model and the low-Re stress-ω RSM model by Menter. The simulations were done in Fluent 6.3.26. Second order discretization schemes were used, SIMPLEC is used as the pressure-velocity coupling algorithm. Oscillatory convergence was present for the majority of the simulations, in which the result was averaged over a large number of

iterations as discussed by Ramponi and Blocken [40] and Blocken [6]. The simulations were done in 3D, as initial 2D simulations deviated significantly from those in 3D, implying that the flow is three dimensional. Simulations were done both for Re = 1000 and Re = 2500. A grid sensitivity analysis was performed and a structured mesh with 3.4 million cells proved to give nearly grid independent results. This mesh resulted in $y^* < 1$ for all surfaces.

The comparison between the simulations and experimental data are shown in figure 3.22 for Re = 1000. The best results are obtained with the low-Re k-ϵ model. This model was developed for recirculating flows in pipe expansions and uses damping functions to have more accurate modelling of the near wall flow. The RNG k-ϵ model showed the worst performance of the four models, deviating significantly from the experimental values measured by the PIV system. This is an interesting result as the RNG k-ϵ model is a popular model for simulating indoor airflows, and has been proven several times to give good results for fully turbulent flow. These simulations show, however, that if the flow is transitional in significant parts of the flow domain, the RNG k-ϵ model should be used with caution.

The SST k-ω model and the RSM model also showed decent performance for this flow. However, when visualizing the entire flow field, as can be done with PIV, in particular the RSM model failed to predict the center of the recirculation zone. The turbulence model performance was fairly similar for the simulation with Re = 2500.

(a) x = 0.2L   (b) x = 0.5L   (c) x = 0.8L
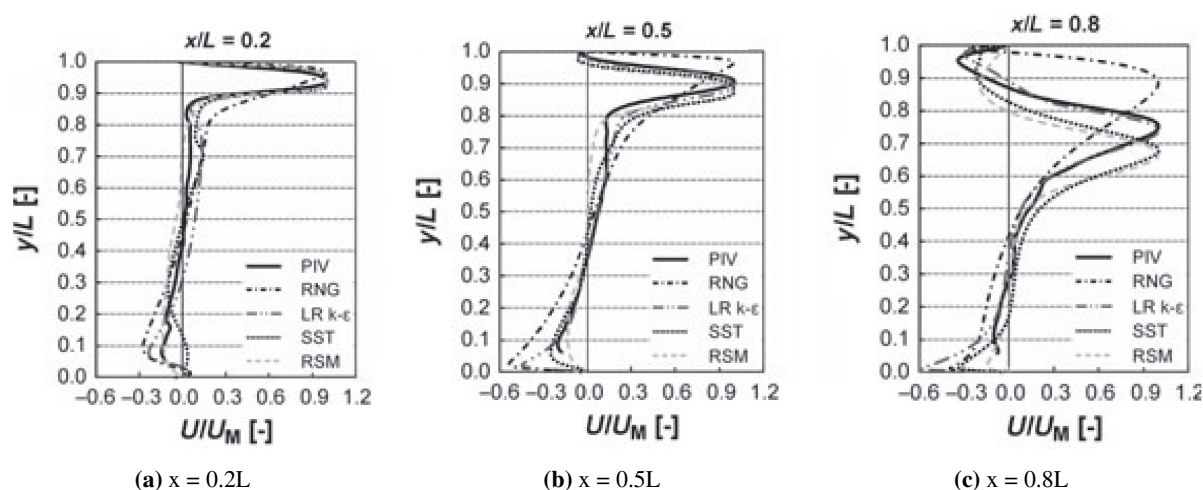
Figure 3.22: Simulations of B5 by van Hoff et al. Comparison of four different turbulence models – RNG k-ϵ, low-Reynolds k-ϵ, SST k-ω and RSM – with experimental data (figure from van Hooff et al. [21] p. 242).

The authors also did comparisons of the values for turbulent kinetic energy. Again the RNG k-ϵ model showed the largest deviation from the experiment, significantly overpredicting the value of k in the wall jet region. The authors conclude this overprediction results in a delayed separation of the wall jet due to the adverse pressure gradient.

Finally, the authors calculated the air change efficiency obtained with the different models. The largest difference between the models was as much as 44%, indicating that the differences in the predicted flow pattern have a big impact on this parameter. The simulations show, however, that although the flow is transitional, two of the two-equation RANS models – SST k-ω and low-Re k-ϵ – are able to give quite accurate results.

Simulations by van Hooff et al. 2017

Another simulation by van Hooff et al. was done in 2017 [23], this time focusing on the impact of physical and numerical diffusion. As presented in the theory section, numerical diffusion is an artificial viscosity that can become too high when using first order upwind schemes, or if the grid is too coarse. Physical diffusion consists of viscous and turbulent diffusion, and its impact is here assessed by varying the turbulent intensity at the inlet.

The simulations were again done in ANSYS Fluent with Re = 2500. The low-Reynolds k-ϵ model by Chang et al. [9] were used due to its success in the previous study [21]. Five different meshes were created to assess the impact of numerical diffusion, ranging from 84 thousand cells to 5.3 million cells. Furthermore, three different discretization schemes were tested: first order upwind, second order upwind and QUICK for the convection terms. PV coupling was done by the SIMPLEC algorithm. Five different values for the turbulent intensity were tested: 1%, 10%, 21%, 50% and 100%, in order to assess the impact of physical diffusion.

The results showed that numerical diffusion both from the use of first order upwind schemes and a coarse grid gave erroneous results. However, the difference between using first order upwind schemes and second order upwind schemes on the coarse grid were comparable to the difference between using second order upwind schemes on the coarse grid and a grid with 22 times more cells. From this result, the authors conclude the use of first order upwind schemes must be avoided at all cost. Based on a grid sensitivity analysis where a Grid Convergence Index (GCI) was calculated, the second finest grid with 1.9 million cells gave satisfying grid independence when second order schemes were used.

The effect on the velocity field of excessive turbulence intensity was very similar to that of excessive numerical diffusion, as both resulted in decreased velocity gradients and delayed detachment on the jet. The reference case with T_i = 21% proved to be the most accurate while in particular the simulations with 50% and 100% showed large deviations from the experimental values. This study therefore shows that it is important to choose a correct value for T_i. As other studies on Benchmark 2 – e.g. Joubert et al. [27] and the project work preceding this thesis – have concluded that the results are fairly independent of the inlet value of T_i, this seems to be case dependent.

The authors also looked at the effect of numerical and physical diffusion on contaminant transport. Here two opposite effects were observed. Increased numerical diffusion reduced the velocity gradients, thus reducing the production of turbulent kinetic energy again reducing the turbulent mass flux. While an increase in T_i increases the production of k and thus increase the turbulent mass flux.

Simulations by Cao and Meyers

Cao and Meyers [8] did simulations on benchmark 5 in 2013, looking at the effect of the turbulent boundary conditions at the inlet. The same conclusion was reached as in the simulation by van Hooff et al. [23], that the value of the turbulent intensity has a significant impact on the flow field for this benchmark. Cao et al. also looked at the impact of the turbulent length scale imposed at the inlet. This parameter had little impact on the flow field, but changed the concentration of indoor pollutants by a factor of 2 when this was included in the simulations.

The simulations were done in ANSYS Fluent, using the low-Reynolds k-ϵ model by Chang et al. and the k-ω SST model. A mesh with 1.25 millions cells was used after performing a "grid refinement

study". Two different types of geometries were used, one with and one without the contraction upstream of the inlet. This had little impact on the velocity field, however some differences were seen in the value of turbulent intensity which could affect pollutant dispersion.

The SIMPLE algorithm was used for pressure-velocity coupling, second order upwind schemes were used for the convective terms and the convergence criteria was residuals below 10^{-5}. The turbulent length scales tested were 10^{-2}, 10^{-4} and 10^{-3}, corresponding to the values obtained from using 7% of the hydraulic diameter, the length of the mesh opening sections in the upstream screens and a value in between, respectively. The turbulent intensities at the inlet ranged from 5% to 30% with a 5% interval.

Simulations by van Hooff et al. 2014

The simulations by van Hooff et al. [24] from 2014 focused on the validity of the standard gradient-diffusion hypothesis used in RANS turbulence models. More precisely, the pollutant dispersion of simulations using LES and RANS were compared to see if there were deviations between the calculated pollutant concentrations. The LES simulation showed there were counter-gradient mechanisms present inside the enclosure, thus the standard gradient-diffusion hypothesis is not valid in the entire enclosure. However, convective mass flux was one order of magnitude larger than the turbulent mass flux, thus results were fairly similar. The result indicates that for the case of benchmark 5 it is most important to obtain the correct mean flow pattern to accurately model the pollutant dispersion. Comparisons between the mean velocity profiles for the LES, RANS and PIV measurements are also presented in the report, and the LES simulations have very good compliance with the PIV measurements. The RANS models used were the same low-Reynolds k-ϵ and RSM model used in the previously mentioned study by van Hooff et al. [21] and they showed similar performance in this study i.e. the low-Reynolds k-ϵ gave the best results.

The simulations were done with Fluent 6.3.26. For the RANS simulations, the settings were similar as to those described in [21]. The transport equation for the pollutant was solved after the steady flow field was obtained. For the LES simulation the dynamic Smagorinsky Sub Grid Scale (SGS) model is used. The filtered momentum equation was discretized with a bounded central scheme, second order upwind scheme were used for the concentration equation. Time integration was second order implicit and PV coupling were done with the PISO algorithm. The time step was based on a maximum CFL number of 1.

3.2.6 Benchmark 6 – Impinging jet

Simulations by Chen et al.

In the same article that describes the experiment of Benchmark 6 [10], the authors present CFD simulations of the benchmark flow. The SST k-ω model and RNG k-ϵ model are used to simulate the flow, using Fluent 13.0. Simulations were done in 3D as this benchmark geometry cannot be approximated as 2D. Three different mesh sizes were tested with both models, consisting of 2.5, 4.9 and 6.1 million cells. The grid sensitivity analysis concludes that the two finest meshes give very similar results, thus the mesh used for the validation is the mesh with 4.9 million cells. The mesh was refined near the walls to keep $y^+ < 1$. The SIMPLE algorithm was used for PV coupling, and second order upwind schemes were used for the convective terms.

Both turbulence models give satisfactory results, and are capable of capturing the main features of

the flow. The results are shown in figures 3.23 and 3.24. The profiles are normalized with the local maximum velocity U_{max} or V_{max}.

As can be seen from figure 3.23 the SST k-ω model performs slightly better for the vertical velocity profiles close to the impingement zone, while both models under predict the velocity in the outer layer of the wall jet at x = 0.7m and x = 1 m. However, the authors argue this is the area of highest turbulent intensity and consequently also the largest area of uncertainty with the hot wire measurements.

(a) x = 0.3 m

(b) x = 0.5 m

(c) x = 0.7 m

(d) x = 1 m
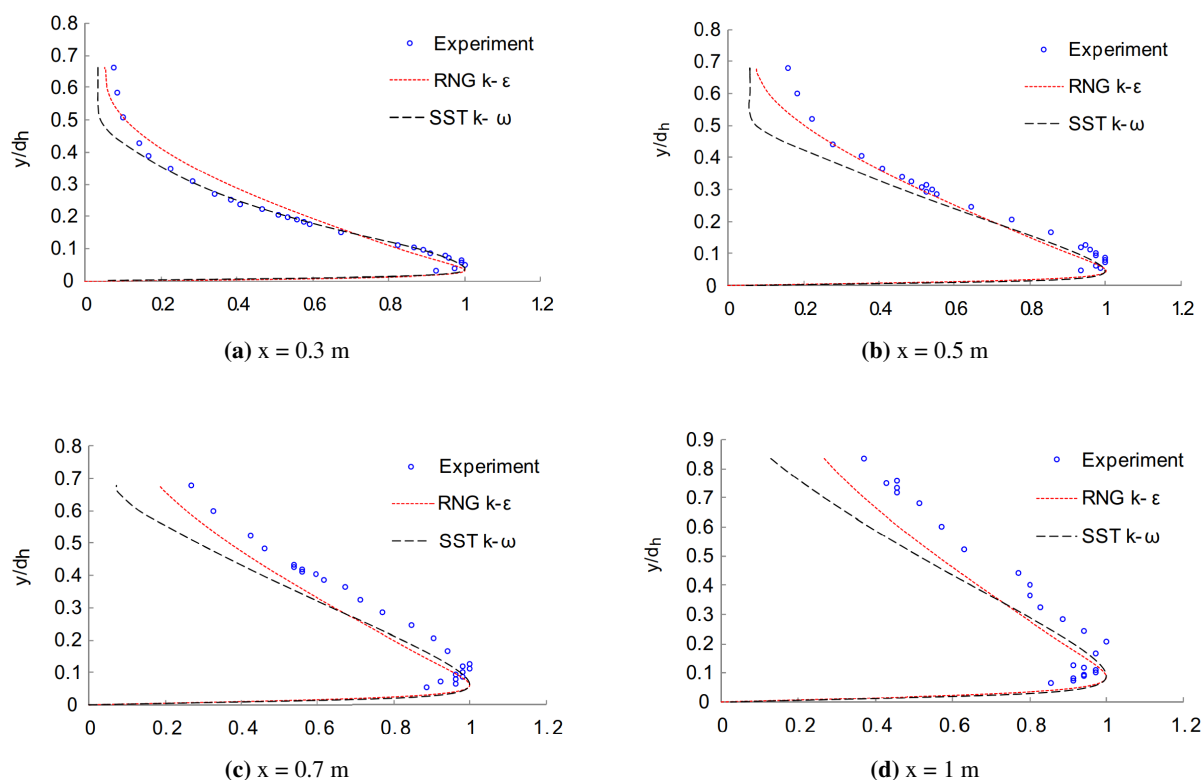
Figure 3.23: Vertical velocity profiles at midplane for various x-locations of benchmark 6 obtained by Chen et al. for the SST k-ω model and the RNG k-ϵ model. U/U_{max} on x-axis (figures from Chen et al. [10] p. 160).

The horizontal velocity profiles can be seen in figure 3.24. Both models are capable of getting the correct velocity profile here. For the position closest to the floor, a local peak in the velocity is observed in the simulated profiles because of a recirculation vortex in the corner with the wall and floor. This was not captured by the measurements because of difficulties measuring this area of the cavity.
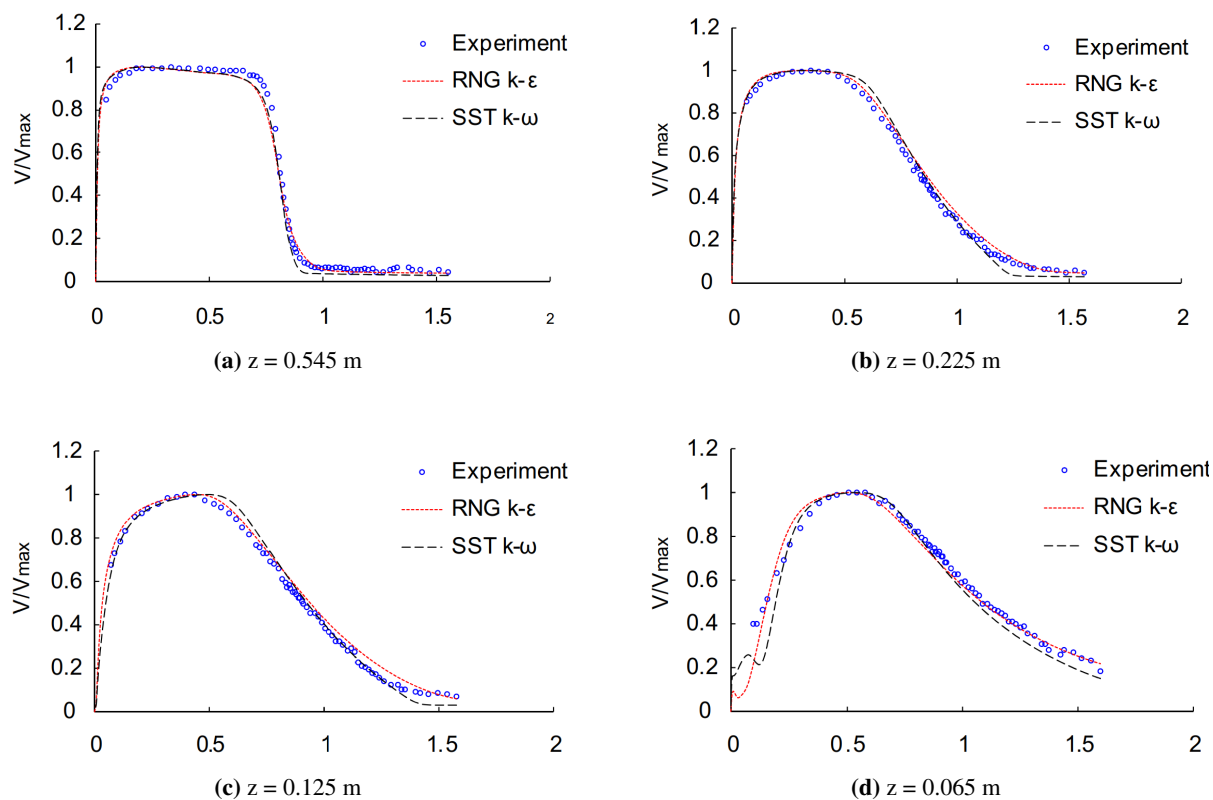
Figure 3.24: Horizontal velocity profiles at midplane for various y-locations of benchmark 6 obtained by Chen et al. for the SST k-ω model and the RNG k-ϵ model. U/U_{max} on x-axis (figures from Chen et al. [10] p. 159).

To summarize good results are achieved with both RANS turbulence models indicating that although several papers argue these models have some shortcomings in modelling an impinging jet (e.g. Karimipanah [28]), these shortcomings are not in the way of producing a satisfactory result for B6.

Simulations by Taghinia et al.

In the same paper that presents LES simulations of B2 and B4 Taghinia et al. [43] also present LES simulations of B6. The same DSM and RAST models are used and the general settings such as numerical schemes are similar and described in section 3.2.2.

A grid with 6.5 million cells is used as this gave similar results to a grid with 8 million cells in a grid sensitivity analysis. A separate LES simulation a pipe flow with the same diameter as the inlet of B6 was done, and the outflow of this simulation was imposed as the inlet boundary condition for this simulation. Once again the LES results by Taghinia et al. give very good results. The velocity profiles at four available x-locations is shown in figure 3.25. The match is also very good for the velocity profile below the inlet and for the decay of maximum velocity.

(a) x = 0.3 m

(b) x = 0.5 m

(c) x = 0.7 m

(d) x = 1 m
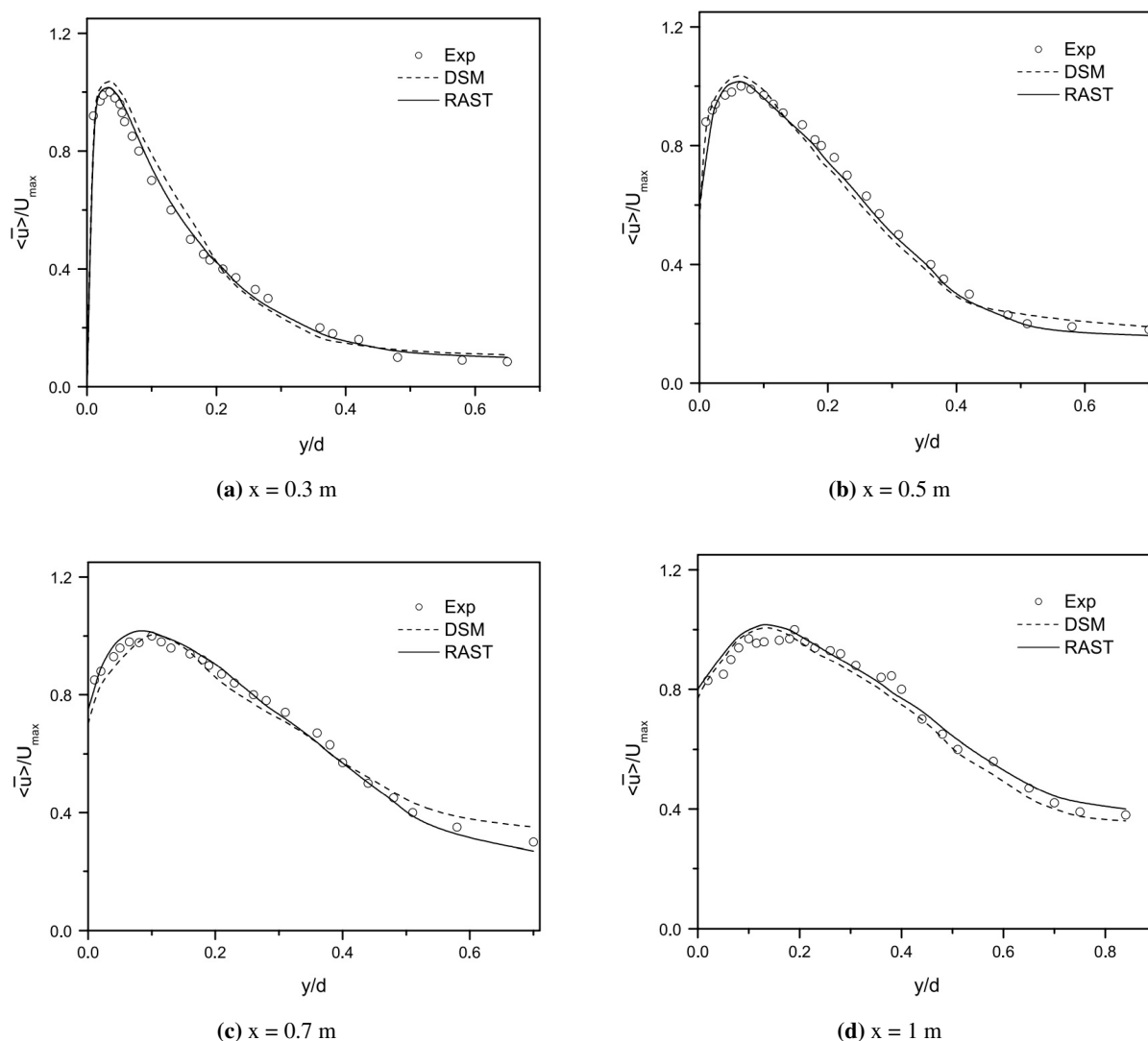
Figure 3.25: Comparison between experiments and LES simulation by Taghinia et al. for B6. Vertical profiles (figures from Taghinia et al. [43] p. 2891).

Also for Benchmark 6, the authors conclude that the RAST model gives slightly better results, but the difference is very small. More interesting is the fact that the LES results are better than the RANS results obtained by Chen et al. [10], seen in particular at the profiles furthest away from the inlet at x = 0.7m and x = 1m if one compares figure 3.25 and figure 3.23.

3.2.7   Benchmark 7 – Wall jet

Simulations of a plane wall jet with several different RANS turbulence models have been done by Yan et al. [46]. ANSYS Fluent 14.5 were used in the simulations. The flow domain used in the simulations were slightly different from the experimental configuration described by Ericsson et al. [16]. The dimensions of the flow domain used in the simulations are shown in figure 3.26. The inlet slot height is 12.7 mm and the length of the lower wall is 4572 mm. The lower and left wall are solid walls with no-slip boundary condition imposed while the right and upper borders are both modelled as pressure outlets. Simulations were done at four different Reynolds numbers: 10000, 20000, 30000 and 40000. Despite the geometry and Reynolds number being different from the experiment described by Ericsson (Re = 9600, h = 9.6 mm and L = 7m), the results from the simulations are compared with
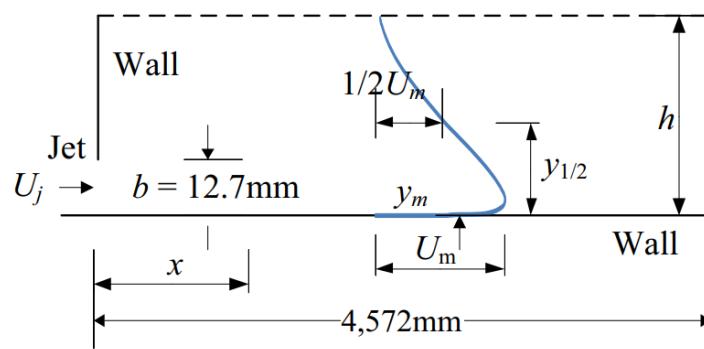
Figure 3.26: Flow domain and dimensions used in the simulations by Yan et al.
(figure from Yan et al. [46] p. 215).

the experimental data from this experiment. The reason being that it was shown by Launder and Rodi [30] that the mean velocity profile is universal and independent of Re when the distance normal to the wall is scaled by the normal distance to where the velocity is half of the maximum ($y_{1/2}$) and the streamwise velocity is scaled by its maximum value at the same streamwise location (U_m). Hence, it is this universal profile that is compared. In this thesis the z-axis is used for the height in B7, thus $z_{1/2}$ is used for $y_{1/2}$ in the results section.

The RANS simulations were done in 2D. A grid sensitivity analysis was performed, simulating with three different mesh sizes: 30 000, 47 120 and 100 000 cells. The analysis concluded the intermediate mesh with 47 120 cells was sufficient to obtain accurate results. The mesh was refined near the wall to keep $y^+ < 1$. The SIMPLEC algorithm was used for pressure-velocity coupling and the simulations were done in steady state. Enhanced wall treatment was used for near wall modelling. Second order upwind schemes were applied for momentum, k and ϵ/ω. The convergence criteria was residuals below 10^{-6}.

The results from the simulations are shown in figure 3.27. Figure 3.27a shows the universal velocity profiles obtained with several turbulence models at x/h = 100 and Re = 20 000. These profiles are compared with the experimental one. Figure 3.27b shows the maximum velocity decay. This decay is dependent on Reynolds number [46], thus instead of comparing directly with the experiments by Eriksson, there is an upper and lower bound based on a review by George et al. [18] of several experiments. The turbulence models in the legend are as follows:

- SKE = Standard k-ϵ

- RNGKE = RNG k-ϵ

- RKE = Realiazable k-ϵ

- SKW = Standard k-ω

- SSTKW = SST k-ω

- LRSM = Linear Pressure-Strain RSM model

- SWRSM = Stress-ω RSM model

(a) Universal profile scaled with $y_{1/2}$ and U_m at x/h = 100

(b) Maximum velocity decay. Upper and lower bound are based on several experiments.
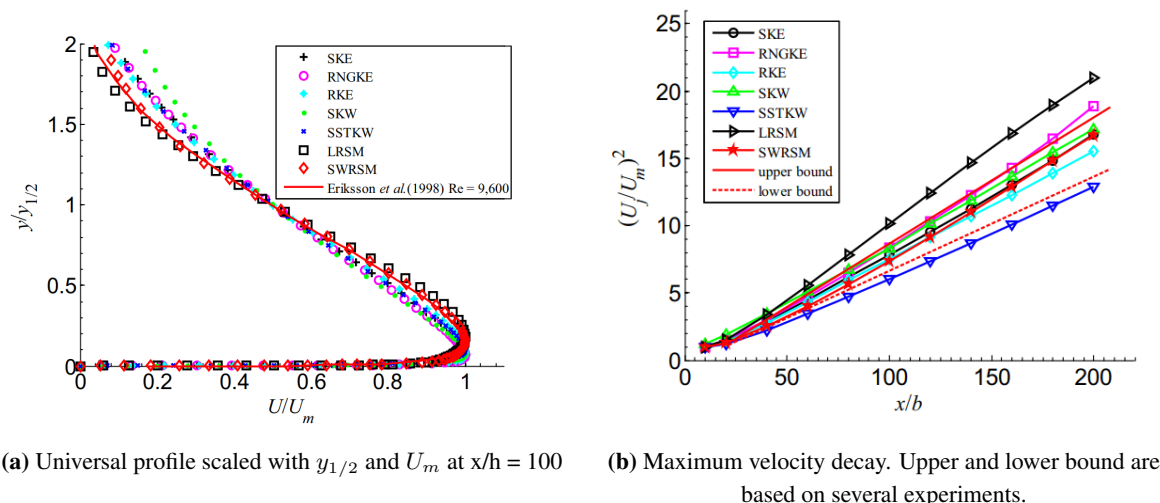
Figure 3.27: Comparison between experiments and simulations by Yan et al. for benchmark 7 (figures from Yan et al. [46] p. 217).

It can be observed from figure 3.27a that all the two-equation turbulence models – that is everyone except the two RSM models – predicted a profile that is shifted closer to the wall compared with the experiments. The two RSM models give closer agreement with experiments. It is hard to say anything about which of the two-equation models that give the best result looking at figure 3.27a. Looking instead at figure 3.27b it is clear that the result from the LRSM model give a too large decay rate compared with the experiment while the decay rate with the SST k-ω is too small compared with the experiment. The RNG k-ϵ model lies on the upper bound of the experiment up until x/h = 150, from where it exceeds the experimental values. The remaining models lie within the range of experimental data.

Yan et al. [46] did also LES simulations of the wall jet in the same paper, comparing the results with the experimental data by Eriksson [16] and the result with the Stress-ω RSM model. The LES model used was the Dynamic Smagorinsky Model (DSM), and the three dimensional grid had 4.3 million cells and $y^+ < 1$.

The LES showed a good fit to the experimental data and the authors conclude the performance of the LES simulation is slightly better than for the Stress-ω RSM model when scaled with the outer variables, U_m and $y_{1/2}$. Furthermore, the LES simulation was significantly better at predicting the Reynolds stresses, as the RSM model over predicted the turbulent quantities in the outer region of the jet while the LES result collapses very well on the experimental data.

3.3   Summary of benchmarks and simulations

Table 3.2 has been created to summarize the performance of the various RANS turbulence models in the literate accounted for in this section. The table presents how well the turbulence models have produced results that are in agreement with the experimental data from the benchmarks. The table is split into 2D and 3D simulations, as the simulation by Ito et al. [25] showed that this can influence the performance of a turbulence model. B1 was split into the two columns with the different Reynolds numbers as the performance varied between the two. For B5 the two Reynolds numbers are in the same column as the turbulence models performed similar for both. The table states the inlet Reynolds number and flow

Table 3.2: Summary of turbulence model performance in literature. Color indicate agreement with experiments. Reference to literature included.

Benchmark	B1	B2	B3	B4	B5	B6	B7
Re inlet	500	5000	7100	684	1000/2500	10013	9600
Flow regime	Transitional	Fully turbulent	Fully turbulent	Unknown	Transitional	Fully turbulent	Fully turbulent
2D Std. k-ε	X	[14] [25] (green)	X	X	X	X	[46] (yellow)
2D RNG k-ε	X	X	X	X	X	X	[46] (yellow)
2D realizable k-ε	X	[14] (red)	X	X	X	X	[46] (yellow)
2D Std. k-ω	X	[14] [25] (yellow)	X	X	X	X	[46] (yellow)
2D SST k-ω	X	[14] [25] (red)	X	X	X	X	[46] (yellow)
2D Low-Re k-ε	X	Std.* [14] (green)	X	L&B [5] (green)	X	X	X
2D Low-Re k-ε	X	AKN[14][25] (yellow)	X	J&L [5] (red)	X	X	X
3D Std. k-ε	X	[25] [38] (green)	[31] (green)	X	X	X	X
3D RNG k-ε	[33] (yellow)	X	[31] (green)	[29] (green)	[21] (red)	[10] (green)	X
3D realizable k-ε	[33] (yellow)	X	X	X	X	X	X
3D Std. k-ω	X	X	X	[29] (yellow)	X	X	X
3D SST k-ω	[33] (red)	[25] (green)	[31] (green)	[29] (green)	[21] (green)	[10] (green)	X
3D Low-Re k-ε	X	AKN [25] (green)	X	X	Chang [21] (green)	X	X
LES	X	[43] (green)	X	[43] (green)	[24] (green)	[43] (green)	[46] (green)

Legend: Good (green) Moderate (yellow) Bad (red) X = not tested

regime of the benchmarks based on what is stated in the experiment reports. It is assumed that what flow regime is present is an important parameter for the how well the models perform. For B4 no flow regime is stated, thus it is reported as unknown. The low-Re k-ϵ models include several models so the abbreviation for each model is shown in each cell. To know exactly which model this is, the reader is encouraged to look up the simulation in the literature review or the referenced article. The table also highlights which turbulence models that have not been tested on the different benchmarks – based on the literature in this section. To have a clean and readable table other parameters than the turbulence model have been left out, but these have been accounted for in the preceding pages.

The idea behind the table is that it can serve as a guideline for selection of turbulence model in mixing ventilation scenarios, by showing how the various turbulence models perform for the different benchmarks in a compact way. The conclusions that can be drawn from such a table will strengthen when the result from one research group is reproduced by one or more different groups, as this implies that the good or bad performance is in fact caused by the turbulence model, and not a different parameter. The reference to the article which the result is taken from is included in the table. Most of the results are only based on one simulation, so very strong conclusions cannot be drawn only from this. The table should be interpreted as one that highlights trends rather than gives specific advice for each Benchmark. The performance indicator – Good, Moderate, Bad – is based on a qualitative interpretation of the result from the author of this thesis and the description of the performance in the respective articles. A similar table is presented in section 6, where the turbulence model performance from the results from this thesis is summarized. It is indicated whether these results are in agreement with table 3.2.

Looking more closely at table 3.2 it can be seen that none of the RANS turbulence models perform well for all the benchmarks. The two most used turbulence models are the RNG k-ϵ model and the SST k-ω model. These two models perform moderate or good for most of the benchmarks, but also has one case of bad agreement with experiments. For RNG k-ϵ this is B5 and for SST k-ω B1 at Re = 4000. It can also be observed that the realizable k-ϵ model – which is the most recent k-ϵ model – has been used little in literature. It is also clear that for all the benchmarks where LES has been used, good results have been obtained.

Table 3.3 complements table 3.2 by providing a comparison of the geometry for the different cavity benchmarks. B6 and B7 are not included since they have fundamentally different geometries. Note that here all the Reynolds numbers that have been used in the experiments are shown in the table, while in table 3.2 the Reynolds numbers refer to what has been used in the simulations. The Richardson number is also reported, using the inlet height as length scale, to give an indication of the buoyancy force for B3 and B4. This number is small for B4 and very small for B3.

Table 3.3: Summary of benchmarks 1-5 geometry and flow regime

Benchmark	h/H	t/H	L/H	W/H	Re	Ri
B1	0.200	NA	25	2	500 4000	NA
B2	0.056	0.160	3	1	5000	NA
B3	0.056	0.160	3	4.7	2400 4700 7100	$\sim 10^{-6}$
B4	0.017	0.023	1	0.29	684	0.04
B5	0.010	0.017	1	1	1000 2500	NA

3.4   The realism of the benchmarks

The benchmarks presented in this thesis have been picked because they represent many of the same challenges as simulating a real mixing ventilation problem. However, connecting the benchmarks to reality is not a straightforward procedure. Say one would like to simulate a mixing ventilation case of a single cell office. Which benchmark should one pick to validate the CFD code for such a simulation? It would depend on the geometry of the room, the air flow rate, the inlet Reynolds number, the temperature of the walls etc. There is, however, not so simple to determine the Reynolds number of every inlet diffuser available on the market. Some diffuser geometries are complex and do not have an obvious length scale like the simple inlets in the benchmarks. It would be beneficial to know the flow regime in the majority of the room, but this is difficult to know with certainty in the design stage of a building.

If one scales up the benchmark to have a typical office ceiling height of 3 meters, and then scales the velocity such that the Reynolds number is constant, one obtains the flow rates seen in table 3.4. These are compared with the air flow rate values one would get by following the Norwegian standard TEK17 [12] when assuming an occupant density of 5 $m^2/pers$. This value is taken from the Sintef Prosjektrapport 42 [13]. TEK17 gives guideline airflow rate values of 26 $m^3/hper$ to account for occupancy and 3.6 m^3/hm^2 to account for emitting materials. Combining this with the occupant density we get:

$$\frac{Flow\ rate}{Floor\ area} = (26/5 + 3.6)\ m^3/(h\ m^2) = 8.8\ m^3/(h\ m^2) = 2.44\ l/(s\ m^2)$$

Since many of the benchmarks have geometries that are quite far from what would be a normal cell office these values should be interpreted with scrutiny. Benchmarks with a large width relative to the length and height will naturally have a larger flow rate in this context, as the flow is constructed to be 2D and the inlet spans the entire width for all benchmarks 1 to 5. Nonetheless, they can give an indication of whether the flow rates in the benchmarks are large, medium or small compared to a real case.

Table 3.4: Benchmark flow rates when scaled to H = 3m for all benchmarks. Values
are compared with the flow rates obtained using TEK17 for an office building.

Benchmark	Re	H [m]	L [m]	W [m]	Floor area [m2]	Flow rate [l/s]	Flow rate TEK17 [l/s]
B1	500	3	45	6	270	45.5	660
B2	5000	3	9	3	27	227.4	66
B3	7100	3	6.3	14.1	89	1517	218
B4	684	3	3	0.86	2.6	9.0	6.3
B5	1000	3	3	3	27	45	22

Taking a closer look at the values in table 3.4 one can see that for benchmark 2 and 3 have large flow rates compared to the standard. For benchmark 3 in particular this is partly because of the large room width, but this nonetheless indicates that the flow rates are larger than for most realistic applications. Benchmark 4 and 5 have values that are closer to the standard and based on this it looks like the benchmarks with a slot Reynolds number in the transitional regime have the most realistic flow rates. Benchmark 1 gets a very high flow rate in the standard because of its very long geometry and to compare these values are not of great interest.

It is out of the scope of this thesis to establish a way to determine the correct benchmark for a realistic ventilation scenario. This section serves more as a warning for the use of RANS turbulence models for ventilation purposes. It has been shown in the literature review there is no one single RANS turbulence model that seems capable of reproducing the flow of every benchmark with satisfying accuracy. This is despite the fact that geometrically the benchmarks are very similar, and probably caused by the differences in flow regime and Reynolds number. This implies that it can be difficult to say if the result is correct when simulating a real case with a RANS turbulence model, specially if the flow regime of the simulation is unknown.

4   Method

All simulations except the simulations of B5 have been done in ANSYS Fluent R2 or 19.2. The difference in version is because the most time consuming simulations were done on a workstation where version 19.2 was installed. It is assumed that the difference in ANSYS Fluent version has no impact on the solution. The benchmark 5 simulations were done in OpenFOAM 7. This was simply because they were done first, when the intention was to use OpenFOAM 7 for the entire thesis, however, a switch was made because the availability in computational power was larger for Fluent.

4.1   Methodical procedure

If one accounts for all the possible settings, models and parameters that are involved in CFD simulations, it becomes clear that a sensitivity analysis looking at all settings quickly becomes much larger than what is feasible for a master thesis. To narrow the scope, this master thesis primarily looks at how different two-equation RANS turbulence models perform for the benchmarks presented in section 3.1. This approach is based on the findings from the preceding project assignment, where the choice of turbulence model seemed to have the biggest impact on the result. Four turbulence models have been tested for all the benchmarks that have been simulated in this thesis: standard k-ϵ, RNG k-ϵ, realizable k-ϵ and SST k-ω. Additional models have been included for some Benchmarks – typically if they have proven successful in literature. The impact of turbulent boundary conditions at the inlet and type of wall treatment have also been investigated for some benchmarks, as these parameters also seemed to have a significant impact on the solution.

In order to evaluate the performance of different turbulence models, the result from simulating with various models have been compared with the experimental data from the benchmarks. Primarily these comparisons have been of the mean velocity profile at the lines where measurements have been performed. The experimental data have been collected by downloading data files when they have been available. This was the case for B2 and B5. In the cases when data files have not been available the digitizer software "WebPlotDigitizer 4.3" have been used to extract the data from existing plots. This approach adds some additional uncertainty to the experimental data. However, this uncertainty is smaller than the uncertainty of the measurements themselves. The mean velocity profiles have been made dimensionless by dividing with either the bulk inlet velocity, or the local maximum velocity for each profile. The former approach has been used for all the cavity Benchmarks, that is Benchmark 2-5, as this gives the opportunity to compare results from different Benchmarks.

Different options were considered as a quantitative metric on the compliance between the predicted velocities from the simulations and the measured velocities from the experiment. One option considered was to use FAC 1.25, which is what is used by Kosutova et al. [29] and the formula is given in equation 3.2. However, this formula contains a defined and slightly arbitrary threshold of 25%. This could be problematic as two simulations where one has many values just within this threshold, and another has very accurate values they will get the same value for FAC 1.25, even though one is clearly superior. Furthermore, since the formula divides by the measured value, one needs a very small difference between the predicted and measured value to be within the threshold, when the values are close to zero. There is however no obvious reason for why one should require higher accuracy for values close to zero in a mixing ventilation scenario. For this reason, it was also ruled out to use a metric based on the percentage error.

In this thesis, it was decided to use the Root Mean Square Error (RMSE). This is a common way to evaluate the deviation between a predicted and observed value and does not have the same deficiencies as described above. The formula for RMSE is shown in equation 4.1, where P_i is the predicted value by the simulation, O_i is the measured value and N is the measurement sample size. One drawback with RMSE is that it is in general not suitable for comparing different data sets as it is scale dependent. However, for Benchmark 2-5 all the velocities are made dimensionless by dividing with the bulk inlet velocity, and it is these dimensionless velocities that are used in equation 4.1. This scales the values to be within the same range, thus enabling at least an approximate comparison of RMSE values for these benchmarks. It was also considered to use the Mean Absolute Error (MAE) shown in equation 4.2, however, RMSE was favoured since this penalizes outliers that are desirable to avoid in a CFD simulation.

$$RMSE = \sqrt{\frac{\sum_{i=1}^{N}(P_i - O_i)^2}{N}} \tag{4.1}$$

$$MAE = \frac{\sum_{i=1}^{N}|P_i - O_i|}{N} \tag{4.2}$$

For each benchmark a grid sensitivity analysis has been conducted. The approach has been to create at least three meshes with different number of cells, where the mesh sizes tested have been loosely based on what has been done before in the literature. The three different solutions have then been plotted against experimental data. From this one mesh has been selected based on a trade-off between accuracy and computational requirement. All meshes – independent of number of elements – have been constructed to have y^+ less than five on the walls in order to put the nearest wall cell in the viscous-sub layer. Some meshes have values higher than this in small parts of the cavity, in particular at the inlet section where the boundary layers are thin, but at the very least y^+ is less than 10. All meshes except the B5 meshes have been constructed in ANSYS meshing using the "Multizone" method. The B5 meshes were constructed on an earlier stage with the "Sweep" method, and have as a consequence uniform spacing in the y-direction i.e. no wall refinement on the front and back walls.

All the benchmarks have been simulated with the exact Reynolds number reported in the literature review. This Reynolds number has been calculated with the bulk inlet velocity. For some benchmarks the simulation has been performed on a scaled geometry compared to the experiment, e.g. this is common in literature for B2 to have an inlet velocity similar to an actual ventilation system. This does not affect the comparison with experimental data as long as the Reynolds number is equal and the velocity is scaled with the same reference velocity – in this case the bulk inlet velocity U_{in}.

4.2   Default solver settings

"Enhanced wall treatment" has been used as the default wall treatment option in ANSYS Fluent. The effect of different wall treatment options have however been investigated for some benchmarks, and have been found to have an impact on the final solution. For the OpenFOAM simulations, the wall boundary condition is a bit more complex as each variable needs its own setting. The choices for the OpenFOAM wall boundary conditions are based on the recommendations by Joel Guerrero [19]. Exactly what settings have been used can be seen in the OpenFOAM Dict files attached in Appendix C.

All the walls have been modelled as smooth, no-slip walls. The fact that the walls are smooth and without roughness is an assumption that is commonly used in literature. It is further justified by the

fact that the walls have to be made of glass to allow LDV/PIV measurements. Nonetheless, the impact of adding roughness was tested for B2. This impact was negligible for roughness heights less than 1 cm for a model scale H = 3m, which greatly exceeds typical roughness heights for glass (scaled from experiment size). It is therefore reasonable to believe that the smooth wall assumption does not induce any errors.

Second order upwind schemes have been used for the convective terms of all the variables in all the ANSYS Fluent simulations. The effect of applying different numerical schemes was tested in the project assignment and the result indicated that as long as first order upwind schemes are avoided the impact is quite small. For the OpenFOAM simulations, linearUpwind schemes – equivalent to second order upwind in Fluent – have been used for momentum, while limitedLinear schemes with a limiter factor of 1 have been used for k, ϵ and ω.

The simulations have been done in steady state. However, in many of the benchmark simulations, a converged steady state solution has not been reached. Instead, residuals and monitored parameters such as the drag coefficients on the floor and ceiling have oscillated. This is not an unknown phenomenon when simulating airflows inside buildings, and in these cases the averaging technique described by B. Blocken [6] has been applied. This technique is to average the solution over a large number of iterations to get a statistically independent solution. The number of iterations required is case dependent and must be investigated for each benchmark. It must also be decided when to start the averaging, as one would avoid starting this process before the solution has started oscillated around the statistically independent solution. Thus, the averaging technique introduces two more parameters that can affect the final solution. An alternative is to simulate these cases in transient mode and average over sufficiently many time steps. This is computationally more expensive as the time step used in a transient simulation is typically small to have a satisfying CFL condition. In this thesis, the averaging has been started when it was made certain that the drag coefficients on the floor and ceiling had started to oscillate around a steady value. The number of iterations to average over was case dependent and stopped when additional averaging no longer impacted the result.

The SIMPLE algorithm is used as default for pressure-velocity coupling. In some instances, the "Coupled" option in Fluent has been used initially with the "pseudo transient" option enabled as this had an increase in convergence speed for some cases. However, in every solution which has been averaged over a large number of residuals the PV coupling algorithm has always been changed back to SIMPLE before the averaging was started. The SIMPLE algorithm was selected as this is frequently used in literature. The ANSYS Fluent user guide [4] accounts for how the different PV coupling algorithms can improve convergence and stability.

A summary of the default solver settings that have been used for ANSYS Fluent simulations is presented in table 4.1. These are the settings that have been used unless otherwise is specified for a specific simulation in section 5.

Table 4.1: Default solver settings ANSYS Fluent.

PV coupling	SIMPLE
Numerical scheme: gradient	Least squares cell based
Numerical scheme: pressure	Second order
Numerical scheme: momentum	Second order upwind
Numerical scheme: k	Second order upwind
Numerical scheme: ϵ/ω	Second order upwind
Near-wall treatment ($k - \epsilon$ models)	Enhanced wall treatment

5   Results and discussion

5.1   Benchmark 2

Benchmark 2 was simulated extensively in the project assignment preceding this master thesis, however, the majority of the simulations were in 2D. Good results were obtained in 2D with the standard and RNG k-ϵ models, while larger discrepancy with experiments was seen with the standard and SST k-ω models and the realizable k-ϵ model. The results from the project assignment were very similar to the 2D results obtained by Dreau et al. [14] and Rong and Nielsen [41]. However, the 3D simulations of Benchmark 2 done in the project assignment deviated significantly from the experimental data and from the simulation by Ito et al. [25]. For this reason, additional 3D simulations of benchmark 2 have been done to investigate what might have caused the poor results in the project assignment.

When simulating B2 in 3D oscillatory convergence is observed for most turbulence models, an issue that is not mentioned in the paper by Ito et al. [25] or the paper by Olmedo and Nielsen [38] who both simulated B2 in 3D. However, the number of turbulence models tested in these two papers is quite limited and the only model used in both papers is the standard k-ϵ model.

5.1.1   Grid sensitivity analysis

The grid sensitivity analysis for Benchmark 2 was carried out with the standard k-ϵ model, as previous simulations had proven this was the only model which showed good convergence for this benchmark. Three meshes were created: a coarse mesh with 342 thousand cells, a medium mesh with 703 thousand cells, and a fine mesh with 4.1 million cells. All these meshes have wall refinement and are improved from the meshes used in project assignment in the sense that they also have wall refinement on the front and back walls. The coarsest mesh nonetheless had some y^+ values well above 5. However, the average y^+ values were well below 5 for all the walls. The turbulent intensity at the inlet was set to 4 % which is what was measured by Nielsen [35], and the length scale used to compute ϵ and ω was ℓ = h/10. The result from the grid sensitivity analysis is shown in figure 5.1. All solutions have been simulated until residuals were lower than 10^{-5} and the drag coefficient on the top and bottom walls reached stable values.

(a) Vertical line: x = H

(b) Vertical line: x = 2H

(c) Horizontal line: z = h/2

(d) Horizontal line: z = H - h/2
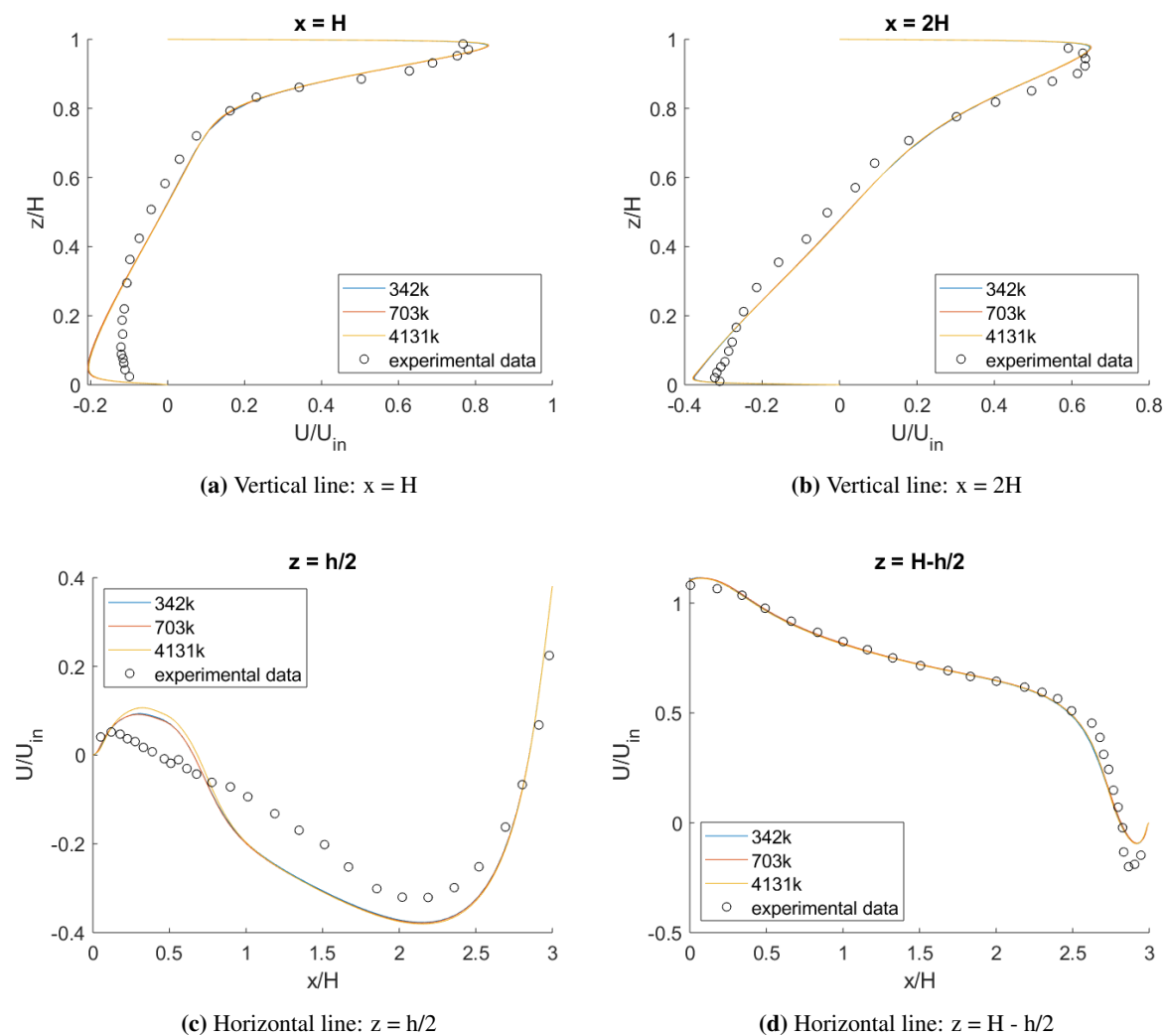
Figure 5.1: Grid sensitivity analysis for Benchmark 2 using the standard k-ϵ model.
Legend refers to number of cells in the mesh.

It can be observed from figure 5.1 that the three solutions nearly overlap, except for the left part of figure 5.1c, where the fine solution deviates slightly from the medium and coarse. Seeing only this relatively small difference and since all the three meshes have a fairly satisfying y^+ condition at the walls, it was decided that the coarse mesh was sufficient for the turbulence model comparison. The savings in computational time was substantial compared to the fine mesh. The coarse mesh also has a similar number of cells to the simulations by Olmedo and Nielsen [38] and the mesh Ito et al. [25] use for the standard k-ϵ model. The layout of the coarse mesh is shown in Appendix A figure A.1. y^+ values for the coarse mesh is shown in table 5.1.

Table 5.1: Average and maximum y^+ values at the different cavity walls for B2 coarse mesh.

	Ceiling	Right wall	Floor	Left Wall	Front Wall	Back wall
Average	2.7	2.8	2.5	1.3	3.8	3.8
Max	6.7	8.2	5.6	2.6	12.8	12.8

5.1.2 Turbulence modelling

Five turbulence models were tested on Benchmark 2 in 3D: standard k-ϵ, RNG k-ϵ, realizable k-ϵ, AKN low-Re k-ϵ and SST k-ω. The AKN low-Re model was included as this was used by Ito et al. [25] and gave satisfying results. All the simulations were initially done on the coarse mesh with 342 thousand cells. The standard k-ϵ and the AKN low-Re k-ϵ simulations converged to a steady state solution, while the remaining models gave oscillating residuals and a flow pattern changing between the iterations. For the solutions with oscillatory convergence the solution was averaged of a large number of iterations, 9000 for RNG k-ϵ the simulation, 10 000 for the SST k-ω simulation and 6000 for the realizable k-ϵ simulation. The SST k-ω simulation was also simulated on the fine 4.1 million cells mesh and an even finer 8 million cells mesh as this model apparently converged to a satisfying steady state solution in the paper by Ito et al. [25]. The solution changes slightly on finer meshes however neither simulation gives as good compliance with the experimental data as the plot presented by Ito et al. (figure 3.14). The results indicate that the differences with the SST k-ω model are caused by a different parameter than the mesh. The results from the different turbulence models are shown in figure 5.2. The abbreviations used for the various turbulence models in the legend of figure 5.2 – and similar figures for the other benchmarks – is described in table 5.2.

Table 5.2: Turbulence model legend abbreviations.

Standard k-ϵ	stdke
RNG k-ϵ	RNG
realizable k-ϵ	realizable
Standard k-ω	stdkw
SST k-ω	SST
AKN low-Re k-ϵ	AKN
Stress-ω RSM	RSM

(a) Vertical line: x = H

(b) Vertical line: x = 2H

(c) Horizontal line: z = h/2

(d) Horizontal line: z = H - h/2
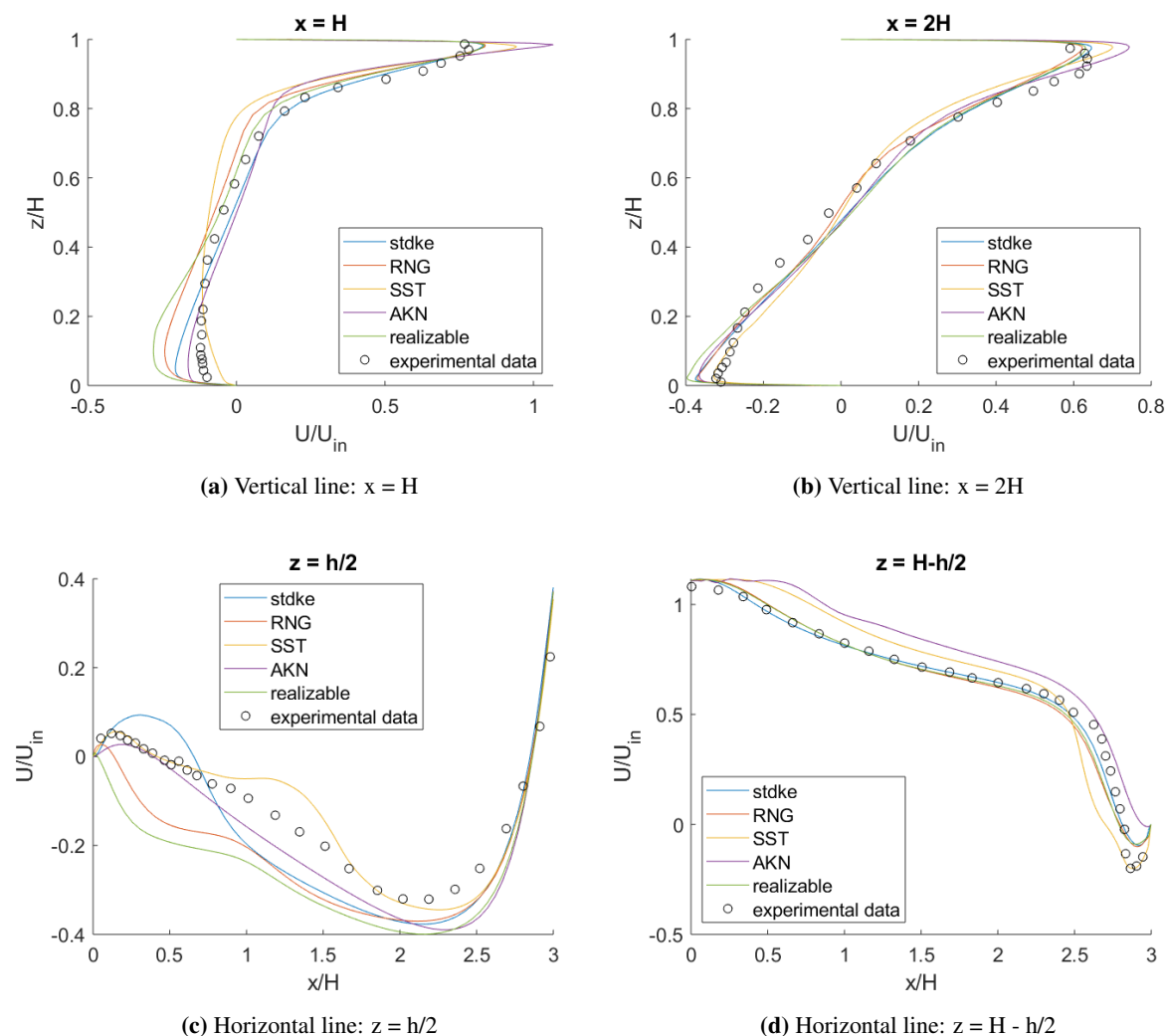
Figure 5.2: Turbulence model comparison for benchmark 2 in 3D. SST k-ω simulation is on the fine mesh while the remaining models are simulated on the coarse mesh.

From figure 5.2 it is clear that neither turbulence model gives a perfect fit with the experimental data. In particular, in figure 5.2c the deviation between the simulation results and the experimental data is quite evident. In the left part of this figure, the experimental data indicates there is a small velocity in the positive x-direction, while the RNG and realizable k-ϵ simulation gives a solution where the flow is going in the negative x-direction. This suggests that these simulated solutions have different flow pattern than the experimental one in this part of the cavity. Obvious differences can also be seen in figure 5.2a, where different predictions in the jet velocity as well as the velocity along the floor can be observed between the models. Velocity contours in the midplane for the different turbulence models are shown in Appendix B figure B.1. Here it is observed that the size of the recirculation zone is much smaller with the SST k-ω model than for the other models. It also predicts a secondary vortex in the impingement region of a different shape than the k-ϵ models.

Table 5.3: RMSE values from using different turbulence models on B2.

	x = H	x = 2H	z = h/2	z = H - h/2	Average
stdke	0.055	0.045	0.071	0.059	0.057
RNG	0.089	0.045	0.100	0.081	0.079
SST	0.098	0.061	0.036	0.151	0.086
AKN	0.103	0.057	0.055	0.140	0.089
realizable	0.102	0.054	0.136	0.077	0.092

Looking at table 5.3 one can observe that the highest RMSE values are obtained with the AKN low-Re k-ϵ model and the SST model at z = H -h/2, because of the overpredicted jet velocity from these models. Some high values are seen also at z = h/2 for the realizable and RNG k-ϵ models, and as discussed above these models have a poor fit to experimental data at this location. It is also clear from table 5.3 that the location where the models overall have the best fit to the experimental data is at x = 2H. Looking at the average values the standard k-ϵ model quite clearly gets the lowest value for RMSE, indicating it has the best compliance with the experimental data. The highest value is obtained with the realizable k-ϵ model, but this is only marginally worse than AKN low-Re k-ϵ and the SST k-ω model.

In addition to differences between the experimental data and the simulations, there are large differences between the various turbulence models themselves for this benchmark. This is a bit surprising as the benchmark is supposedly fully turbulent and should therefore be suitable to model with RANS turbulence models. The largest differences between the models can be observed in the part of the cavity that is beneath the inlet, i.e. the left part of figure 5.2c. One possible explanation to why the turbulence models have difficulties modelling this part of the cavity is that the flow has lost its turbulent characteristics in this part of the cavity, thus is dominated by the transitional regime. Looking at the flow structures visible in the RNG k-ϵ and realizable k-ϵ simulations makes this more credible, as large vortex structures are visible in this part of the cavity. This is illustrated in figure 5.3 where velocity contours at an isosurface with z = h/2, from the realizable k-ϵ simulation is shown.
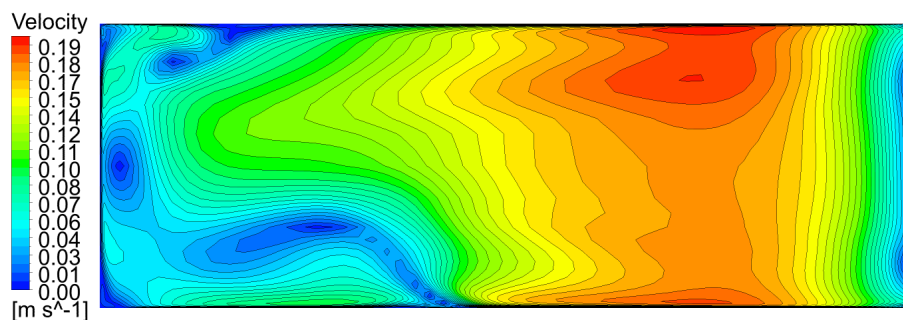
(a) Simulation stopped after 8500 iterations
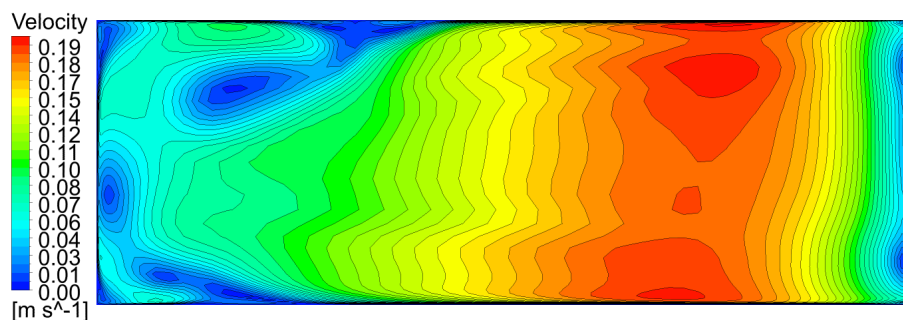
(b) Simulation stopped after 8600 iterations

Figure 5.3: Velocity contours at an isosurface z = h/2 from the realizable k-ϵ
simulation, taken at two instances with 100 iterations separating them.
Three-dimensional vortex structures visible.

Figure 5.3 shows that when simulated with the realizable k-ϵ model benchmark 2 is transient in nature. In the left part of the cavity there is a vortex moving from side to side that circulates around the z axis. This implies that the flow is both transient and three dimensional, however as the fit with the experimental data is not very good with this model, it is not necessarily the correct solution. These vortex structures observed here – and similar with the RNG k-ϵ model – can however explain why the solution does not converge. It also raises doubt to whether the flow is fully turbulent in the entire cavity since such vortex structures are more typical for the transitional flow regime.

The best fit with the experimental data was obtained with the k-ϵ model and with this model the flow has no transient behaviour. Instead for the moving vortex observed in figure 5.3, a symmetric pattern that is observed where most of the air flows along the walls. This is shown in figure 5.4. This pattern is fixed in time, but has also some clear three-dimensional flow structures. It seems that the question of transient vs steady state is turbulence models dependent. To the question of 2D vs 3D the answer seems to be 3D for all turbulence models.
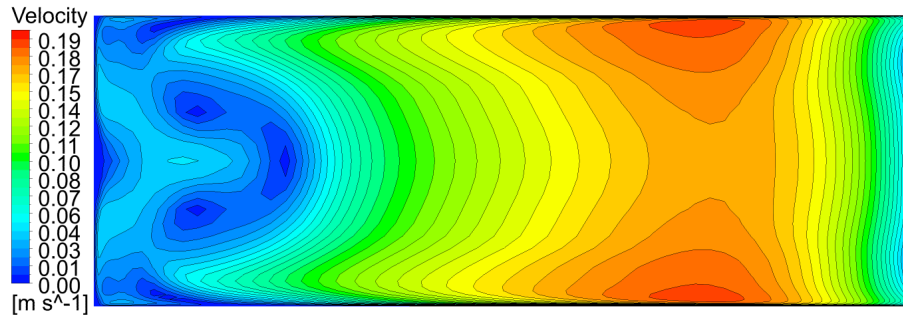
Figure 5.4: Velocity contours at an isosurface z = h/2 from the standard k-ϵ
simulation.

5.1.3   Near wall treatment

In the 3D simulations by Ito et al. [25] the wall modelling approach was reported as "wall function
(Generalized log-law)" for the standard k-ϵ model. It can be assumed that this refers to the option
of using standard wall functions in ANSYS Fluent – which was reported as the used software.
Furthermore, it was also reported that the mesh had no wall refinement for the k-ϵ simulation. This is
the correct approach when using wall functions, because the nearest wall cell then should be placed in
the log-law layer, thus y^+ should be above 30.

This approach was also tested in this thesis. A mesh similar to the coarse, but without any wall
refinement was created. Along the floor, the nearest wall cell was in fact stretched out to increase the
number of cells with y^+ above 30. The total number of cells for this mesh was 108 thousand. The
standard k-ϵ model was used both with standard wall functions, non-equilibrium wall functions and
scalable wall functions. A description of the different wall functions can be found in the Fluent theory
guide [3]. How the wall functions compare to the use of Enhanced wall treatment on the coarse 342
thousand cell mesh can bee seen in figure 5.5.

Looking at figure 5.5 it is clear that the solution changes depending on what type of wall treatment
that is selected. The use of Enhanced wall treatment gives slightly higher velocity in the jet and
along the floor. In the jet, using Enhanced wall treatment gives the best compliance with experiments,
however, along the floor, this profile is furthest away from the experimental values. This can also be
observed in table 5.4, where enhanced all treatment has the highest value at z = h/2, but the lowest at z
= H - h/2. The solutions with standard and scalable wall functions are almost inseparable, indicating
there is little difference between these options when simulated on a mesh where the majority of cells
have y^+ above 30. The non-Equilibrium wall functions – which is an adjusted version of standard wall
functions to account for pressure gradient effects – gives a noticeable different result from the standard
and scalable wall functions.

(a) Vertical line: x = H

(b) Vertical line: x = 2H

(c) Horizontal line: z = h/2

(d) Horizontal line: z = H - h/2
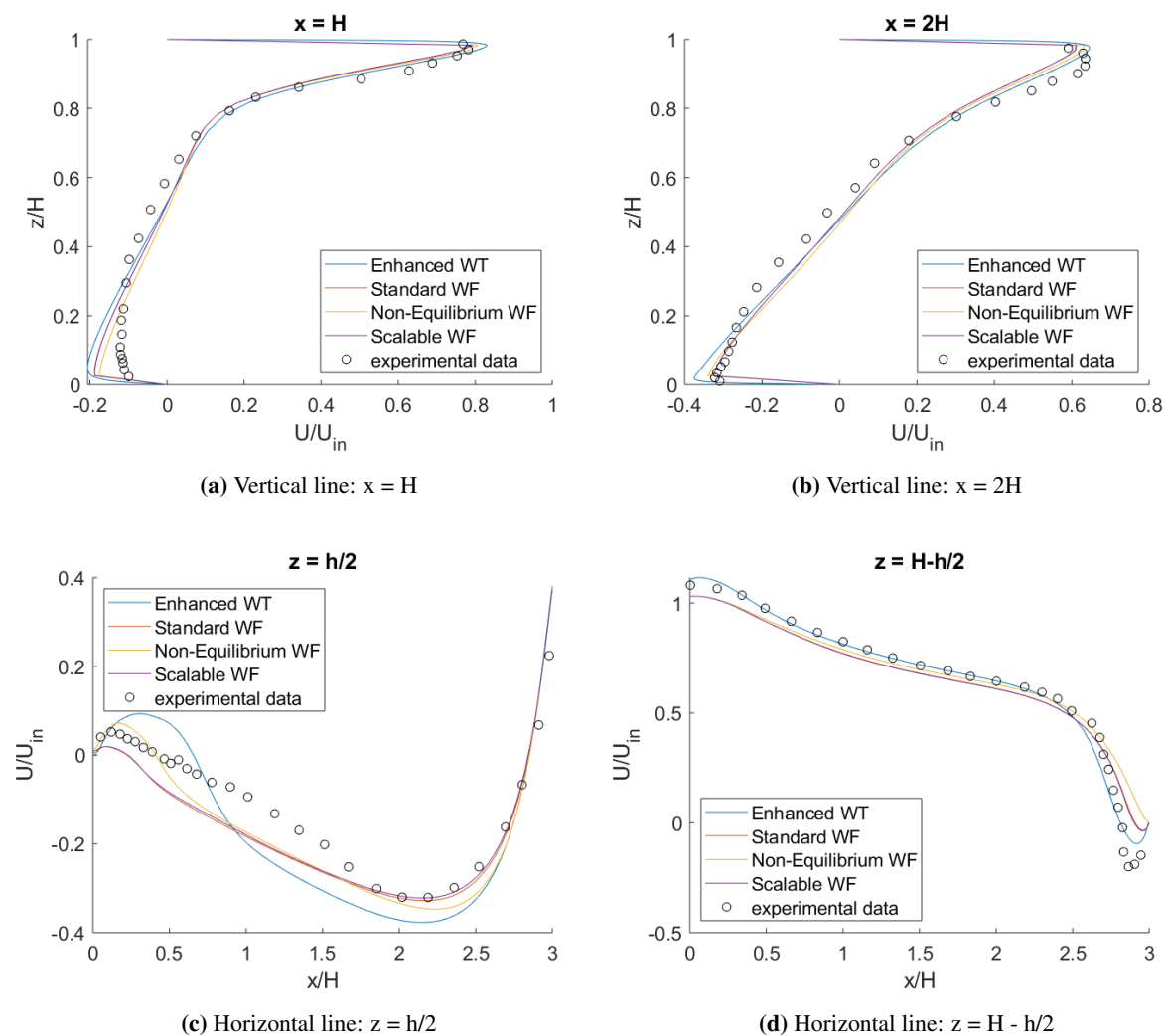
Figure 5.5: Wall treatment option comparison for standard k-ϵ model. Enhanced wall treatment simulation on the coarse mesh, while the three remaining options were simulated on a similar mesh, but with no wall refinement.

Table 5.4: RMSE values for different wall modelling options using the standard k-ϵ model on B2.

	x = H	x = 2H	z = h/2	z = H - h/2	Average
Enhanced WT	0.052	0.045	0.071	0.059	0.057
Standard WF	0.062	0.052	0.060	0.101	0.069
Non-Eq. WF	0.054	0.050	0.050	0.140	0.074
Scalable WF	0.062	0.053	0.058	0.098	0.067

Looking at the average values in table 5.4, Enhanced wall treatment has the lowest average value for RMSE. However, this is mainly because of a much lower value at z = H - h/2, where the wall function solutions both underpredict the velocity in the jet and are incapable of capturing the secondary vortex in

the corner. The last point is probably not because of the wall functions themselves, but rather because the mesh with wall function is too coarse in the corner to resolve this small vortex. This gives a large deviation from the experiment in the corner that is penalized heavily by the RMSE formula. In the other parts of the cavity, the RMSE values are quite similar despite some differences in the shape of the velocity profiles. From figure 5.5 and table 5.4 it is not clear that any particular type of wall modelling gives superior results, but one can conclude that it is a parameter that has a significant impact on the solution. In the CFD community, there is still a consensus that most accurate approach is to resolve the boundary layers, and in particular this is important for accurate modelling of heat transfer which is absent in this benchmark flow.

These results are similar to those obtained by Ito et al. [25] when using wall functions , seen in figure 3.14 of this thesis. It should be pointed out that the y-axis scale of the figure for z = h/2 is slightly different, thus the solutions are more similar than what might be the first impression.

5.1.4   Turbulent inlet parameters

For B2 it was also tested how varying the turbulent intensity, T_i, at the inlet impacted the solution. This was tested with the standard k-ϵ model since this had proven to give the best results for Benchmark 2. Simulations were run with T_i at the inlet varying between 4%, 20% and 50%. The turbulent length scale at the inlet remained constant and equal to h/10 for all the simulations. The result is shown in figure 5.6.

Looking at figure 5.6 it is clear that the inlet value for T_i has a very small impact on the solution for B2. The only visible difference can be seen in the left part of figure 5.6d, right after the inlet, where it can be seen that a higher value for T_i gives slightly lower jet velocity. However, overall the impact on the solution is very small.

(a) Vertical line: x = H

(b) Vertical line: x = 2H

(c) Horizontal line: z = h/2

(d) Horizontal line: z = H - h/2
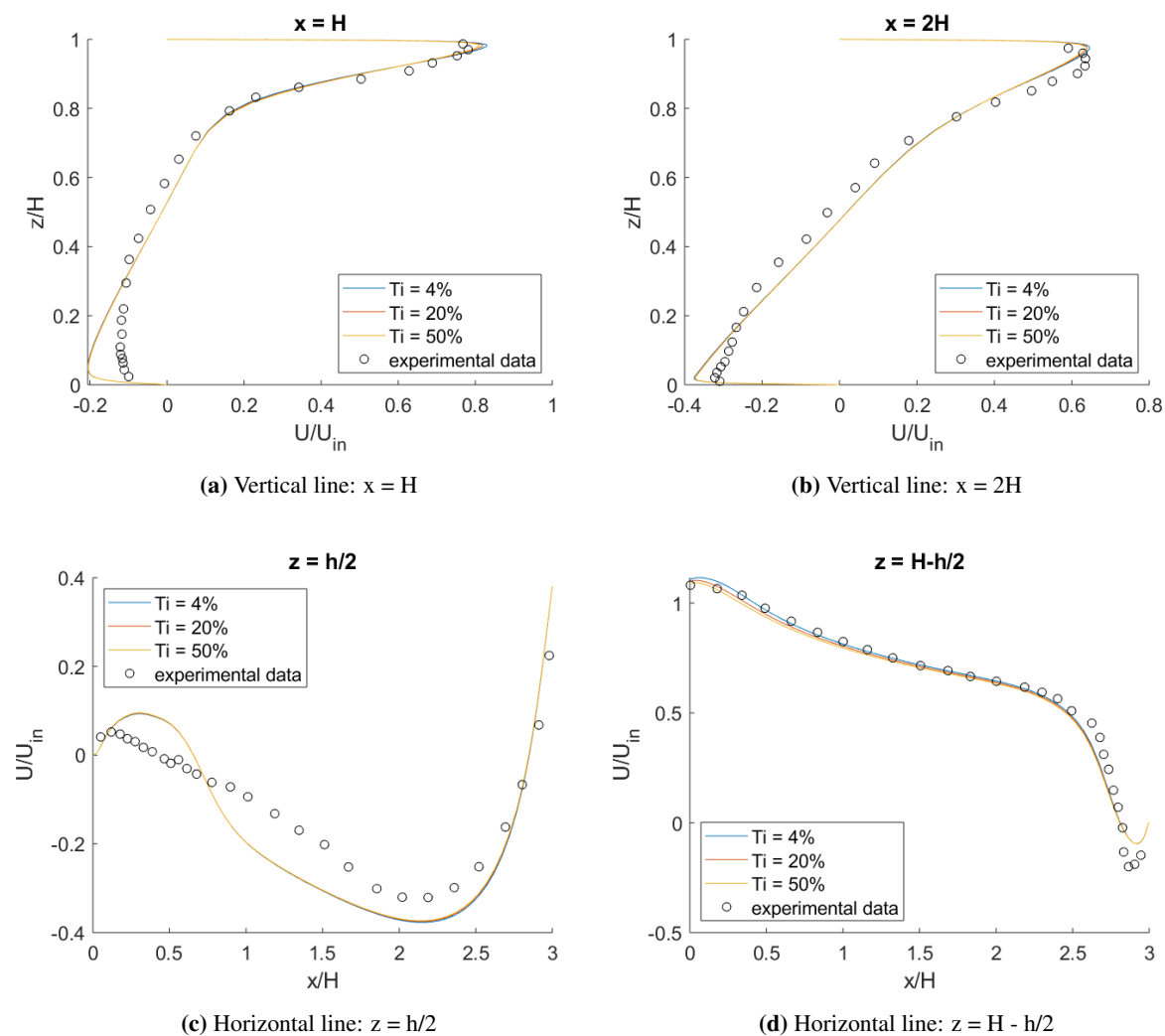
Figure 5.6: Comparison of velocity profiles for different values of T_i imposed at the inlet.

5.2   Benchmark 3

Benchmark 3 was simulated for the case with Re = 7100 to enable comparisons with Limane et al. [31]. The benchmark is simulated as an isothermal case, as the main motivation for this simulation was to see how B3 compares to B2 as both cases are supposedly fully turbulent. Furthermore, the buoyancy effects are very limited for this benchmark and the velocity measurements were also done for an isothermal case. Simulations were done in 3D only.

5.2.1   Grid sensitivity analysis

Four different meshes were created for benchmark 3. A very coarse mesh with 521 thousand cells, a coarse mesh with 854 thousand cells, a medium mesh with 1.7 million cells and a fine mesh with 6.3 million cells. For this benchmark, it was particularly challenging to keep $y^+ < 5$ at the walls because of the high inlet velocity. This needed a very thin cell near the wall, leading to very high aspect ratios for the coarsest meshes. The two coarsest meshes have a significant amount of cells with $y^+ > 5$. While the medium and the fine mesh can be said to have satisfying y^+ values. Overall the meshes have more cells than the meshes for B2 since this benchmark is considerably wider – thus more divisions are needed in

the y-direction – and additionally a higher level of wall refinement was needed.

The results from the mesh size comparison can bee seen in figure 5.7. The standard k-ϵ model was used. Turbulent intensity at the inlet was set to $T_i = 5\%$ and the hydraulic diameter was used for the calculation of ϵ – i.e. $\ell = 0.07D_h$. This is similar to the values used by Limane et al. [31]. The simulation converged to a steady state solution in all four cases. Small oscillations were seen in the residuals, but at very low values, around 10^{-6} for velocity, k and ϵ, and around 10^{-3} for continuity. It was tested to average over 1000 iterations, but this had a negligible impact on the result. The velocity profiles are plotted at the same locations as for B2, and taken at the midplane, however for B3 experimental data are only available at x = 2H.

(a) x = H

(b) x = 2H

(c) z = h/2

(d) z = H - h/2
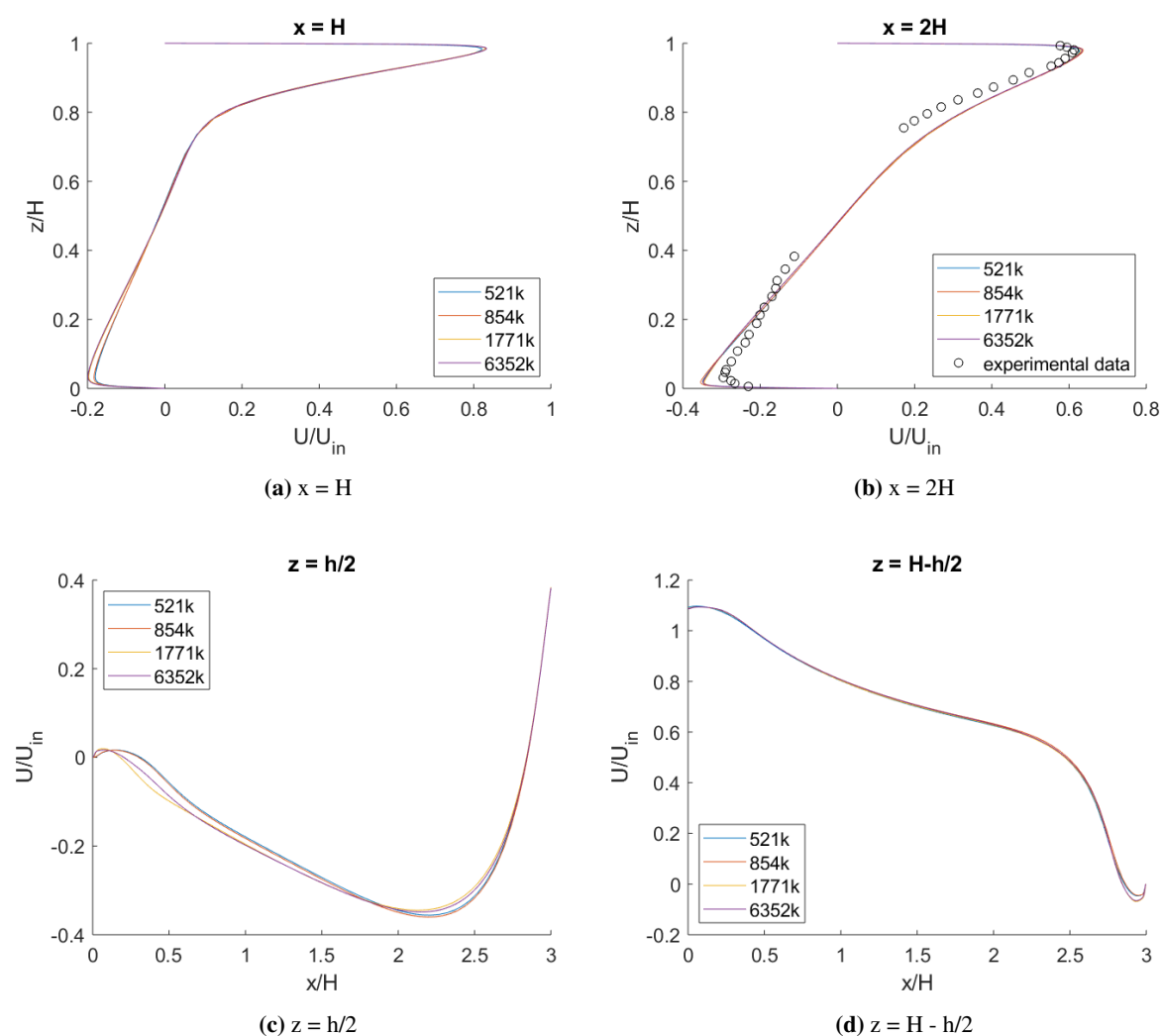
Figure 5.7: Grid sensitivity analysis of benchmark 3, using the standard k-ϵ model.
Legend refers to number of cells in mesh.

Looking at figure 5.7 some small differences can be seen between the fours solutions. Similarly to B2, the larges differences are seen at the line z = h/2. Here the two coarse meshes, which have very similar solutions, deviate from the medium and fine mesh. A small difference can also be seen between the medium and fine mesh in figure 5.7c at 0 < x/H < 0.5. Except for this the medium and fine solution are very similar, thus it was decided to use the medium mesh as the computational requirement for the fine mesh is very large. The layout of the medium mesh is shown in appendix A figure A.2. y^+ values

for the medium mesh is shown in table 5.5. The values at the front and back walls are not satisfying, however, since the cavity is so wide this should not have a huge influence.

Table 5.5: Average and maximum y^+ values at the different cavity walls for B3 medium mesh.

	Ceiling	Right wall	Floor	Left Wall	Front Wall	Back wall
Average	1.1	1.2	2.1	1.1	33.3	33.3
Max	2.8	5.3	4.2	3.0	78.8	78.8

5.2.2   Turbulence modelling

Four turbulence models were tested on B3, standard k-ϵ, RNG k-ϵ, realizable k-ϵ and SST k-ω. The velocity profiles obtained with the different models are shown in figure 5.8.

(a) x = H

(b) x = 2H

(c) z = h/2

(d) z = H - h/2
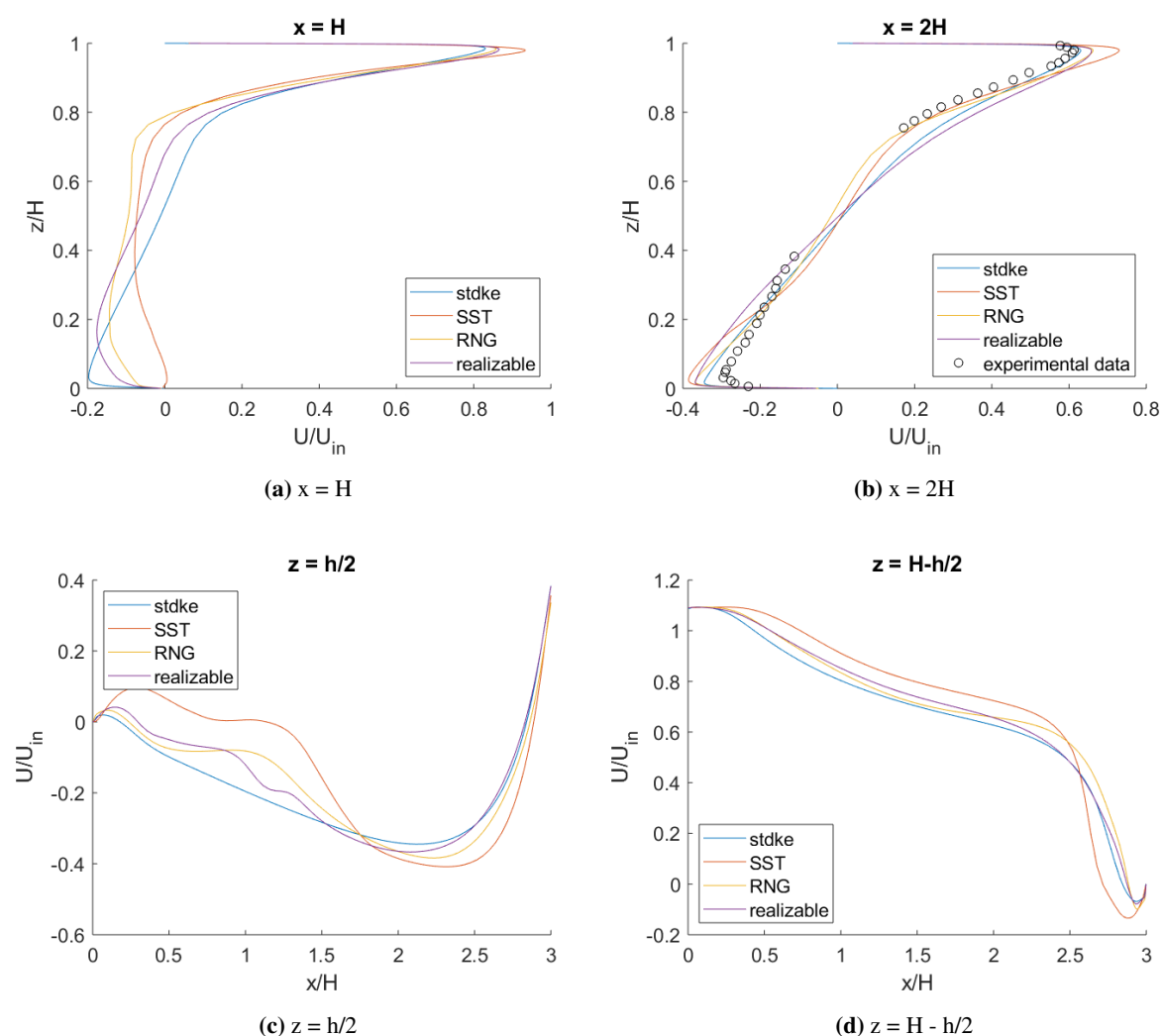
Figure 5.8: Turbulence model comparison for Benchmark 3.

Since B3 only has experimental data at x = 2H, it is more difficult to know which model overall gives the best agreement with experiments. Furthermore, it was the experimental data at x = 2H which had the best agreement with the simulations for B2. Nonetheless, the results for B3 are in many ways similar to those obtained for B2 with the same turbulence models. Looking at figure 5.8d the SST k-ω model predicts a higher jet velocity than the other models, similar to what was seen for B2. Looking at the left part of figure 5.8c it is once again seen velocity profiles with local extrema. However, this also looks like the figure with the largest deviation from the B2 result. The SST k-ω model predicts a large zone with positive values for U, and the immediate dip in velocity seen with the RNG and realizable k-ϵ models for B2 is not seen here. Looking at the RMSE values in table 5.6 the standard and RNG k-ϵ models seem to give the best agreement with experiments at x = 2H, which was also the case for B2.

Table 5.6: RMSE values for the different turbulence models tested on B3.

	stdke	SST	RNG	realizable
x = 2H	0.047	0.071	0.050	0.075

The B3 simulation has an even higher Reynolds number than B2, 7100, thus it is even more likely that this flow is fully turbulent. For B3 one more model converged to a steady state solution – the realizable k-ϵ model – while oscillations are still seen in the mean flow field for the RNG k-ϵ and the SST k-ω model. These oscillations are caused by secondary flow structures emerging in the left part of the cavity that change location from iteration to iteration. For the RNG k-ϵ model these secondary flow structures are vortices close to the corners with the front and back walls. Since B3 is much wider than B2, these vortices have a smaller impact on the velocity profiles in the midplane where the data are extracted from. For the SST k-ω model, small vortices are seen across the whole width W and the flow pattern is in general more chaotic. This is shown in Appendix B figure B.4 where velocity contours at an isosurface z = h/2 are plotted. Velocity contours in the midplane are also shown in figure B.3.

In he's PhD. thesis Nielsen [34] addresses the question of a stable or unstable flow in chapter 2.4.3, looking at B3, but varying the length of the cavity from L/H = 6 to L/H = 2. From flow visualization photos it is shown that the flow is unsteady for L/H = 6 and L/H = 5. For L/H = 4 there are still weak oscillations in the flow, but he writes: "In practice, however, we may consider the flow as steady in the main part of the model" ([34] p. 33). For L/H = 3, which is the case for this simulation, it is concluded that the flow is steady and two-dimensional. Thus, B3 is probably close to the limit of stable vs unstable flow and some turbulence models produce a stable solution and some an unstable solution. This might also be the case for B2.

Comparing the results in figure 5.8 to the results from Limane et al. [31] in figure 3.18, it looks like the simulation by Limane et al. [31] has slightly better agreement with the experimental data. In general, the velocity is slightly lower in the top and bottom part of the cavity, thus avoiding the overprediction seen in figure 5.8. This may be caused by Limane et al. [31] simulating without any inlet and outlet lengths. It is shown later that for B4 this slightly decreases the velocity along the ceiling and floor. Limane et al. [31] do not mention oscillating residuals, and reports that the simulation was stopped after residuals reached constant values less than 10^{-6}. Limane et al. [31] also used the SST k-ω model and the RNG k-ϵ model so this is in contrast to the result obtained in this thesis.

It is interesting that one more turbulence model converges to a steady state solution when the inlet Reynolds number increases. This implies that a higher level of turbulence might favour a steady state solution for the realizable k-ϵ model. There is however not only the inlet Reynolds number that is different from B2, but also the width of the cavity. With all the k-ϵ models vortices are seen in the corners with the front and back walls, thus the transition to a steady state solution with the realizable k-ϵ model can also be caused by these vortices no longer interacting with each other.

5.3 Benchmark 4

Since B4 is non-isothermal a selection must be made for buoyancy modelling and a discretization scheme must be selected for the energy equation. The buoyancy effects were modelled with the incompressible ideal gal law. This is suitable for incompressible flows. It was also tested to use the Boussinesq approximation, and very small differences were observed. The energy equation was discretized with the second order upwind scheme.

5.3.1 Grid sensitivity analysis

Since B4 is described in the experiment report [5] as a 2D flow and has been successfully simulated in 2D by Blay et al. [5], an initial grid sensitivity study was done in 2D to reduce computational times. Four different 2D meshes were created, with 4, 7, 18 and 39 thousand cells. All meshes had mesh refinement near the walls to keep $y^+ < 5$. The RNG k-ϵ model was used for the grid sensitivity analysis. The inlet turbulent intensity was set to $T_i = 6$ % which is what was measured by Blay et al. [5], and the hydraulic diameter was used to calculate ϵ and ω. Following the same procedure as the two papers presented in the literature review for this benchmark ([29] and [5]) the meshes were created without inlet and outlet length l and b. There is no picture of the actual experimental setup in the report, thus it is not possible to know exactly what conditions are present upstream and downstream of the inlet and outlet. The simulations by Blay et al. [5] and Kosutova et al. [29] have however shown that good results can be obtained by simulating without inlet and outlet lengths.

As can be seen from figure 5.9 the differences in the predicted velocities for the four different meshes are very small. Thus, it was concluded that the 7k mesh is sufficient for further simulations. The layout of the 7k mesh is shown in appendix A figure A.3. The y^+ values are displayed in table 5.7.

There is however not such great compliance between the experiments and the simulations. The velocity is over predicted along the floor and the temperature is under predicted in the entire room. As Kosutova et al. [29] got a better result with the RNG k-ϵ model simulating in 3D, this result might suggest that the flow should be simulated in 3D, as the front and back walls would add more friction and reduce the velocity. Benchmark 4 is the narrowest cavity with W = 0.3H.

(a) Velocity profile: z = H/2, y = W/2

(b) Velocity profile: x = L/2, y = W/2

(c) Temperature profile: z = H/2, y = W/2

(d) Temperature profile: x = L/2, y = W/2
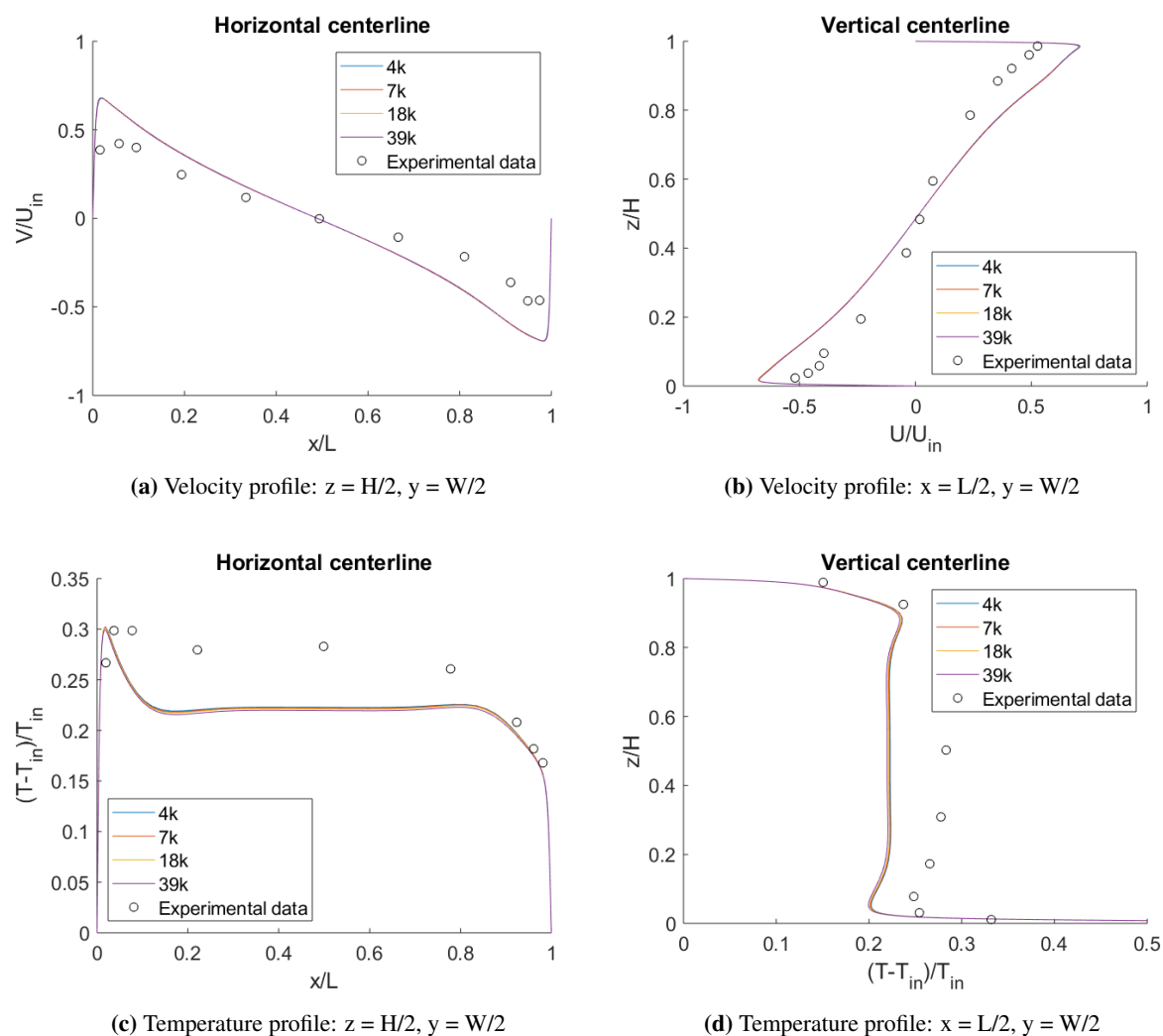
Figure 5.9: Comparison between simulations and experimental data for different mesh refinements using the RNG k-ϵ model. Legend refers to number of cells in the mesh.

Table 5.7: Average and maximum y^+ values at the different cavity walls for B4 with 7k mesh.

	Ceiling	Right wall	Floor	Left Wall
Average	1.5	1.5	1.6	1.46
Max	5.6	5.7	6.0	2.9

5.3.2   Geometrical configuration

In this subsection both the validity of the assumption of a 2D flow and the assumption of zero inlet and outlet lengths are tested.

Impact of inlet and outlet length

To test this a mesh was created with l = b = 0.3 m. Other than this the mesh was equal to the mesh with

7 thousand cells. The result can be seen in figure 5.10. This was only tested in 2D.

(a) Velocity profile: z = H/2, y = W/2

(b) Velocity profile: x = L/2, y = W/2

(c) Temperature profile: z = H/2, y = W/2

(d) Temperature profile: x = L/2, y = W/2
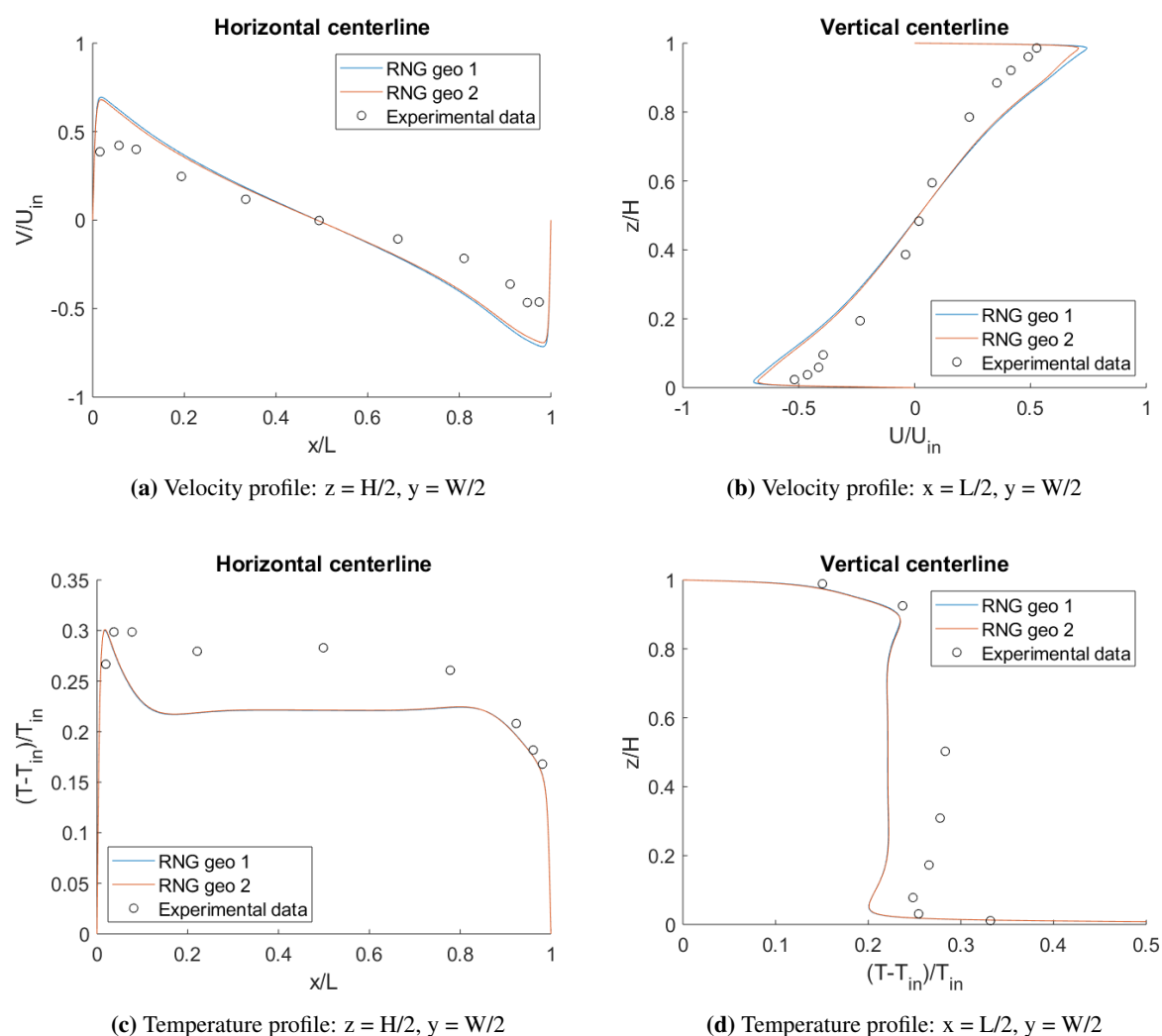
Figure 5.10: Comparison between simulations and experimental data for different geometrical configurations using the RNG k-ϵ model. Geo 1 refers to with inlet and outlet lengths and Geo 2 to with zero inlet and outlet lengths.

As seen in the figures the profiles are very similar and do not depend heavily on the choice of inlet and outlet geometry. There are however noticeable smaller velocities in the jet when simulating without any inlet and outlet lengths. This is possibly because the uniform velocity profile is imposed straight into the cavity without any inlet length, increasing the velocity gradients in the shear layers and thus increases the deceleration of the flow. Overall however, the difference is very small and it is therefore concluded that it is sufficient to simulate without any inlet and outlet lengths for this benchmark. This conclusion was also extrapolated to 3D, as it simplifies the geometry and reduce computational times. It is also what has been done in literature for this benchmark. It can't be known with certainty that the conclusion would be the same in 3D, but as good results are obtained without inlet and outlet lengths in 3D by Kosutova et al. [29] and the 2D investigation implies the difference is small, it is a well judged assumption.

3D vs 2D

Still using the RNG k-ϵ model the flow was simulated in both 2D and 3D and the results were compared
with the experimental data. The 3D mesh was based on the 2D mesh with 7 thousand cells, then extend-
ing the mesh in the third dimension with 27 divisions. The mesh was refined near the front and back
walls to have a maximum y^+ value of 5.8 and an average value of 1.3. Other than this the y^+ values
were very similar to the 2D mesh. The 2D vs 3D comparison is shown in figure 5.11.

(a) Velocity profile: z = H/2, y = W/2

(b) Velocity profile: x = L/2, y = W/2

(c) Temperature profile: z = H/2, y = W/2

(d) Temperature profile: x = L/2, y = W/2
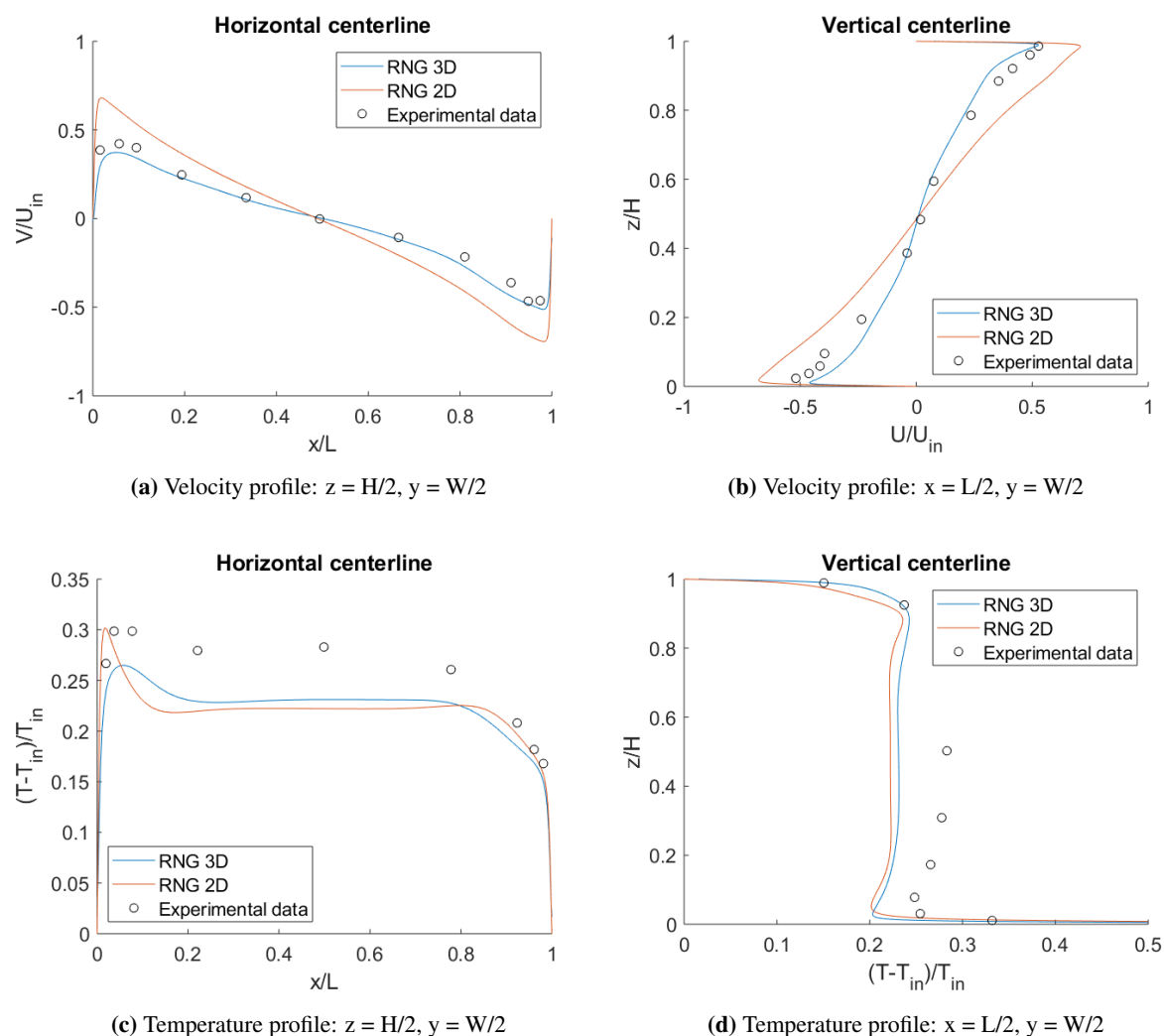
Figure 5.11: Comparison between simulations and experimental data simulating in
2D and 3D using the RNG k-ϵ model.

Obvious differences can be seen between the two solutions. Looking at the velocity profiles in
figure 5.11 the compliance between the simulations and the experimental data is significantly improved
by simulating in 3D. The 3D velocity profile is in fact very similar to that of Kosutova et al. [29], and
thus strengthens the hypothesis that the RNG k-ϵ model is capable of simulating this flow. Looking at
the temperature, the fit is also improved by simulating in 3D, however, the improvement is smaller than
for the velocity.

Based on these results it seems that although the benchmark flow was designed to be 2D, it should
be simulated in 3D to get the best results. The most likely explanation is that this cavity is so narrow
that the friction from the front and back walls are significantly affecting the velocity in the flow.

5.3.3 Turbulence modelling

Five different RANS turbulence models were tested on benchmark 4. The comparison is done in 3D as the results from the 3D vs 2D comparison suggested this is the more correct approach for this benchmark. The five models are the standard k-ϵ, RNG k-ϵ, realizable k-ϵ, standard k-ω and SST k-ω. Each simulation gave oscillatory residuals, thus the results were averaged over 2000 iterations for each model. Testing with the RNG k-ϵ revealed there was no difference between averaging over 250 iterations and 1000 iterations, but as this could be model dependent 2000 was used to be certain the result would not be dependent on the number of averaged iterations. Figure 5.12 show the velocity and temperature profiles obtained with the different models.

(a) Velocity profile: z = H/2, y = W/2

(b) Velocity profile: x = L/2, y = W/2

(c) Temperature profile: z = H/2, y = W/2

(d) Temperature profile: x = L/2, y = W/2
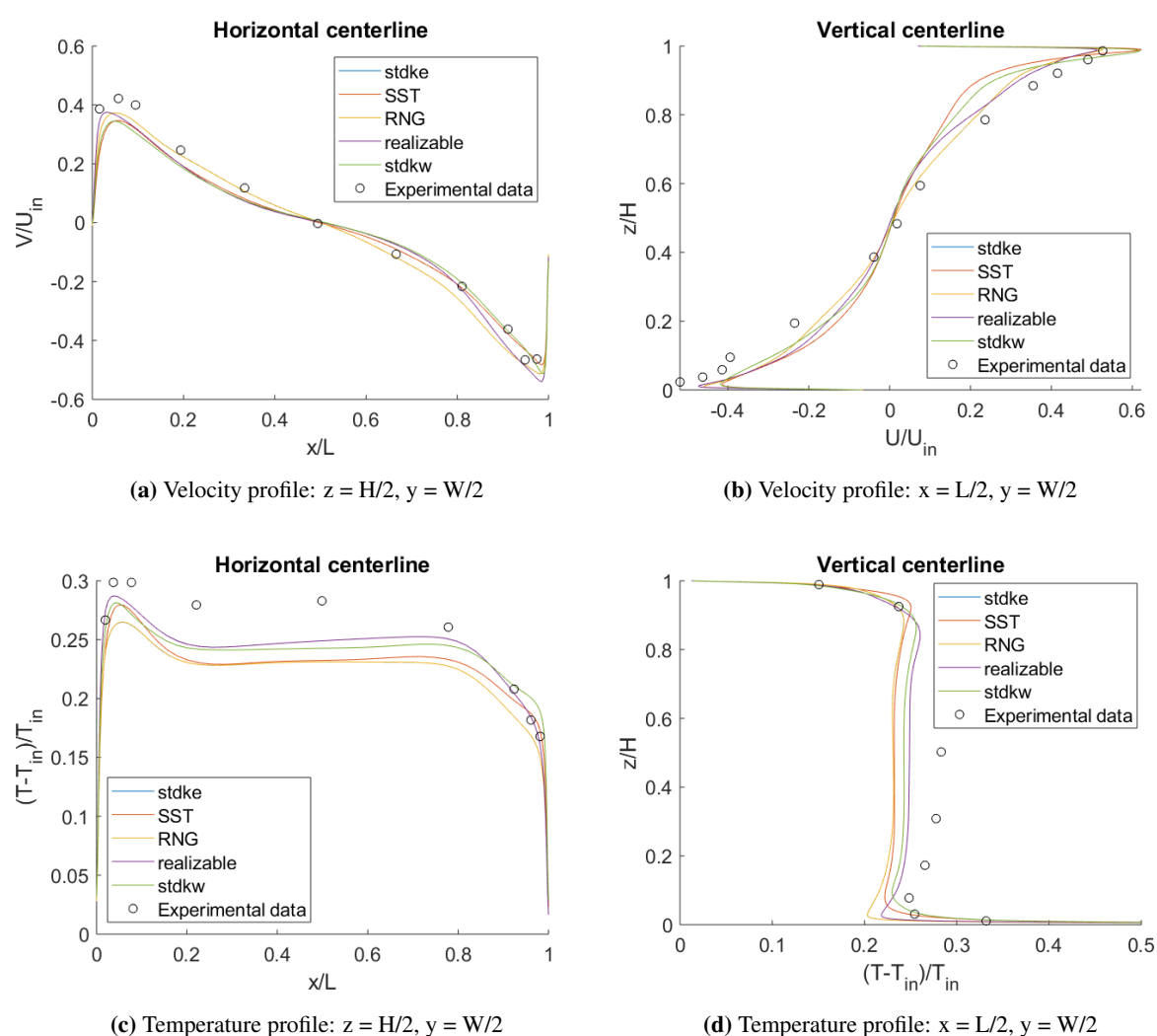
Figure 5.12: Comparison between five different turbulence models and experimental data for Benchmark 4.

Looking at figure 5.12 one can see that neither turbulence model gives a completely erroneous result, all are capable of predicting a fairly correct flow pattern in the cavity. There are however some differences. The two k-ω models overpredict the maximum velocity for the jet along the ceiling, and the velocity gradient in the negative z-direction is too high resulting in a too low velocity

in the upper part of the room compared to both the experiments and the k-ϵ models. All models underpredict the velocity in the jet along the floor, and also here the k-ω models are furthest away from the experimental value. The velocity contours at the midplane are shown in Appendix B figure B.5.

Looking at the temperature profiles in figure 5.12 most noticeable is probably that all models underpredict the temperature in the room. The temperature is too low in both the vertical and horizontal profiles for the majority of the experimental data points. Furthermore, the increase in temperature along the left wall seen in figure 5.12c is sharper than the experimental data indicates. Thus, the result indicates that the turbulence models underpredict the mixing of hot air with cold, as the concentration of hot air in the left part of the room seems to be too high. The realizable k-ϵ model gives the best agreement between simulation and experiment, but the differences are quite small.

Table 5.8: RMSE values for the different turbulence models tested on B4.

	z = H/2 velocity	x = L/2 velocity	z = H/2 temp.	x = L/2 temp.	Average velocity	Average temp.
stdke	0.049	0.066	0.035	0.044	0.057	0.040
SST	0.061	0.100	0.029	0.034	0.080	0.032
RNG	0.049	0.066	0.035	0.044	0.057	0.040
realizable	0.049	0.067	0.019	0.028	0.058	0.024
stdkw	0.060	0.077	0.024	0.028	0.069	0.026

Table 5.8 shows the RMSE values for the different turbulence models used on B4. The average values for velocity are noticeably lower than the average RMSE values for B2 in table 5.4, however, a comparison should be made with care as the set of measurement lines are dissimilar. The largest deviation between experiments and the simulations seemed to be in the vicinity of the corners for B2. For B4 the two lines of measurements are in the center of the cavity, and therefore no measurements have been done in the corners. Nonetheless, the difference between the turbulence models seems to be smaller for B4 and the overall compliance with experiments slightly better than for B2. It is hard to know exactly why this is the case. One possible explanation is that B4 is narrower and the flow is more constrained by the walls. Hence, the largest possible error is smaller.

All models show moderate to good performance, but the k-ϵ models seem to be the better option for benchmark 4. These three models give slightly better results for the velocity profiles. In particular the realizable k-ϵ model seems to be the best option as it gives the most correct estimation of the room temperature. The SST k-ω model gives the overall worst performance, and it also gives a slightly odd flow pattern seen in figure B.5d.

5.3.4   Transient vs steady state

As mentioned previously all the 3D steady state simulations gave oscillatory residuals, and the results were therefore averaged over 2000 iterations for all the turbulence models. The type of oscillatory

behaviour is shown in figure 5.13. As discussed in section 4, this lack of convergence is typical for the ventilated cavity flow. The method of averaging over the residuals is the most cost effective way to obtain a statistically independent solution that is satisfactory for many cases. However, since the 3D mesh of benchmark 4 is quite small due to the small width this benchmark was selected for comparing the results from a steady state simulation with taking the average over several iterations and a transient simulation and then averaging over time. A transient RANS simulations is commonly referred to as an Unsteady-RANS (URANS) simulation.

(a) RNG k-ϵ **(b)** SST k-ω
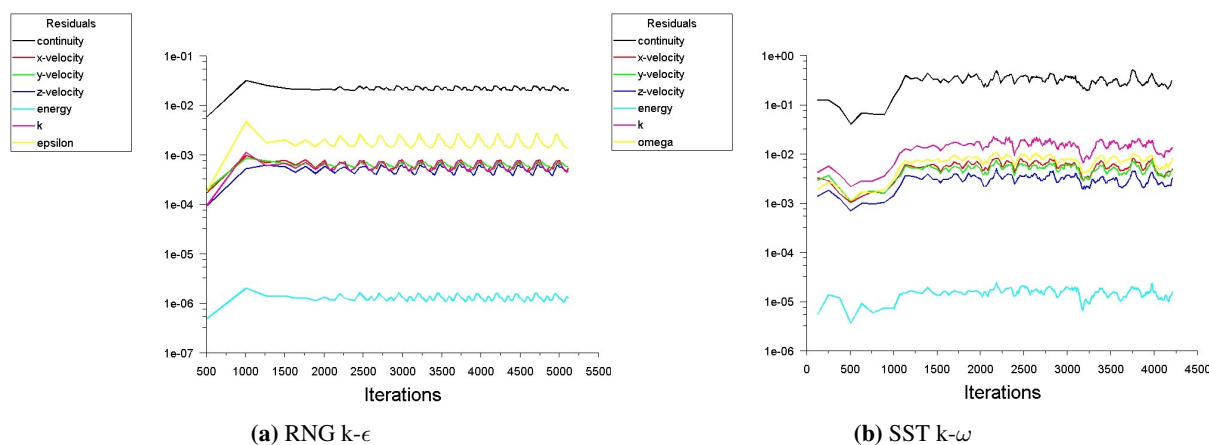
Figure 5.13: Examples of oscillatory behaviour obtained when simulating B4 in 3D.

Simulations were run again in transient mode for three turbulence models: RNG k-ϵ, realizable k-ϵ and SST k-ω. The settings for the transient simulations were kept equal to the steady state simulations, other than the switch to transient mode and a selected time step of 0.004 seconds. This kept the maximum Courant number below 2 for the entire simulation. The transient simulation was started with the data from the steady state simulation as running from t=0 was very time consuming. It was tested with the realizable k-ϵ model to average over a time span of 40, 80 and 120 seconds. Very little difference was observed between averaging over 80 and 120 seconds, thus the results from averaging over 80 seconds are presented for all models. Figures 5.14, 5.15 and 5.16 show the results using the RNG k-ϵ model, the realizable k-ϵ model and the SST k-ω model, respectively.

(a) Velocity profile: z = H/2, y = W/2

(b) Velocity profile: x = L/2, y = W/2

(c) Temperature profile: z = H/2, y = W/2

(d) Temperature profile: x = L/2, y = W/2
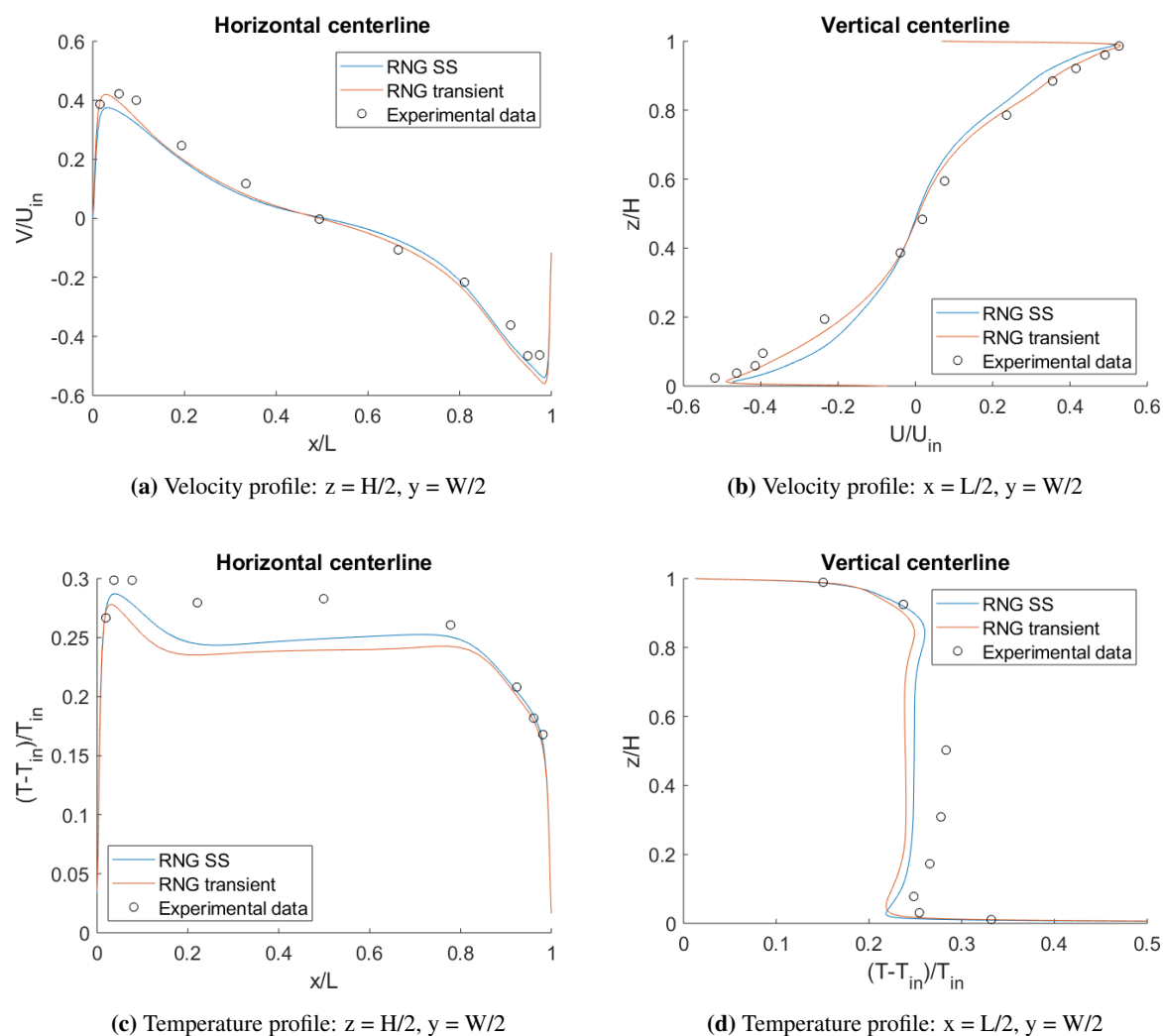
Figure 5.14: Comparison between steady state and transient simulation with RNG k-ϵ model.

Looking at figures 5.14 to 5.16 one can see that there is a slight difference between simulating in steady state and transient for all three turbulence models. There are however differences in the magnitude of the difference and whether simulating in transient is an improvement or not.

For the RNG k-ϵ model the difference is the smallest and neither method is significantly better than any other. The transient simulation gives a slightly better prediction of the velocity along the left wall and the floor, but is slightly worse along the right wall. For temperature the difference is marginal.

With the realizable k-ϵ model the transient velocity profile is in better agreement with the experiments. The steady state simulation gives too low velocities in both the upper and lower part of the cavity and this error is smaller for the transient simulation. However, when we look at the temperature profile the transient simulation gives a larger error compared to the experiment. Thus, overall one cannot conclude that the transient simulation shows better compliance with experiments.

(a) Velocity profile: z = H/2, y = W/2

(b) Velocity profile: z = H/2, y = W/2

(c) Temperature profile: z = H/2, y = W/2

(d) Temperature profile: x = L/2, y = W/2
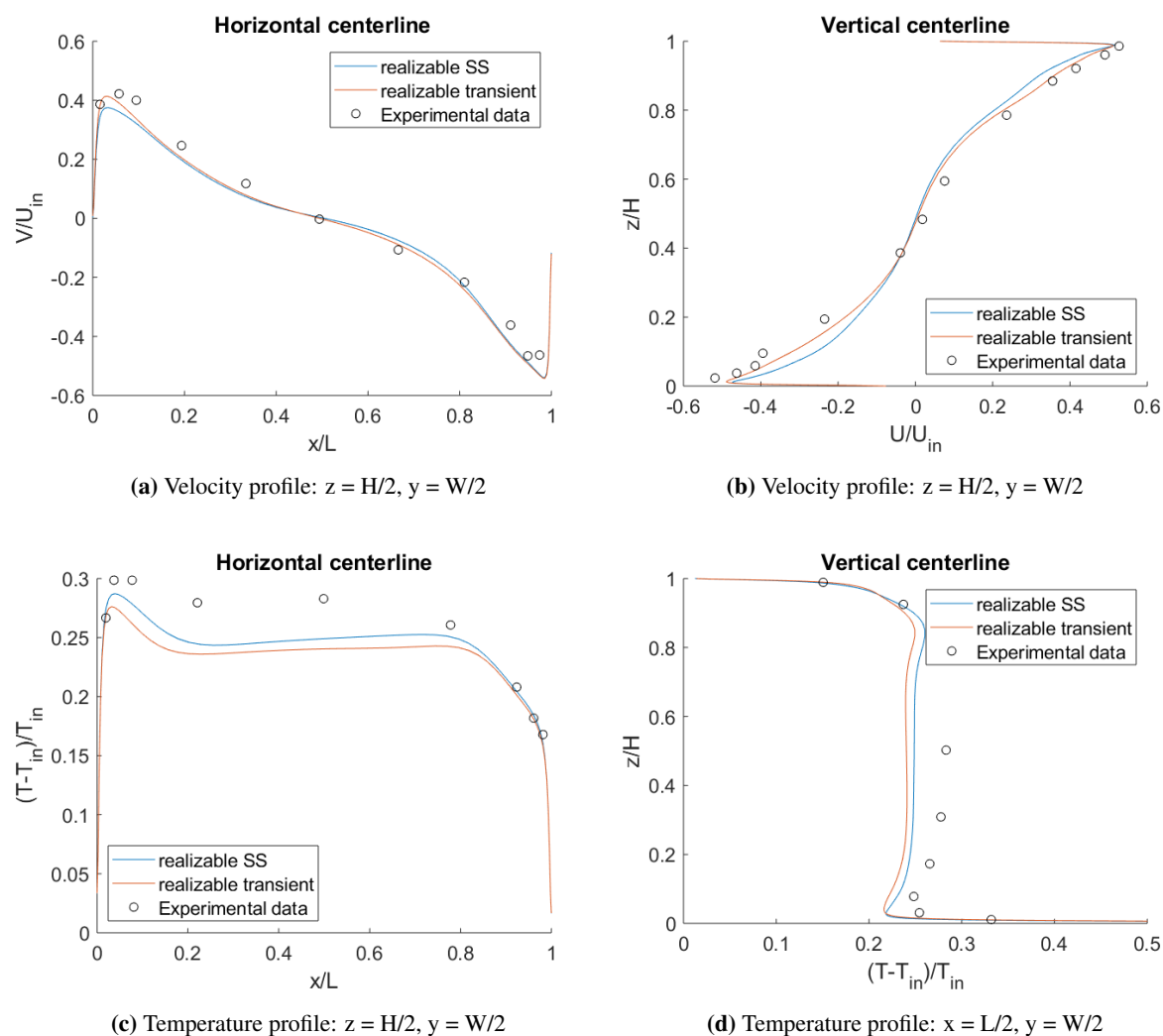
Figure 5.15: Comparison between steady state and transient simulation with
realizable k-ϵ model.

Using the SST k-ω model there is a difference in the velocity profile, however, the deviation from
the experiments seen in the steady state simulation is not significantly improved switching to a transient
simulation. The only improvement is a small reduction in the overprediction of the maximum velocity
of the inlet jet. However, looking at the temperature profiles the transient simulation is significantly
closer to the experimental data, both in values and in terms of the shape of the profile, since the velocity
peak in the left side of the room is too sharp in the steady state simulation.

Overall, switching to a transient simulation improves the velocity prediction with the realizable
k-ϵ model and the temperature prediction with the SST k-ω model. The temperature prediction with
the realizable k-ϵ model gets slightly worse when changing to a transient simulation, while for the
remaining profiles the difference is quite small. This is not strong enough indications to say that one
should simulate benchmark 4 in transient mode, but the fact that clear differences are observed that are
dependent on turbulence model and possibly also other parameters show that more research is needed
to conclude on this topic.

(a) Velocity profile: z = H/2, y = W/2

(b) Velocity profile: x = L/2, y = W/2

(c) Temperature profile: z = H/2, y = W/2

(d) Temperature profile: x = L/2, y = W/2
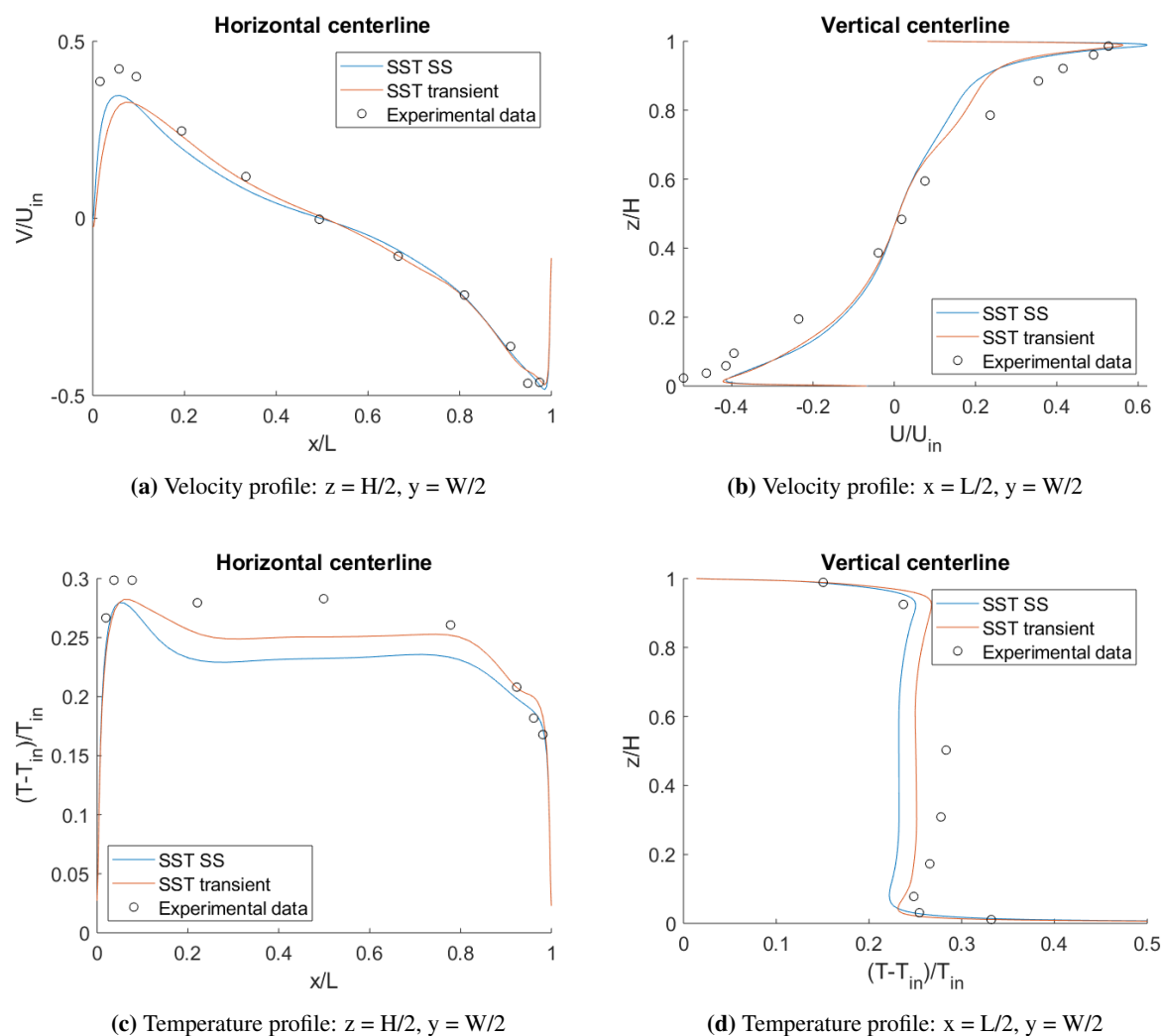
Figure 5.16: Comparison between steady state and transient simulation with SST
k-ω model.

5.4   Benchmark 5

Benchmark 5 was simulated using OpenFOAM 7 and not ANSYS Fluent like the other simulations. Only the case of Re = 1000 has been simulated and is what is presented in this section.

5.4.1   Grid sensitivity analysis

The grid sensitivity analysis of Benchmark 5 was done with the SST k-ω model as this had provided good results in the study by van Hooff et al. [21]. Simulations were only done in 3D, since van Hooff et al. [21] reported the flow cannot be approximated as 2D. Three meshes were created: a coarse mesh with 295 thousand cells, a medium mesh with 1.2 million cells and a fine mesh with 2.2 million cells. Similar to in the study by van Hooff et al. [21] oscillating residuals were observed for the simulation, thus the solution was averaged over 2000 iterations. 800 iterations were sufficient to give a very nearly statistically independent solution for the medium mesh. Therefore, 2000 was used as default, as different meshes could require a higher number of iterations. The meshes were structured and refined

near the walls to keep y^+ below 5, however, they had uniform spacing in the y-direction, thus there were no refinement near the front and back walls as mentioned in section 4. The upstream contraction is included in the mesh in order to make results comparable to those by van Hooff et al. [21]

The inlet turbulent intensity was set 6%, which was reported to match the experimental value by van Hooff et al. [21] and ω was calculated from the hydraulic diameter of the inlet. linearUpwind schemes was used for convective momentum terms, while limitedLinear with a limiter factor of 1 was used for k and ω. SimpleFoam was used as the OpenFOAM solver. As boundary condition at the walls omegaWallFunction was used for ω and kLowReWallFunction was used for k. A full description of the settings used in the OpenFOAM simulation can be seen in the Dict files attached in Appendix C.

The result from the grid sensitivity analysis can be seen in figure 5.17. The velocities are scaled with the bulk inlet velocity, and not the local maximum velocity for each profile as done by van Hooff et al. [21]. This was to see differences in the prediction of maximum velocity. The experimental data are shown with a dotted line rather than circles because the data points are very close together for B5.

(a) Vertical line: x = 0.3L

(b) Vertical line: x = 0.5L

(c) Vertical line: x = 0.8L
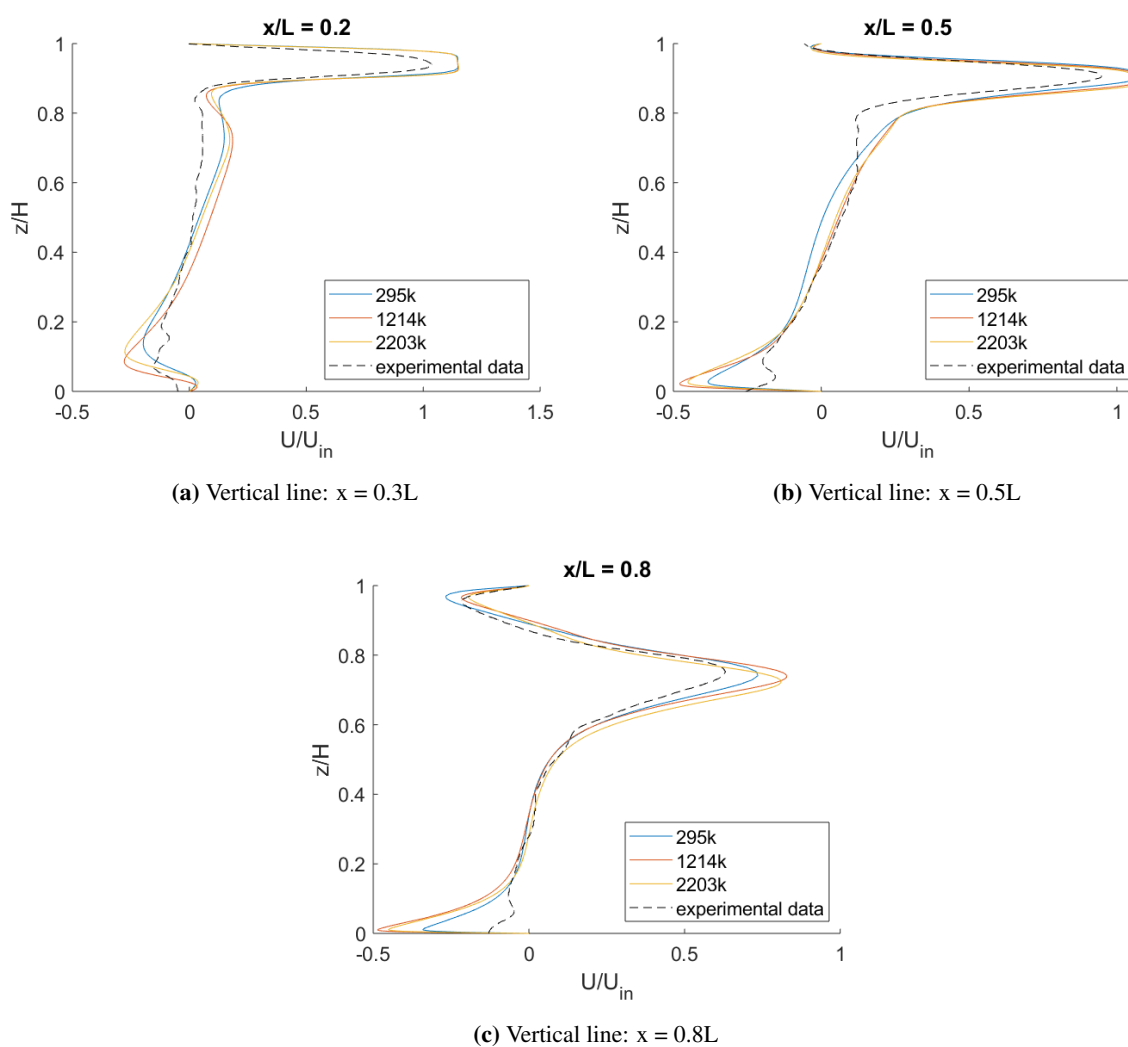
Figure 5.17: Grid sensitivity analysis for Benchmark 5 using the SST k-ω model. Legend refers to number of cells in the mesh.

Some differences can be observed between the three solutions in figure 5.17. In particular, different

velocities are predicted right above the floor, and different peak velocities in the jet at x = 0.8H. Some differences are seen between all three solutions, but overall the difference between the coarse and medium mesh is bigger than the difference between the medium and fine. For this reason, the medium mesh was selected for the remaining simulations. This is a slightly coarser mesh than that used by van Hooff et al. [21] where the mesh had 3.4 million cells, but is very similar to the mesh size used by Cao and Meyers [8] of 1.25 million. The layout of the medium mesh is shown in Appendix A figure A.4. The y^+ values of the medium mesh are shown in table 5.9. As can be observed in the table, the combination of a quite refined mesh and low inlet Reynolds number gives very low y^+ values.

Table 5.9: Average and maximum y^+ values at the different cavity walls for B5 with medium mesh.

	Ceiling	Right wall	Floor	Left Wall	Front wall	Back wall
Average	0.002	0.02	0.05	0.002	3.9	3.3
Max	0.1	1.1	1.2	0.1	41.8	41.5

5.4.2   Turbulence modelling

Four different turbulence models were tested on Benchmark 5. Standard k-ϵ, RNG k-ϵ, realizable k-ϵ and SST k-ω. The result is shown in figure 5.18. All models showed some degree of oscillating residuals, but the standard and RNG k-ϵ models had much more high frequent oscillations at lower values. These models seem to converge to a steady state solution, while the realizable k-ϵ and SST k-ω model have visible changes in the mean flow field from iteration to iteration. Thus, the same is seen for this Benchmark 5 as for Benchmark 2, whether the simulation converges to a steady state solution or not seems to be turbulence model dependent. To illustrate the differences in convergence the residuals from the four simulations are shown in figure 5.19

(a) Vertical line: x = 0.3L

(b) Vertical line: x = 0.5L

(c) Vertical line: x = 0.8L
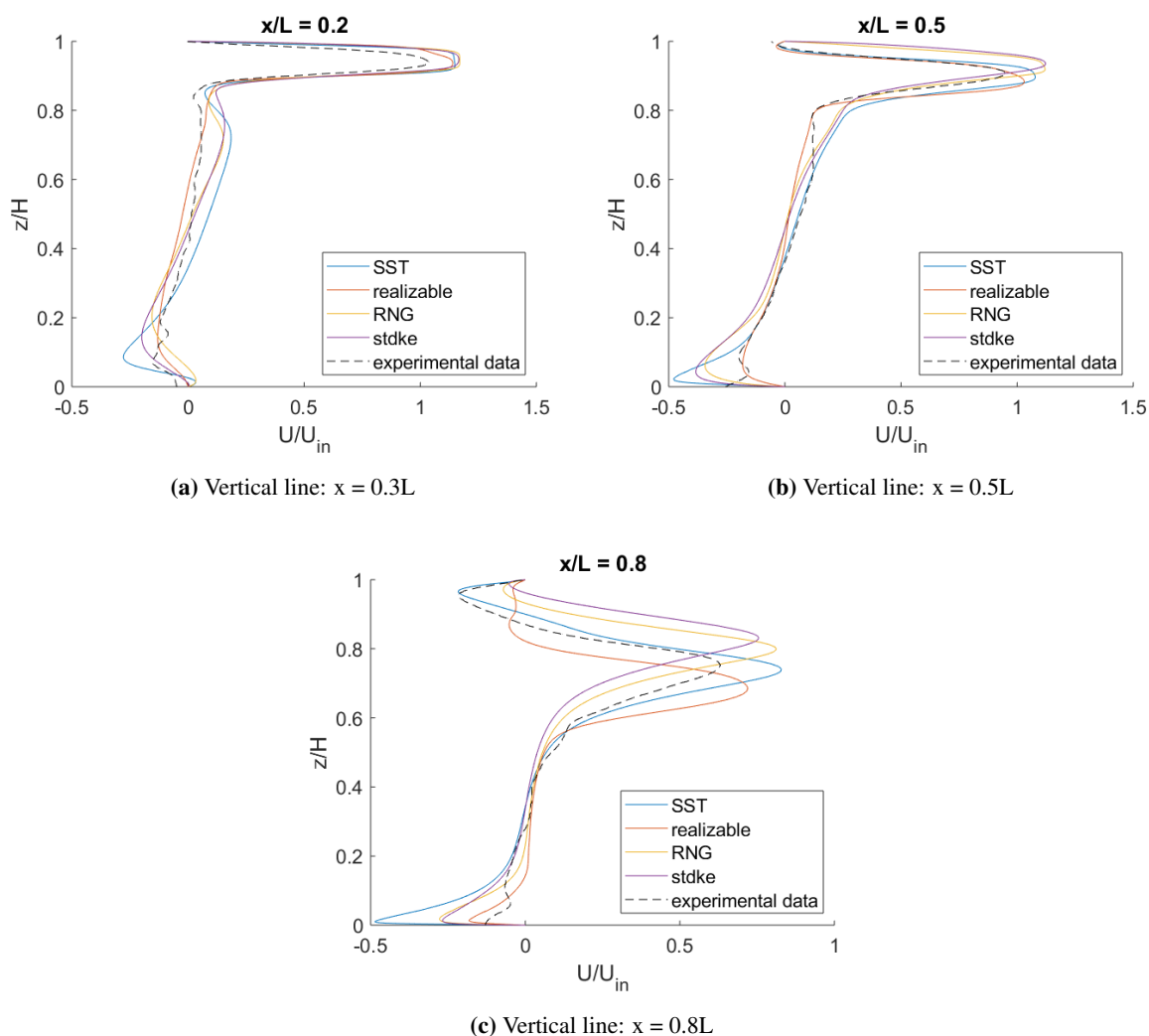
Figure 5.18: Turbulence model comparison for Benchmark 5 simulated on medium mesh.

Looking at the turbulence model performance in figure 5.18 it can be observed that the SST k-ω model gives a very good prediction of the detachment point for the inlet jet. This can be seen from the top part of figure 5.18c where the three other models seem to predict detachment further away from the inlet. All the models seem to overpredict the maximum velocity in the jet at all three lines of measurement. Large differences can also be observed in the velocity right above the floor, however here the measurements are inaccurate because of reflections from the glass floor, thus one cannot know which models give the most correct value. Overall the models give significantly different solutions, but neither is a perfect fit to the experimental data. The SST k-ω model seems to perform best, while the standard k-ϵ shows the largest deviation with experiments, at least in figure 5.18c. The velocity contours at the midplane are shown in Appendix B figure B.6. Here it is seen how different the models predict the jet detachment, and in general how the flow pattern varies significantly between the models.

Table 5.10: RMSE values for different turbulence models tested on B5. Values with
z/H < 0.15 have been omitted because of inaccurate measurements in this region.

	x/L = 0.2	x/L = 0.5	x/L = 0.8	Average
SST	0.112	0.088	0.077	0.092
realizable	0.094	0.085	0.146	0.108
RNG	0.107	0.153	0.167	0.143
stdke	0.109	0.180	0.230	0.173

The fact that the SST k-ω model gives the best compliance with experiments can also be seen in table 5.10, as it gets the lowest RMSE value. In particular, the SST k-ω model gives superior compliance at x/L = 0.8. The realizable k-ϵ model seems to have the second best fit, while the RNG k-ϵ and the standard k-ϵ get the highest RMSE values. If one compares the RMSE values for B5 with those from B2 in table 5.3 and B4 in table 5.8, one quickly realizes that overall the average values are much higher. Again, a direct comparison should be made with care as the set of experimental values are different. However, the differences are so large that it is still an indication that B5 is significantly harder to model for the RANS turbulence models than B2 and B4. When comparing with B2, it is natural to say that this is most likely because of the transitional flow regime of B5, compared to the supposed turbulent flow regime of B2. As RANS turbulence models are known to struggle with the transitional regime, this is an expected result. However, comparing B5 to B4, the inlet Reynolds numbers are more comparable – 684 for B4 and 1000 for B5. The flow regime of B4 is not known from the experiment report [5], however based on the inlet Reynolds number it is most likely transitional. Thus, the fact that the RANS turbulence models seem more capable of modelling B4 must be caused by something else. One possibility is the narrower and more constrained geometry of B4, another is that the buoyancy effects present in B4 has a significant impact and a third possibility is the fact that B4 has a much smaller ratio of h/H than B5 – 0.017 compared to 0.1. This means that although the Reynolds numbers are nearly the same B4 has a higher inlet velocity, causing higher velocity gradients that affect the generation of turbulence. It should however once again be stressed that the experimental values for B4 are not measured in the vicinity of the cavity corners. For both B2 and B5 this seems to be the areas with the largest deviation between simulation and experiments and the highest RMSE values, and this is most likely partly the reason why B4 has lower values.

(a) SST k-ω

(b) Realizable k-ϵ

(c) RNG k-ϵ

(d) Std. k-ϵ
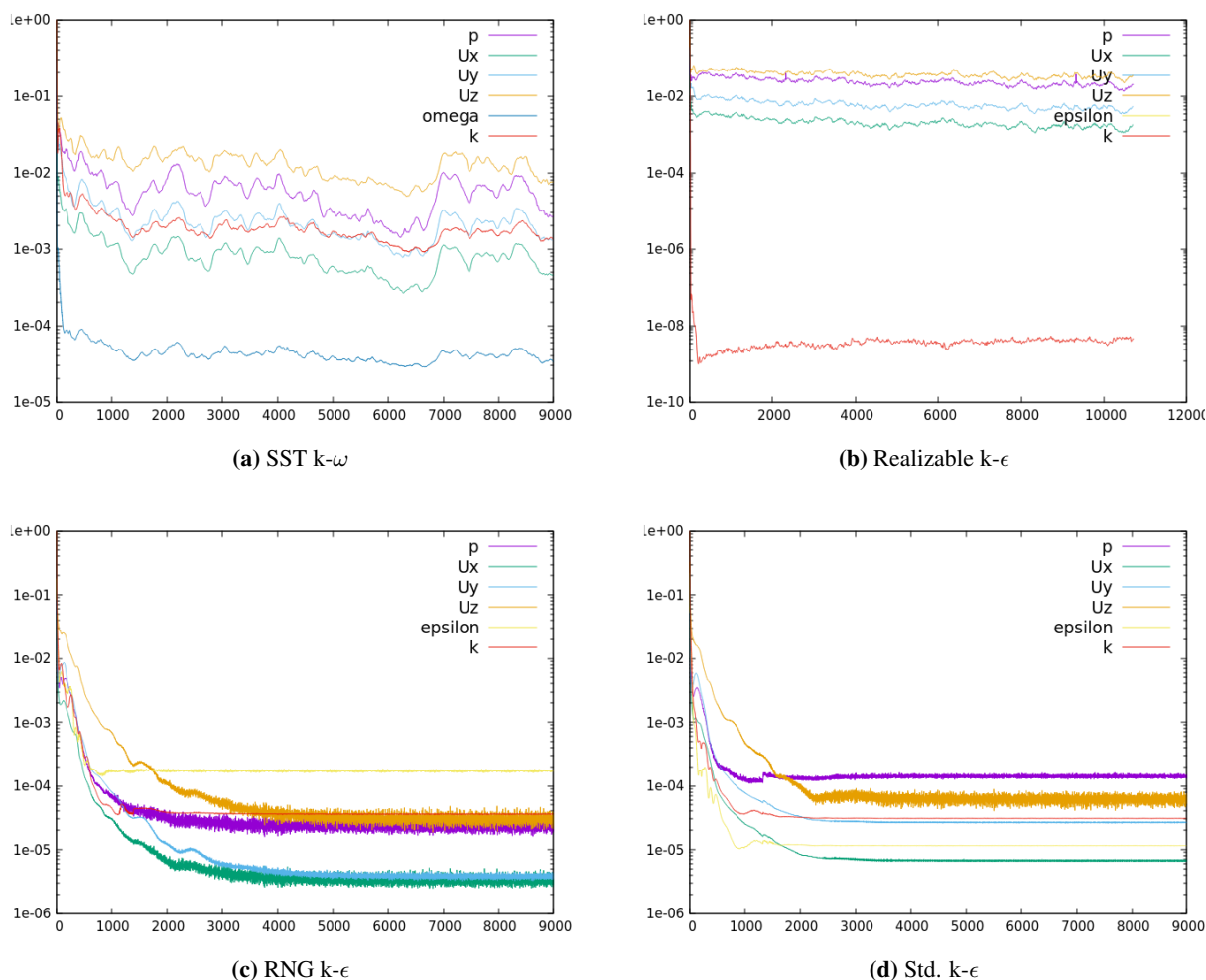
Figure 5.19: Residuals for the four different turbulence model simulations of
Benchmark 5.

It is interesting that the same situation regarding convergence and fluctuations in the mean flow field is observed in both Benchmark 2 and 5. The benchmarks have very different inlet Reynolds numbers – 5000 and 1000. B2 has been declared fully turbulent by the creators of the experiment [35] and B5 has been declared as a case of transitional flow [21]. That B5 is a transitional case was confirmed by injecting fluorescent dye in the center of the inlet opening: "From the flow visualizations, it can be concluded that transitional flow appears to be present for Re up to at least 2500." (van Hooff et al. [20] p. 502). Looking at the performance of the k-ϵ model however, it gives reason to believe that B2 is in fact fully turbulent and B5 is transitional. The standard k-ϵ model had the best performance of the turbulence models tested for B2 while it had the worst for B5. The standard k-ϵ model is a high Reynolds number turbulence model, known to struggle in the transitional regime, thus this behaviour seems to be in line with the believed flow regimes.

There are some plausible explanations to why these mean flow field oscillations are observed for both B2 and B5. One is that B2 could be transitional in some parts of the cavity. Second, it seems related to the choice of turbulence model, the SST k-ω and realizable k-ϵ models give oscillations in both cases, while the standard k-ϵ model converges to a steady state solution in both cases. This could be related to how the turbulence models handle certain aspects of the cavity flows that is not strictly related to the flow regime. Thirdly, it could be related to a numerical issue, but the fact that similar

oscillations are observed for many benchmarks and by several researchers makes this less likely.

5.4.3   Turbulent inlet parameters

It was also tested how varying the turbulence intensity imposed at the inlet affected the velocity profiles for Benchmark 5. This was also tested by van Hooff et al. [23] and Cao and Meyers [8], and both these studies found that this parameter had a significant influence on the velocity field.

The inlet turbulent intensity was set to three different values: 6%, 21% and 50%. The simulations were done with the SST k-ω model on the medium mesh and the solutions were averaged over 2000 iterations. ω was calculated from the hydraulic diameter of the inlet using equation (2.24) in all three cases. Other than this the settings were unchanged from what was reported in section 5.4.1. The velocity profiles obtained with the different values of T_i are shown in figure 5.20.

(a) Vertical line: x = 0.3 H

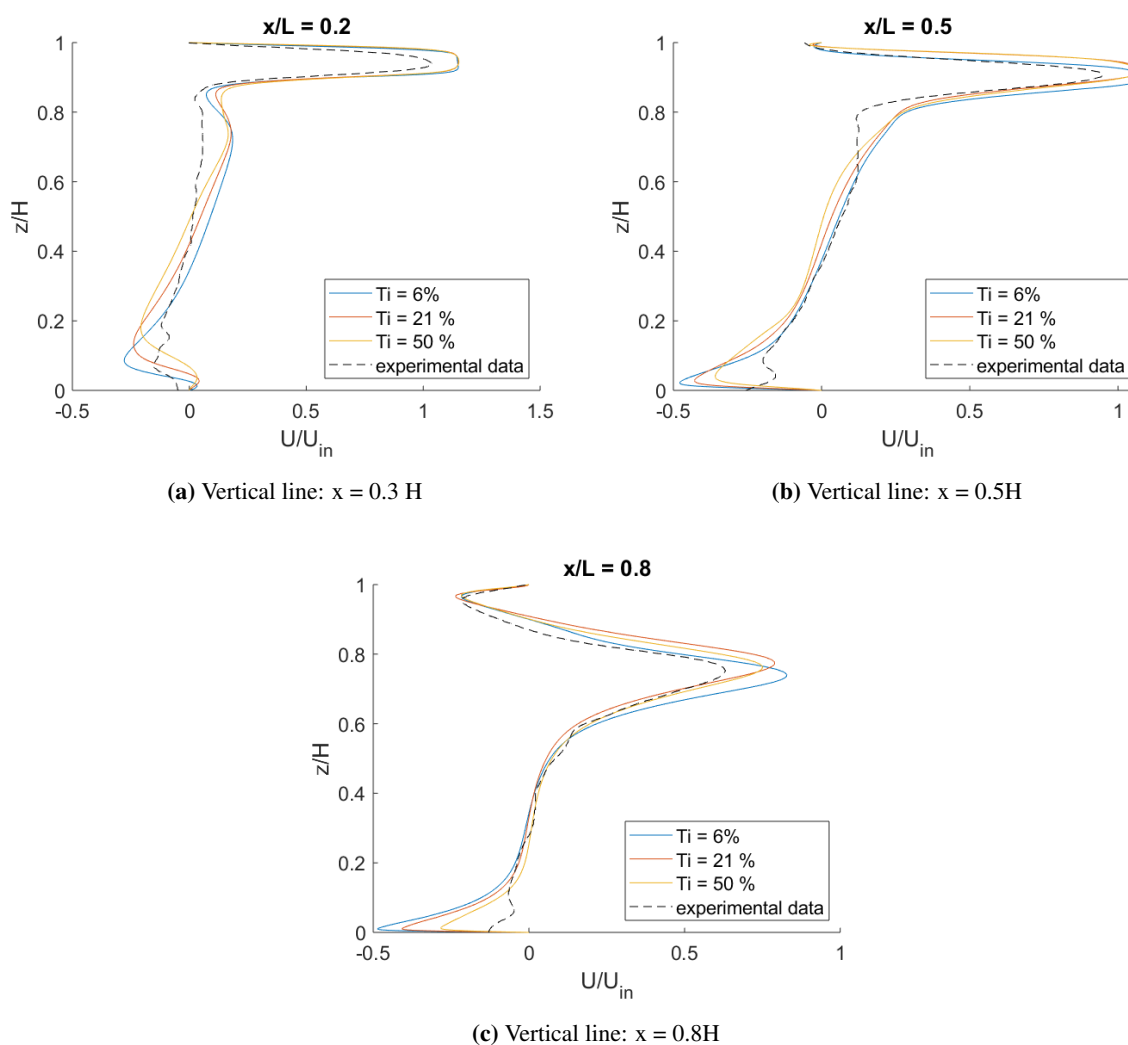(b) Vertical line: x = 0.5H

(c) Vertical line: x = 0.8H

Figure 5.20: Velocity profiles obtained with different values for the inlet turbulent intensity T_i. SST k-ω model on medium mesh.

From figure 5.20 it is clear that the inlet turbulent intensity has some effect on the calculated velocity profile. As one would expect, the maximum velocity at x/L = 0.8 decreases with increasing T_i,

as a higher level of turbulence increases the mixing in the shear layer and decelerate the flow further. The impact is also quite big on the predicted velocity just above the floor. Van Hoof et al. [23] report that increased inlet turbulent intensity reduces velocity gradients and causes a delayed detachment of the jet. The same is seen here, but it seems the effect is much smaller in this study. In the study by van Hoof et al. [23] the jet was still attached to the ceiling at x/L = 0.8 for T_i = 50%, while this is not the case in this study looking at figure 5.20c. The studies are however done for two different Reynolds numbers, Re = 1000 in this study and Re = 2500 in the study by van Hooff et al. [23], and this is likely to affect the result. Van Hooff et al. also used a different turbulence model – the low-Re k-ϵ model by Chang et al. [9] – which is another important difference.

Comparing the impact of changing T_i at the inlet for B2 and B5 – i.e. comparing figure 5.6 and figure 5.20 – it is observed that the impact is much larger for B5. This is something that also has been observed in literature. Thus, it seems like it is more important to have accurate knowledge of the turbulent inlet parameters when a case in the transitional regime is simulated compared to a case that is fully turbulent.

5.5   Benchmark 6 – Impinging jet

5.5.1   Inlet boundary condition

Benchmark 6 is the impinging jet benchmark and the semi-elliptic inlet is located 0.6 m above the floor on which the jet impinges. Various options were tested as boundary condition at the inlet. The experiment article [10] states the bulk inlet velocity is 1.2 m/s. It also mentions measurement of the inlet velocity profile and turbulent kinetic energy, however, this profile is not publicly available and is not plotted in the article. Thus, two different options were tested. One was to impose a uniform velocity profile with a value of 1.2 m/s and another to include a part of the inlet section in the simulation. The former approach gave poor agreement with experiments close to the floor, so the latter was favoured. To avoid making the mesh generation more complicated a separate simulation of the inlet duct was conducted and the profiles of velocity, k and ϵ at the outlet were exported and used as the inlet condition in the actual simulation. For this separate simulation, uniform profiles of velocity, k and ϵ were imposed at the inlet with turbulent intensity equal to 10% and ϵ calculated from the hydraulic diameter. This is also what was used by Chen et al. [10]. The inlet duct length was first set to 2.4 meters, which is the actual length of the inlet pipe, but this gave a very large discrepancy between the simulation and experiment velocities at the horizontal line z = 0.545 m. This line is located only 0.055m beneath the inlet (see figure 3.8), thus this approach is most likely erroneous. A duct length of 0.25 meters gave much better compliance at this location, so this was selected for all the B6 simulations.

5.5.2   Grid sensitivity analysis

Three different semi structured meshes were created for benchmark 6: a coarse mesh with 3.0 million cells, a medium mesh with 5.4 million cells and a fine mesh with 7.1 million cells. All three meshes shared the same layout and were refined in the impingement region and close to the floor where the boundary layer develops. The layout of the medium mesh is shown in Appendix A figure A.5.

The RNG k-ϵ model was selected for the grid sensitivity analysis, as this had already proven to give fairly good results in the simulation by Chen et al. [10]. The meshes were refined near the floor, but it

was hard to achieve a satisfying degree of wall refinement as refining the mesh further lead to some poor quality elements near the floor. Thus, the meshes created were a trade off between wall refinement and element quality. The y^+ values for the medium mesh is shown in table 5.11. As explained they are a bit high in the impingement region, seen from the maximum values, in particular for what is referred to as the "inlet wall" in figure 3.7, which is the wall that forms the corner where the jet impinges together with the floor.

The result from the grid sensitivity analysis can be seen in figures 5.21 and 5.22. The differences between the solutions are rather small, and can hardly be seen without zooming in on the figures. The medium and fine mesh solutions are very close to each other, hence it was decided to use the medium mesh for further simulations. This is also very close to the number of cells in the mesh used by Chen et al. [10].

(a) z = 0.545 m

(b) z = 0.225 m

(c) z = 0.125 m

(d) z = 0.065 m
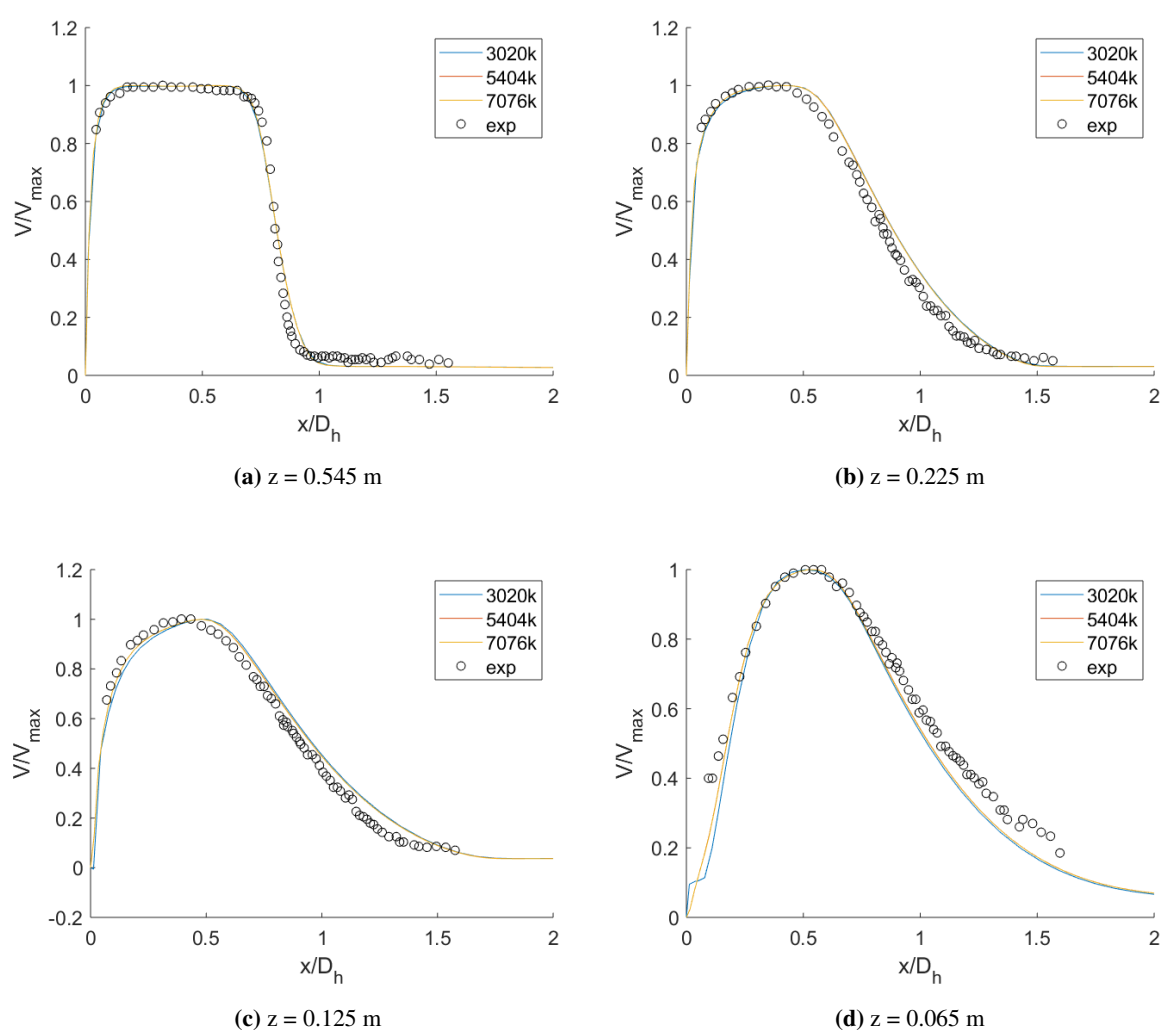
Figure 5.21: Grid sensitivity analysis for Benchmark 6 using the RNG k-ϵ model. Legend refers to number of cells in the mesh. Horizontal lines.

Table 5.11: Average and maximum y^+ values at the different walls for B6 medium mesh.

	Floor	Inlet wall
Average	2.5	8.7
Max	8.1	38.1

(a) x = 0.3 m

(b) x = 0.5 m

(c) x = 0.7 m

(d) x = 1 m
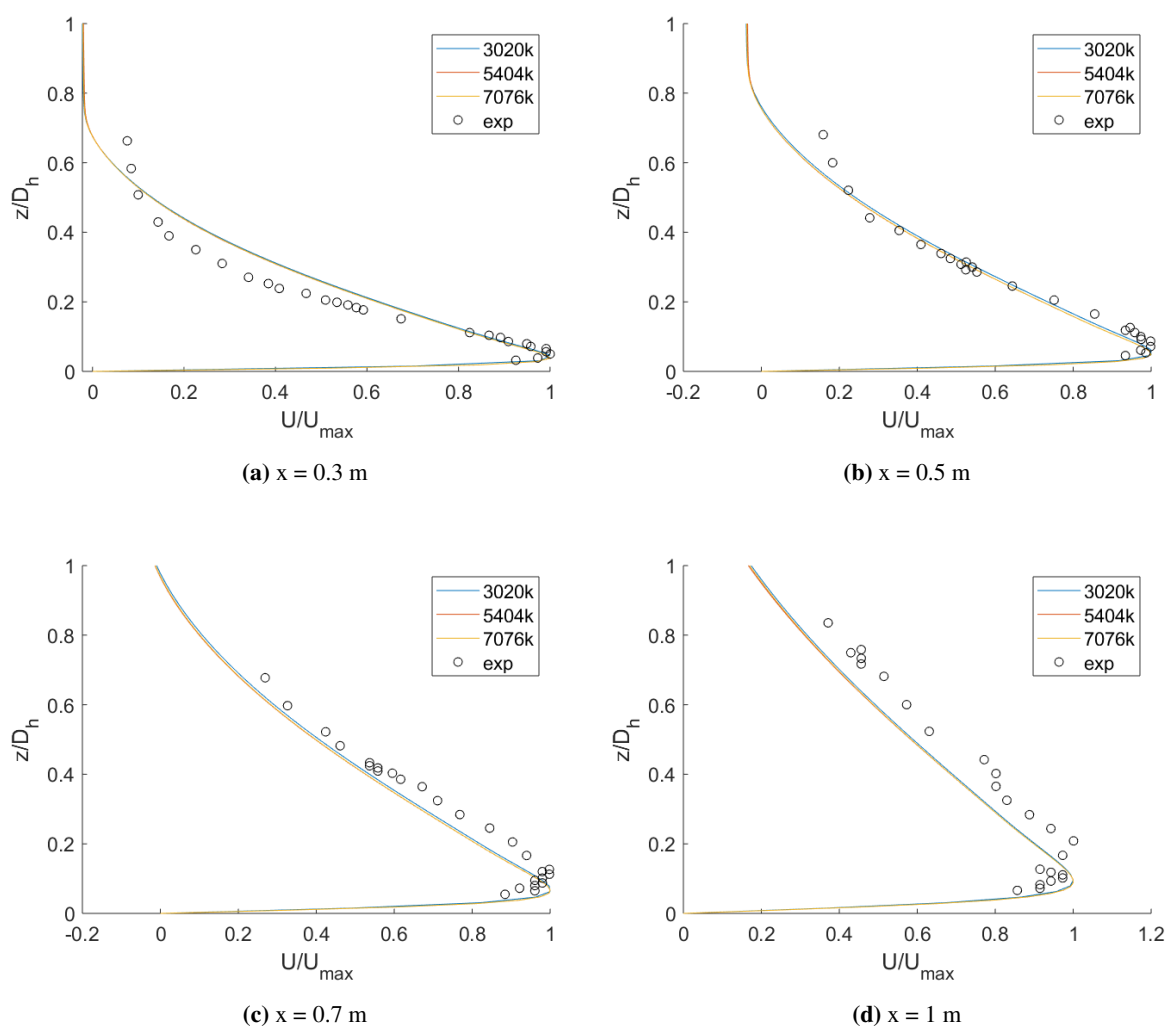
Figure 5.22: Grid sensitivity analysis for Benchmark 6 using the RNG k-ϵ model. Legend refers to number of cells in the mesh. Vertical lines.

5.5.3   Turbulence modelling

Five different turbulence models were tested on Benchmark 6: standard k-ϵ, RNG k-ϵ, realizable k-ϵ, SST k-ω and standard k-ω. All simulations were done on the medium mesh. All three k-ϵ models converged to a steady state solution, while the two k-ω models had oscillating residuals and oscillating drag coefficient on the floor. For the k-ω models, the solutions had to be averaged over 8000 iterations to create a statistically independent solution. The results from the five different models are shown in

figures 5.23 and 5.24.

(a) z = 0.545 m

(b) z = 0.225 m

(c) z = 0.125 m

(d) z = 0.065 m
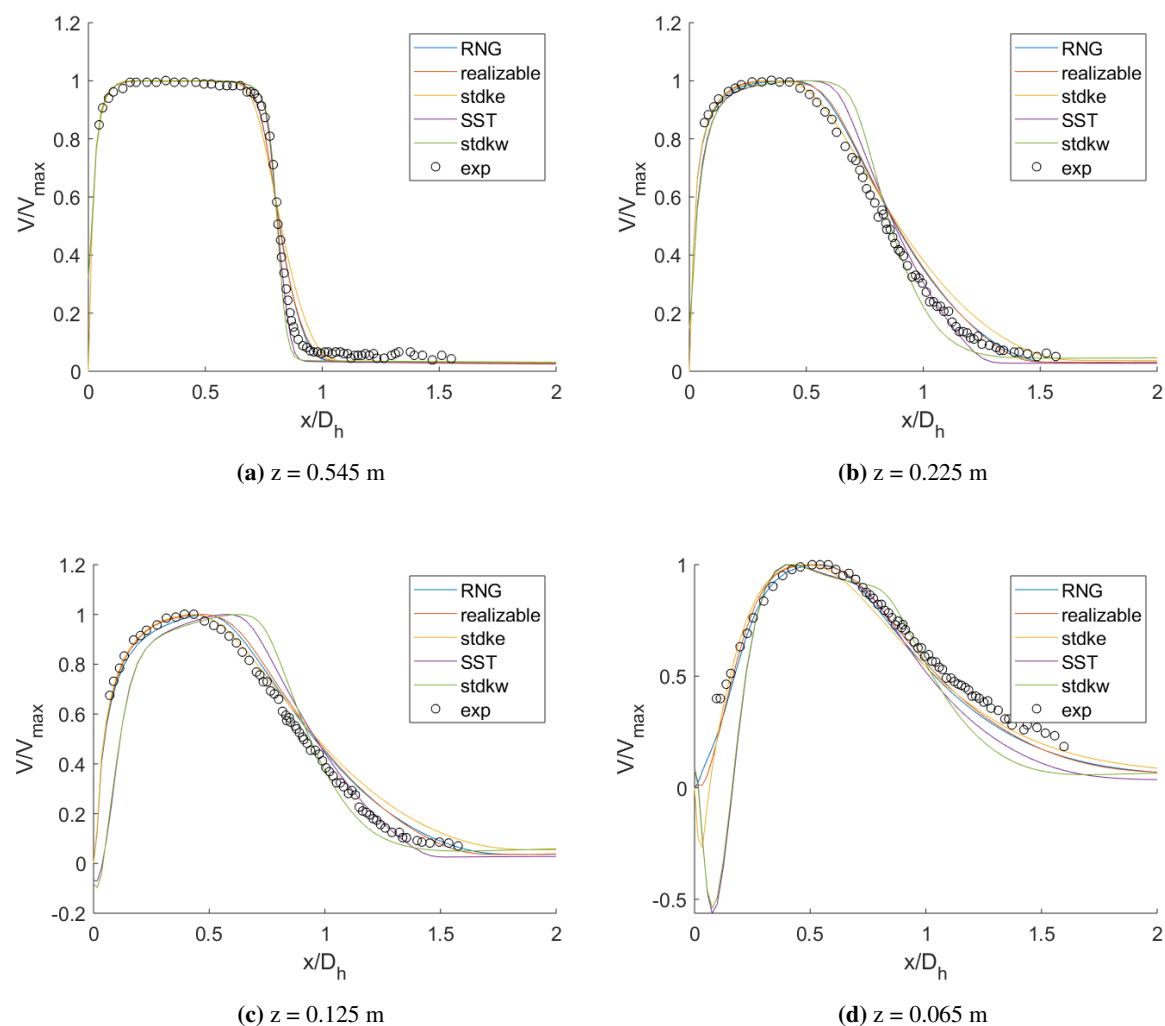
Figure 5.23: Turbulence model comparison of Benchmark 6 using the medium grid.
Horizontal lines.

The largest difference between the five solutions can be seen in figure 5.23d, which is the horizontal line closest to the corner where the jet impinges. Here the SST and standard k-ω models predict a recirculation zone, seen from the negative velocities in the left part of the figure. The standard k-ϵ model also predicts a recirculation zone, however one that is slightly smaller than for the k-ω models. The RNG k-ϵ and realizable k-ϵ models do not predict any recirculation zone at this point. The k-ϵ models seem to have the best fit to the experimental data in the left part of the figure, thus the location, shape and size of the recirculation zone obtained with the k-ω models seem incorrect. It should, however, be noted that it was stated in the experiment report [10] that it was not possible to get good measurements in the region with this secondary vortex, and this is why the measurements stop some distance before the wall. It is also in this impingement region of the flow where oscillations in the mean flow field can be seen for the k-ω models. However, since the k-ϵ models seem to give the best fit, these oscillations might be erroneous. The velocity contours in the impingement region are shown in Appendix B figure B.7.

Looking at figure 5.24 and how the solutions look in the boundary layer at the floor, one can see

that the point with maximum velocity is shifted closer to the floor compared with the experiments. This is the case for all the models, and something that is also seen later for Benchmark 7 – the pure wall jet. Moving further away from the wall larger differences are seen in the solutions. The SST k-ω model seems to predict the lowest velocity here and give the largest error compared with the experimental data in figures 5.24b, 5.24c and 5.24d. In figure 5.24a the velocity in the shear layer is generally overpredicted and the SST k-ω model actually gives the best compliance with experiments.

(a) x = 0.3 m

(b) x = 0.5 m

(c) x = 0.7 m

(d) x = 1 m
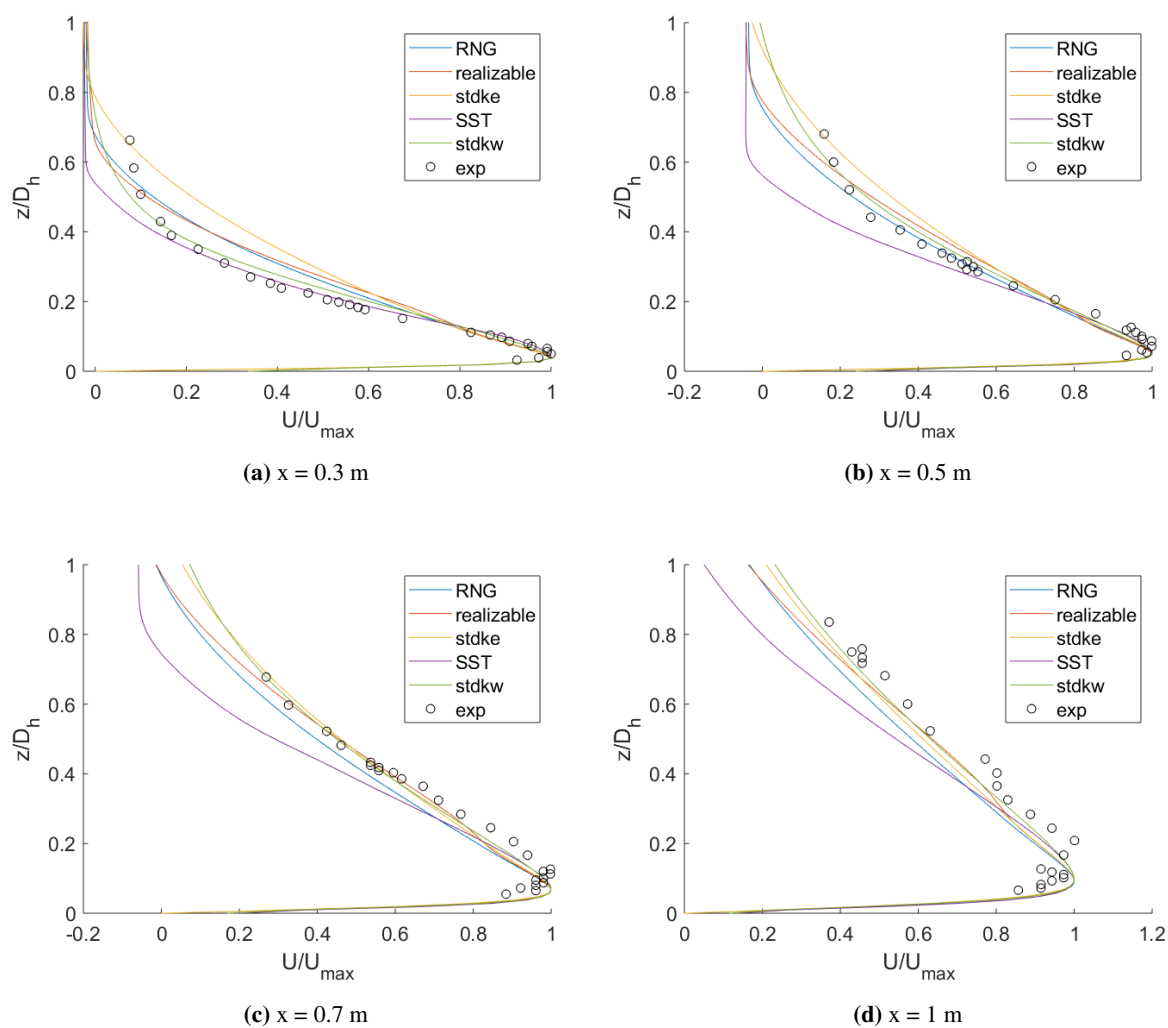
Figure 5.24: Turbulence model comparison on Benchmark 6, using the medium
grid. Vertical lines.

From the RMSE values in table 5.12, it is quite clear that the k-ϵ models have a better fit with the experiments at the horizontal lines of measurement. As expected, the k-ω models get very high values at z = 0.065m. The realizable and RNG k-ϵ models get the lowest average values. Looking at the RMSE values from the vertical lines in table 5.13 the standard k-ω model actually gets the lowest value, indicating it has the best compliance with the experiments here. The worst compliance is obtained with the SST k-ω model. Once again the three k-ϵ models have quite similar values, but the realizable k-ϵ model seems to be marginally better judged from the RMSE values.

Table 5.12: RMSE values for the different turbulence models tested on B6.
Horizontal lines.

	z = 0.545m	z = 0.225m	z = 0.125m	z = 0.065m	Average
RNG	0.042	0.047	0.051	0.059	0.050
realizable	0.042	0.050	0.056	0.053	0.050
stdke	0.063	0.061	0.063	0.058	0.061
SST	0.033	0.059	0.118	0.213	0.106
stdkw	0.045	0.078	0.130	0.216	0.117

Table 5.13: RMSE values for the different turbulence models tested on B6. Vertical
lines.

	x = 0.3m	x = 0.5m	x = 0.7m	x = 1m	Average
RNG	0.075	0.045	0.065	0.084	0.067
realizable	0.092	0.058	0.043	0.064	0.064
stdke	0.107	0.061	0.045	0.066	0.070
SST	0.040	0.090	0.104	0.124	0.089
stdkw	0.050	0.036	0.039	0.050	0.044

Results are fairly similar to the RANS simulations by Chen et al. [10] for the vertical lines. However, the simulations by Chen et al. do not predict any recirculation zone similar to what is seen here at z = 0.065m for the SST k-ω model. Chen et al. did also not mention anything about oscillating residuals for any of the models. One cannot rule out completely that no such behaviour was observed, however, a difference between this simulation and the one by Chen et al. [10] is the wall refinement. Chen et al. [10] claims y^+ was below 1 in their simulations while this simulation only had y^+ below 5.

Overall the k-ϵ models seem to be the better option for Benchmark 6 based on the results in this thesis. However, since the simulation with the SST k-ω model does not match the result obtained by Chen et al. [10] there is some uncertainty to whether another parameter is causing the error seen with this model. This is the second time differences are seen between the results of this thesis and the results in literature when using the SST k-ω model, as it was the same case for B2 when comparing with the results from Ito et al. [25]. There is, therefore, reason to believe that when using the SST k-ω model, the solution is particularly sensitive to parameters other than the turbulence model. This parameter could be the mesh, as this is the hardest to compare with the results from literature. Usually, the number of elements and y^+ value is known, but there are several other factors such as inflation rate, mesh refinement in areas with high gradients and geometrical shape of the cells that can influence the solution. The B6 mesh was particularly challenging to create because of the geometry which does

not allow a completely structured mesh and the high inlet Reynolds number creating high y^+ values. The impingement wall has quite poor wall refinement compared to the other meshes in this thesis and this could be a source of error for the SST k-ω model. Nonetheless, if the mesh is in fact the source of error the k-ϵ models have proven more capable to deal with a lower quality mesh than the SST k-ω model. The idea behind simulating B6 was to see which turbulence models had the best performance in the jet impingement region, and based on the results the conclusion would be to say the k-ϵ models. However, since there is not agreement with literature for the SST k-ω model this is not a very strong conclusion. Another important aspect is that the flow pattern in the impingement region of B6 is quite different from the flow pattern in the impingement region of the other benchmarks. This can be seen by comparing figure B.7 to for instance figure B.6 or B.5. The high Reynolds number and short distance from the inlet to the floor causes the jet to impinge with a lot more momentum and as a consequence, the turn is much sharper than for the other benchmarks and the secondary vortex that is created much smaller. It is therefore a bit uncertain if the results from B6 can be extrapolated to evaluate how well the different turbulence models model the impingement region in the cavity benchmarks. Ideally, B6 should have had a lower Reynolds number to be more comparable with the other benchmarks.

5.6   Benchmark 7 – Wall jet

5.6.1   Grid sensitivity

Five different 2D meshes were created for Benchmark 7, with 19, 26, 41, 77 and 819 thousand cells. Since B7 is a plane 2D wall jet that is unlikely to have any 3D effects, simulations have been done in 2D only. The meshes were refined near the wall in order to resolve the viscous sub-layer. In addition, the meshes were refined in the shear layer between the jet and the nearly quiescent fluid. For the coarsest mesh with 19 thousand cells there was a much coarser refinement in the shear layer compared to the 26 thousand cell mesh while the near wall refinement was equal. Using the same setup as Yan et al. [46] the right and top boundaries were modelled as pressure outlets. The length of the flow domain was shortened compared to the real tank in the experiments as this reduced the number of cells and the area of interest was the left part of the tank. The four meshes all had y^+ below 5, but the two finest meshes with 77 and 819 thousand cells were even more refined with y^+ below 1. The medium mesh with 41 thousand cells had y^+ below 2. The y^+ values for all five meshes are shown in table 5.14.

Table 5.14: Average and maximum y^+ values for B7 meshes. Values calculated at the wall jet wall for 0 < x/h < 200.

	19k	26k	41k	77k	819k
Average	2.0	2.0	1.0	0.5	0.5
Max	4.2	4.5	1.9	1.0	1.0

The inlet dimensions and the inlet velocity was equal to that in the experiments i.e. the Reynolds number was Re = 9600. The non-uniform velocity profile measured with LDV was used as the inlet boundary condition. The inlet turbulent intensity was set to 1% which is what was measured by Eriksson et al. [16], and ϵ and ω was calculated from the hydraulic diameter of the inlet. The layout of

the mesh and the flow domain can be seen in Appendix A figure A.8 for the mesh with 41 thousand cells.

The grid sensitivity analysis was done with the RNG k-ϵ model. The result is shown in figure 5.25. The profile is scaled into the universal wall jet profile by dividing the z coordinate with the distance to half of the maximum velocity $z_{1/2}$ and the velocity U with the local maximum velocity U_{max}.

(a) x/h = 70   **(b)** x/h = 150
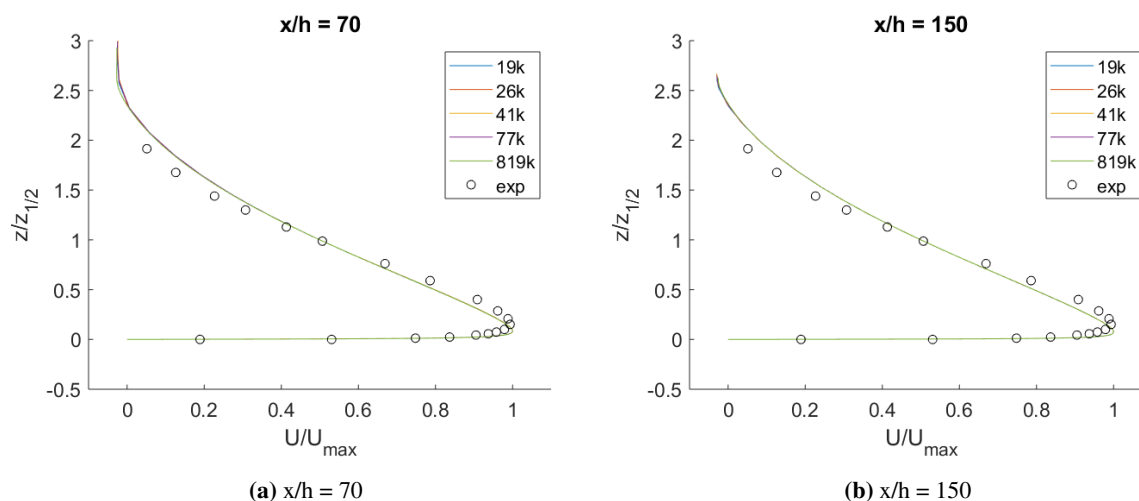
Figure 5.25: Grid sensitivity analysis for Benchmark 7 with RNG k-ϵ turbulence model. Legend refers to number of cells in the mesh.

Looking at figure 5.25 it is hard to see any difference at all between the five meshes as they appear as one line when looking at the full profile. If one zooms in, one can observe that the differences are in the order of 10^{-4}. Overall the solutions are very similar even when increasing the number of cells to a value as high as 819 thousand cells. Thus the 41k mesh was selected for the rest of the simulation to save computational time and can be regarded as a near grid independent solution. This is also very similar to the mesh size used by Yan et al. [46]. It is interesting how small the differences are between the four solutions. The coarsest mesh with 19 thousand cells and limited refinement in the shear layer seems to be fine enough to get a satisfying accuracy. It also shows that there is – at least for the RNG k-ϵ model – a small difference between having y^+ below 5 and y^+ below 1. It also shows a very small difference between the two different locations x/h = 70 and x/h = 150.

Convergence was monitored by plotting the drag coefficient on the floor against the number of iterations. The simulation was stopped when this had been very close to constant for 1000 iterations. A constant value was not reached as the drag coefficient oscillated, but with the order of 10^{-3}. The residuals were also monitored, but did not reach satisfactory low values. In fact, the same oscillatory behaviour was observed as for many of the other Benchmark simulations. This could be because of poorly imposed boundary condition with reverse flow occurring for both the pressure outlets. However, it is interesting that the same convergence issues are observed also with Benchmark 7 that consists only of the wall jet. This implies that the oscillatory behaviour can be caused by the modelling of this particular flow element with RANS turbulence models. The residuals and drag coefficient monitor obtained for the 26k mesh simulation are shown in figure 5.26. Averaging over a large number of iterations had no impact on the solution for B7.

(a) Residuals   **(b)** Drag coefficient
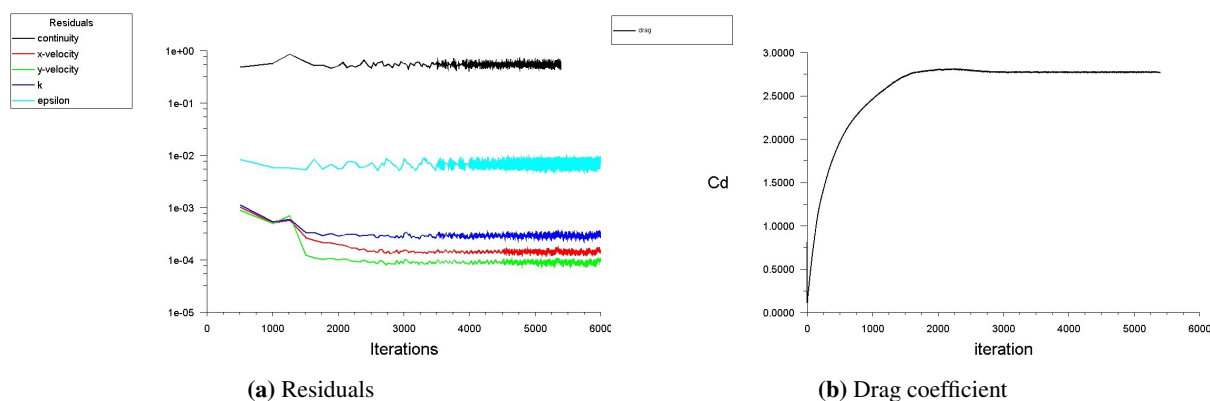
Figure 5.26: Convergence monitors for B7 using the 26k mesh with RNG k-ϵ model.

5.6.2   Turbulence modelling

Six turbulence models were tested on the B7 geometry using the 41k mesh: standard k-ϵ, RNG k-ϵ, realizable k-ϵ, standard k-ω, SST k-ω and the RSM Stress-ω model. The results are shown in figure 5.27.

(a) Full profile   **(b)** Closeup of velocity peak
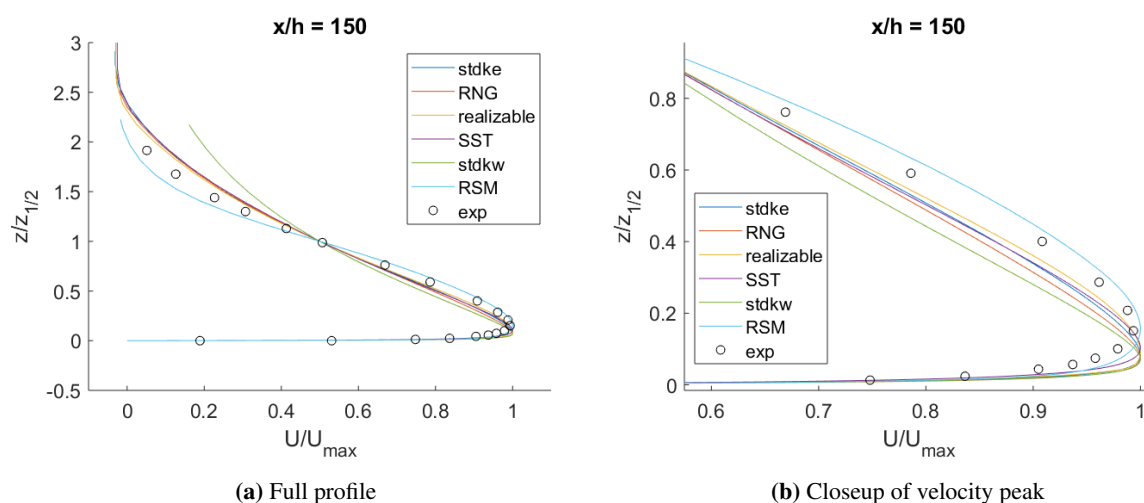
Figure 5.27: Comparison of six turbulence models for Benchmark 7 on 41k mesh.

The most obvious result from looking at figure 5.27 is how the RSM model is different from the two equation models. Close to the wall, the RSM model gives a profile shape that is more similar to that from the experiments, and the point of maximum velocity seems to be at a more correct distance from the wall. Moving away from the wall, however, the velocity is first slightly overpredicted and then underpredicted as we pass the half velocity point. The RSM model also gets the lowest RMSE value, seen in table 5.15, although only marginally better than the SST k-ω model. Nonetheless, overall the RSM model seems to give the best performance for the wall jet which strengthens the conclusion by Yan et al. [46].

Table 5.15: RMSE values for the different turbulence models tested on B7.

	stdke	RNG	realizable	SST	stdkw	RSM
x/h = 150	0.130	0.133	0.129	0.127	0.144	0.126

Looking at the profiles from the two equation models the same trend is observed here as in the paper by Yan et al. [46], that all two equation RANS models set the point of peak velocity too close to the floor compared with the experiments. There are nonetheless some small differences between the models, the SST k-ω model gives the solution where the point of maximum velocity is furthest away from the wall followed by the realizable k-ϵ model. The realizable k-ϵ model gives the least deviation with the experiments if one follows the profile into the shear layer. Looking at table 5.15 the SST k-ω model gets the lowest value, but perhaps more noticeably is how small the differences are between the SST k-ω, standard k-ϵ, RNG k-ϵ and realizable k-ϵ models. The profile obtained with the standard k-ω model is an outlier compared to the other models and this could also be seen from the convergence of this simulation as both the residuals and drag coefficient oscillated with a much larger amplitude than for the other simulations. This result is dissimilar to the result by Yan et al. [46] where the standard k-ω model was much closer to the other turbulence models, hence this might be incorrect due to some other parameter or setting.

The reason the velocity profiles from B7 are plotted with the scaling of z and U as in figure 5.27 is because the experimental data were only available for this particular type of plot from Eriksson et al. [16]. It is however also interesting to plot the profiles and scale with the bulk inlet velocity, since the differences between the models are easier to see, and this is what has been done for the other benchmarks. This is done in figure 5.28.

(a) x/h = 70   **(b)** x/h = 150
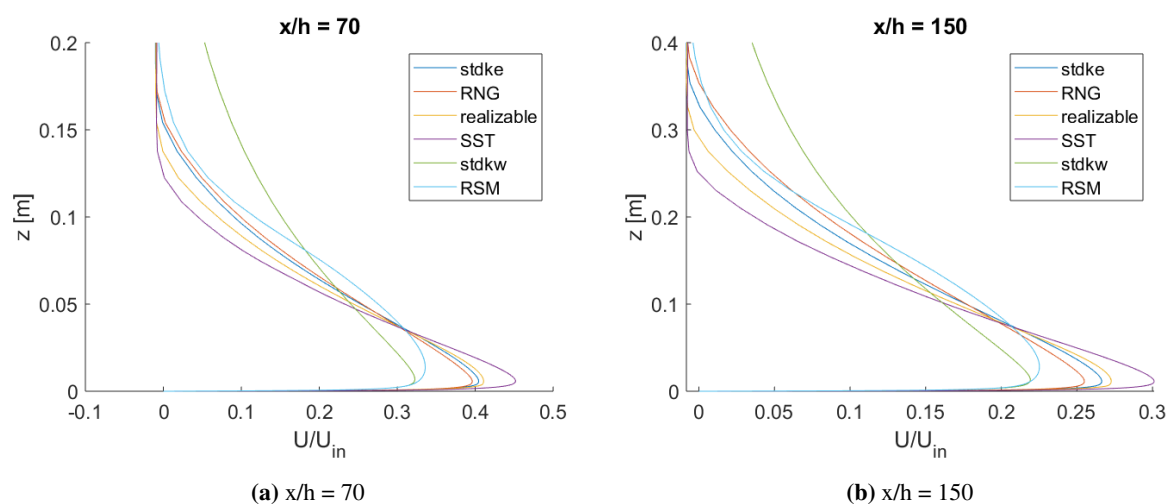
Figure 5.28: Comparison of six turbulence models for Benchmark 7 on 41k mesh.
Velocity scaled with bulk inlet velocity and no scaling on the y axis.

Looking at figure 5.28 it is clear that the different turbulence models give solutions that are more diverse than what is the impression from figure 5.27. The maximum velocity obtained with the different models varies significantly. It was a tendency for Benchmarks 2-4 that the SST k-ω model overestimated the maximum velocity in the jet, and here it is seen that for a pure wall jet it predicts the highest

maximum velocity of the 6 RANS models tested. Eriksson et al. [16] do not present experimental data for this value, but Yan et al. [46] compared the maximum velocity decay for various turbulence models with experimental data – figure 3.27b. They found that the SST k-ω model underpredicts the decay in maximum velocity, thus this result, and what was seen for B2, seems to confirm that the SST k-ω model predicts a too high maximum jet velocity for a fully turbulent jet. The three k-ϵ models predict a fairly similar maximum velocity, while the RSM model predicts a significantly lower value. The RSM model got the lowest RMSE value when applied on figure 5.27, but it is not certain that the same result would be obtained for figure 5.28 if experimental data had been available for this plot. From comparing figure 5.28 to for instance figure 5.2a it seems like the differences observed in the wall jet region in benchmarks 2-4 are – perhaps unsurprisingly – dominated by how the turbulence models model the wall jet. In other words, the influence from the additional features of the cavity flow compared to the pure wall jet seems to have a minor impact in this region. B5 is slightly different, as here the jet impinges and turns much closer to the inlet, losing the wall jet characteristics much sooner. The jet in B5 also has a significantly lower Reynolds number.

The standard k-ω model gave as mentioned previously poor results compared to the other models, and this result was not in line with the results by Yan et al. [46]. It was later discovered that both the convergence and the final solution with the standard k-ω model improved when setting the inlet turbulence intensity to 10% instead of 1%. The standard k-ω model is known to be sensitive to the inlet turbulence parameters and seemed to have some instabilities in the shear layer right after the inlet when $T_i = 1\%$. The result with the $T_i = 10\%$ is shown in appendix B figure B.8.

5.6.3   Near wall treatment

In this thesis, the Enhanced wall treatment option has been used for the majority of the benchmarks and the meshes have been created to have y^+ below 5 at the walls. For benchmark 7 all the options for near wall treatment were tested on the 26k mesh – with the exception of any user defined wall functions – even though theory dictates only Enhanced wall treatment, Menter-Lechner Wall Treatment and arguably Scalable Wall Functions are appropriate for this mesh. The motivation by such a study is to see what effect a user error would have on the wall attached jet flow. The different types of near-wall treatment were tested with the RNG k-ϵ model. The results from using the different near-wall treatment options are shown in figure 5.29.

(a) Full profile   **(b)** Closeup of velocity peak
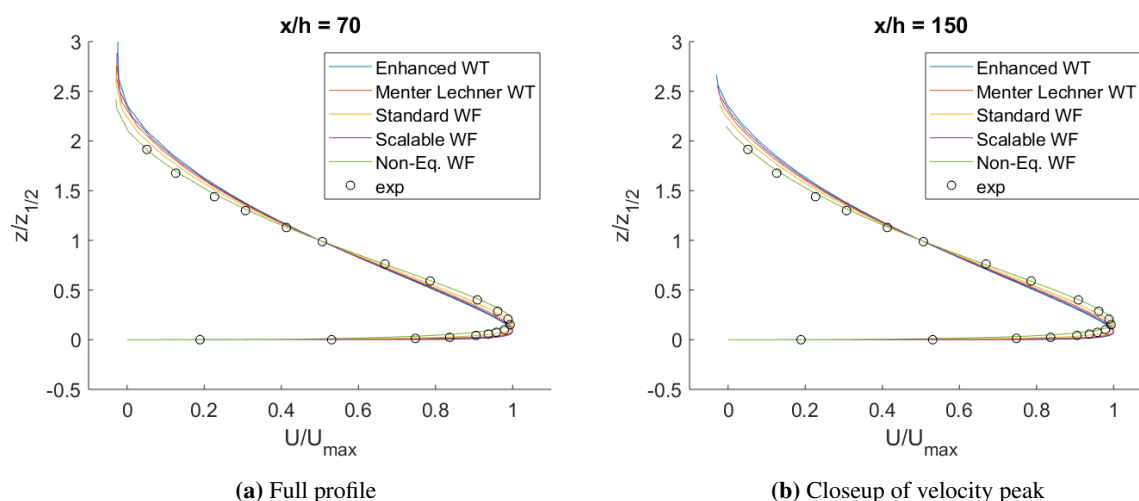
Figure 5.29: Comparison of 5 five different options for near-wall treatment using
the RNG k-ϵ model.

Some interesting results can be observed in figure 5.29. The most obvious is perhaps that the Non-Equilibrium wall functions give a very good result where $0.4 < z/z_{1/2} < 2$. In fact, the two options that give the best prediction of the point of maximum velocity are the Standard wall functions and Non-equilibrium wall functions which in theory are unsuitable to use for this mesh. The two "correct" options – Enhanced wall treatment and Menter-Lechner – give the same result as seen before, a point of maximum velocity too close to the wall compared with the experiments. The difference between using these two options is quite small, but the Menter-Lechner option seems to give a slightly smaller deviation between simulation and experiments. Looking at the RMSE values for the different near wall treatment options in table 5.16, the Standard wall functions actually gets the lowest value. The Non-Equilibrium wall functions do not get such a low value as figure 5.27 might suggest, because the largest deviations are seen close to the wall and these values dominate the average value.

Table 5.16: RMSE values for the different near wall treatment options tested on B7.

	Enhanced WT	Menter-Lechner WT	Standard WF	Scalable WF	Non-eq WF
x/h = 150	0.133	0.133	0.123	0.137	0.137

Another interesting observation done when testing the different near wall treatment options was the impact on the convergence for the simulations. As mentioned previously in section 5.6.1 oscillatory residuals were observed, and this was with the use of Enhanced wall treatment. When switching to Standard wall functions and Non-equilibrium wall functions the residual behavior changed completely with residuals reaching much lower values with no oscillations. This difference is shown in figure 5.30.

(a) Standard wall functions   (b) Enhanced wall treatment
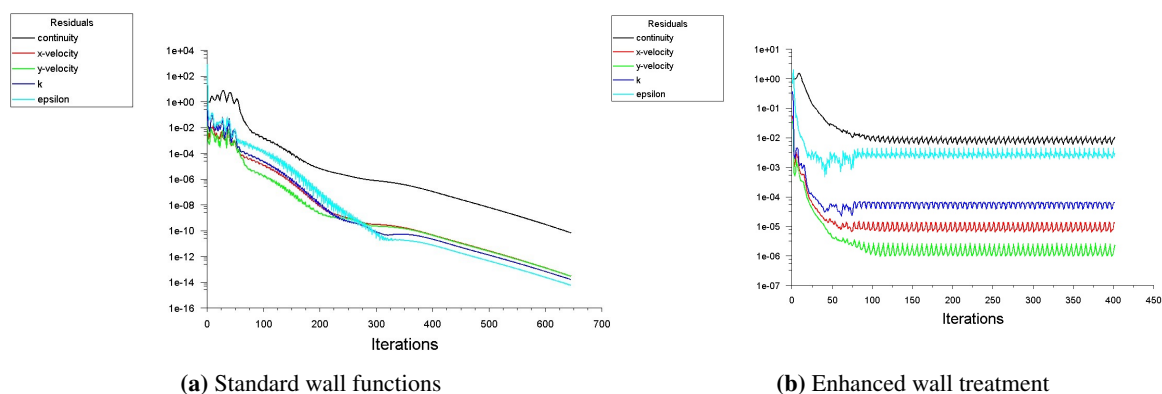
Figure 5.30: Difference in residuals when using Enhanced wall treatment and
Standard wall functions. 26k mesh with RNG k-ϵ model.

With both improved convergence and results when using the Standard wall functions, it could be tempting to conclude this is in fact a more suitable approach for the wall jet than doing what theory dictates and use Enhanced wall treatment. However, one should not rule out that this result is simply "a strike of luck". As both these simulations and the simulations by Yan et al. [46] show, all the two equation RANS turbulence models seem to have some shortcomings in modelling the wall jet. Thus, when you impose one error – using an unsuitable type of near-wall treatment – on top of another – using an inadequate turbulence model – the result could go both ways i.e. the errors could to some extent cancel each other out. That seems to be the case here, and this result is relevant to the discussion introduced by Peng et al. [39] that many errors in CFD are user errors. What this result shows is that when doing an experimental validation of a CFD code, good results can be obtained even when – either by lack of knowledge or accident – best practice guidelines are not followed. However, if one then extrapolates the same code to a more complex problem there is no guarantee the same mistakes once again will cancel each other out.

6   Conclusions

The focus in this thesis has been on the suitability of two-equation RANS turbulence models to model benchmarks that are representative for mixing ventilation systems. The performance of the various turbulence models is summarized in table 6.1, where it is also indicated whether the result is in agreement with the similar table for literature – table 3.2. The performance indicator – good, moderate, bad – has been decided based on a combined evaluation of the RMSE values and the qualitative agreement with the experimental velocity profiles. The results in table 6.1 refer to the results presented in the section "Turbulence modelling" for each benchmark.

The results from benchmarks 2 and 3 indicate that the best turbulence model for these benchmarks is the standard k-ϵ model. The results with the standard k-ϵ model are also in line with what has been done in literature. This implies that the standard k-ϵ model is a good choice when simulating indoor airflows that are fully turbulent, and without strong pressure gradients. The results from Benchmark 2 also indicate that the choice of wall treatment has an impact on the final solution. The results did not significantly deteriorate with the use of wall functions, but the RMSE calculations implied that the use of Enhanced wall treatment on a wall refined mesh gave marginally better results with the standard k-ϵ model. Nonetheless, the savings in computational time can justify the use of wall functions for a case similar to B2.

For Benchmark 4 the three k-ϵ models gave the best agreement with experiments, while for Benchmark 5 the SST k-ω was clearly superior to all the k-ϵ models. This was an interesting result as the inlet Reynolds number is comparable for the two cases. The result implies that other factors are equally important as the inlet Reynolds number when selecting turbulence model. Benchmark 5 has stronger pressure gradients in the wall jet, and the poor results from the k-ϵ models were mainly caused by failing to predict the correct jet detachment point. Another difference between B4 and B5 is the ratio h/H which is much higher for B5. It is hard to say with certainty if the SST k-ω model was superior for B5 because of better performance in the transitional flow regime or better performance in the presence of adverse pressure gradients and jet impingement. The realizable k-ϵ model was the better option of the three k-ϵ models for B4 and arguably B5. The standard k-ϵ model gave the worst performance for B5 and should therefore be used with caution when modelling a transitional flow.

Benchmark 6 was included in the thesis to investigate which turbulence models were better for simulating an impinging jet. The results from B5 had indicated that the SST k-ω model was the best option for the impingement region in B5, however, the same result was not seen for B6. Here the three k-ϵ models again gave the best results, and the SST k-ω model overall the worst. The result with the SST k-ω model was however not consistent with the results from literature. The impinging jet of B6 has a significantly higher Reynolds number than the jet from B5, and in general, the jet impinges with much higher momentum than what is the case in the cavity benchmarks 2-5. Looking at the velocity contours it is questionable how comparable the impingement region in B6 is to the impingement region in the other benchmarks. The secondary vortex seen in B6 is very small and seems to have a smaller influence on the flow than what is the case for the other benchmarks – in particular B5. Nonetheless, B6 is also a case of k-ϵ models performing well for a high Reynolds number, and adds to the trend that the k-ϵ models are better for high Reynolds number flows.

Benchmark 7 showed that all the two-equation RANS models used in this thesis have a tendency to shift the wall jet profile closer to the wall than what is seen with the experimental data. A profile shape

Table 6.1: Summary of turbulence model performance in this thesis. Color indicates agreement with experimental data. Agreement with literature indicated by number of asterisk. No asterisk means this model has not been used in the literature accounted for in the literature review for this benchmark.

Benchmark	B1	B2	B3	B4	B5	B6	B7
Re inlet	500	5000	7100	684	1000	10013	9600
Flow regime	Unknown	Fully turbulent	Fully turbulent	Unknown	Transitional	Fully turbulent	Fully turbulent
2D Std. k-ϵ	X	** (Green)	X	X	X	X	** (Yellow)
2D RNG k-ϵ	X	(Green)	X	(Yellow)	X	X	** (Yellow)
2D realizable k-ϵ	X	** (Red)	X	X	X	X	** (Yellow)
2D Std. k-ω	X	** (Yellow)	X	X	X	X	** (Yellow)
2D SST k-ω	X	** (Red)	X	X	X	X	** (Yellow)
3D Std. k-ϵ	X	** (Green)	** (Green)	(Green)	(Red)	(Green)	X
3D RNG k-ϵ	X	(Yellow)	** (Green)	** (Green)	** (Red)	** (Green)	X
3D realizable k-ϵ	X	(Green)	(Green)	(Green)	(Yellow)	(Green)	X
3D Std. k-ω	X	X	X	** (Yellow)	(Yellow)	(Yellow)	X
3D SST k-ω	X	* (Yellow)	* (Yellow)	** (Yellow)	** (Green)	* (Yellow)	X
3D Low-Re k-ϵ	X	AKN * (Yellow)	X	X	X	X	X

Legend:

Good	Moderate	Bad	X = not tested	** = agreement with literature	* = not agreement with literature

more similar to the experiments was obtained by using a RSM model. It was hard to argue that any of the RANS models were significantly better than the others from the comparison with experimental data. However, when the velocities were scaled with the inlet velocity rather than the local maximum, it was seen that the SST k-ω model predicts a higher maximum jet velocity than the k-ϵ models. There are significant indications that the SST k-ω model in fact consistently overpredicts the maximum jet velocity in a fully turbulent wall jet, both from the results in this thesis and the literature. The benchmark 7 simulations also showed that improved agreement with experiments can be obtained by using wall functions rather than Enhanced wall treatment. This is however not recommended for a mesh with y+ < 5 and is rather an example of how supposedly good results can be obtained even though best practice guidelines are not followed.

The overall goal of this thesis was to establish a best practice use of RANS turbulence models for mixing ventilation applications in indoor airflows, by investigating how different models and other parameters affect the result for several benchmark flows. Some best practice guidelines can be given based on the discoveries in this thesis, but there is also a need for further work on some topics. Primarily, if the flow is known to be fully turbulent, the best option seems to be to use a k-ϵ model, and in particular the standard k-ϵ model. The SST k-ω model has proven to give poorer and more inconsistent results for the fully turbulent benchmarks, and this could be caused by inadequacy in modelling the fully turbulent wall jet, for which it seems to overpredict the maximum velocity. Secondly, if the flow is known to be transitional the conclusion is flipped, as the best option based on B5 is precisely the SST k-ω model and the standard k-ϵ model is the worst. However, the conclusion for the transitional regime is not so strong since different results are seen for B4 and B5 with comparable inlet Reynolds numbers. The differences between B4 and B5 have been pointed out, and it has to be further researched which of these are causing the deviation in turbulence model performance for these benchmarks. Of the k-ϵ models, the realizable model seems to be the better option in the transitional regime based on the agreement with experiments for B4 and B5, but should be used with caution as the flow pattern it predicted for B5 is a bit peculiar. Thirdly, the results from B2 indicate that wall functions can be used when using the standard k-ϵ model for fully turbulent flows, without causing a large deterioration in the result. However, this is only tested for B2 and it has to be further researched when it is tolerable to use wall functions. In general, best practice guidelines for CFD is to resolve the boundary layers. Fourthly, the sensitivity of the inlet values for k and ϵ/ω seems to be larger for low Reynolds number flows and smaller for high Reynolds number flows. It is therefore recommended to choose these parameters with more scrutiny when the inlet Reynolds number is low, while for a high inlet Reynolds number it seems sufficient to do a rough estimate of the inlet turbulent intensity.

The overall recommendations given for the use of RANS turbulence models are in many ways summarized by table 6.1. This table and table 3.2 are also visual reminders that no RANS turbulence model seems capable of modelling all the benchmarks, thus the selection of an appropriate turbulence model is paramount. It is also seen from table 6.1 that the SST k-ω model is often inconsistent with literature, and it has to be further researched what is causing this inconsistency. It is also a reminder that the turbulence model is only one of several parameters that make up a CFD simulation, and essentially all parameters should be selected with care.

Additionally, many of the simulations in this thesis do not converge to a steady state solution even though a steady state solver has been used and the benchmarks are designed to have steady state flows. The exact reason for this is not known, and is a phenomenon that is not discussed in the literature other than for B5. One possible explanation discussed in this thesis is that parts of the cavity can be in the

transitional regime for B2 and B3, however, this is only a hypothesis. There is also a clear dependency on turbulence model to whether the solution converges to a steady state or not. The standard k-ϵ model converges to a steady state solution for all benchmarks while the RNG k-ϵ, realizable k-ϵ and SST k-ω models are more prone to give a non-steady state solution. In the cases with oscillating residuals and monitors, the solution has been averaged over a large number of iterations. This has proven to give satisfactory results for most cases. For B4 it was tested if there are differences between simulating in transient and steady state when such oscillations are seen in the flow. The conclusion was that simulating with a transient solver has an impact on the solution, but did not give significantly better agreement with experiments. It has to be researched further when it is okay to use a steady state solver and when a URANS approach should be used.

Based on the LES results presented in the literature review, it seems like overall LES gives better results than RANS turbulence models for the benchmarks presented in this thesis. Thus, if high accuracy is needed for a simulation it should be considered to use LES instead of RANS. This is a question of accuracy vs computational time, and generally speaking, how accurate results are needed is important to judge prior to a simulation. It has been shown in the thesis that a RANS simulation can give significant deviations with the experimental data, but it could also be argued that for most cases the RANS models seem to predict the correct flow pattern in the majority of the flow domain. Hence, if a simulation does not require a very high level of accuracy, RANS is probably a better option than LES.

7 Further Work

By comparing the results from various benchmarks, the performance of RANS turbulence models has been investigated in this thesis. An effort has been made to highlight what parts of the cavity flow different turbulence models are capable and incapable to model correctly. The problem is that for most cases multiple features change from benchmark to benchmark. For example, comparing B2 to B5 the flow regime has changed, but so has the geometry, h/H ratio and magnitude of the adverse pressure gradient. Thus, it is difficult to know with certainty what is the main cause for the variations in turbulence model performance. Therefore, to continue the work with decomposing the flow and systematically evaluate turbulence model performance, it should be created additional benchmarks which systematically changes one feature at a time. An effort should also be made to carry out measurements at similar locations for the different benchmarks to facilitate an accurate comparison of the results. This would allow a more thorough investigation, and deeper insight, in the performance of RANS turbulence models for mixing ventilation applications, than what can be accomplished with the benchmarks available today.

The main focus of this thesis has been on turbulence model performance, however, it has also been shown that other parameters have had an impact on the solution. The choice of wall treatment affects the solution, and the results in this thesis indicate that good results can be obtained also with the use of wall functions. However, this should be investigated for more benchmarks, as this was only tested for B2 in this thesis. In a such study, the degree of wall refinement in the mesh should also be included as a parameter. Various turbulence models might also depend differently on the choice of wall treatment and this is also something that should be further researched. Furthermore, it should be investigated if the parameters that only have been used with the default setting this thesis – like PV coupling algorithm and numerical schemes – have a significant effect on the solution. However, combining several parameters quickly leads to a very high number of simulations to conduct.

Another parameter which proved to impact the solution in this thesis was the choice of using a steady state or transient solver in the presence of oscillating residuals. It should be further researched for what cases it is sufficient to simulate in steady state and when a URANS simulation will provide better results, as this was only tested for B4 in this thesis. It should also be further investigated what are the causes of these oscillations, as the results from this thesis shown that both turbulence model, wall treatment and Reynolds number are affecting this. To know if there are in fact oscillations in the mean flow, frequency analysis should be conducted for the benchmarks, or the dye injection technique used for B5 could be used.

The SST k-ω model did not provide the same results as the results seen in literature for two of the benchmarks in this thesis – B2 and B6. This implies that this model is sensitive to one or more parameters, and it should be researched what these parameters are, since this model might give the overall best performance if it provides good results also in the fully turbulent regime.

Ultimately, it is essential that the results from a study like this and similar ones can be extrapolated to real cases to have an actual benefit of improved ventilation systems. Thus, research should be made on how to identify the different features of the cavity flow in a real scenario, to know which benchmarks that are most comparable and therefore also which turbulence models are likely to give the best results. The comparison with real flow rates in this thesis suggested that the benchmarks with inlet Reynolds numbers in the transitional regime are the most comparable to a real scenario. However, it should be researched further if this is really the case since it is a bit ambiguous to compare the benchmark

geometry with real offices. Furthermore, as many real scenarios will have significant heat sources and buoyancy effects, similar studies to this should be conducted for benchmark where buoyancy is a more dominant force than what is the case for the benchmarks in this thesis. The results from this thesis are only relevant for mixing ventilation systems where forced convection dominates natural convection. In a real scenario, the room geometry will also be much more complex than what is the case for the benchmarks, and it is important to understand to what extent the geometry can be simplified.

References

[1] Aalborg University, . CFD Benchmarks. URL: `https://www.cfd-benchmarks.com/`.

[2] Abe, K., Kondoh, T., Nagano, Y., 1995. A new turbulence model for predicting fluid flow and heat transfer in separating and reattaching flows—II. Thermal field calculations. International Journal of Heat and Mass Transfer 38, 1467–1481.

[3] ANSYS, 2020a. Fluent R2 Theory Guide.

[4] ANSYS, 2020b. Fluent R2 User Guide.

[5] Blay, D., Mergui, S., Niculae, C., 1992. Confined turbulent mixed convection in the presence of a horizontal buoyant wall jet. Phys. Fluids A Fluid Dyn 4.

[6] Blocken, B., 2015. Computational Fluid Dynamics for Urban Physics: Importance, scales, possibilities, limitations and ten tips and tricks towards accurate and reliable simulations. Building and Environment 91, 219–245.

[7] Bredberg, J., 2000. On the Wall Boundary Condition for Turbulence Models. Internal report 00/4. Department of Thermo and Fluid Dynamics. Chalmers University of Technology.

[8] Cao, S.J., Meyers, J., 2013. Influence of turbulent boundary conditions on RANS simulations of pollutant dispersion in mechanically ventilated enclosures with transitional slot Reynolds number. Building and Environment 59, 397–407.

[9] Chang, K., Hsieh, W., Chen, C., 1995. A Modified Low-ReynoldsNumber Turbulence Model Applicable to Recirculating Flow in Pipe Expansion. Journal of Fluids Engineering 117, 417–423.

[10] Chen, H., Moshfegh, B., Cehlin, M., 2011. Numerical investigation of the flow behaviour of an isothermal impinging jet in a room. Building and Environment 49, 154–166.

[11] Davidson, L., 1990. Calculations of the turbulent buoyancy-driven flow in a rectangular cavity using an efficient solver and two different low Rynolds number k-epsilon turbulence models. Numerical Heat Transfer, Part A: Applications 18, 129–147.

[12] Direktoratet for byggkvalitet, 2017. Byggteknisk forskrift (TEK17).

[13] Dokka, T.H., Klinski, M., Haase, M., Mysen, M., 2009. Kriterier for passivhus- og lavenergi bygg – Yrkesbygg. Technical Report 42. Sintef Byggforsk.

[14] Dréau, J.L., Heiselberg, P., Nielsen, P.V., 2013. Simulation with different turbulence models in an Annex 20 benchmark test using Star-CCM+. DCE Technical report xxx. Department of Civil Engineering. Aalborg University.

[15] ERCOFTAC, . QNET. URL: `https://kbwiki.ercoftac.org`.

[16] Eriksson, J., Karlsson, R., Persson, J., 1998. An experimental study of a two-dimensional plane turbulent wall jet. Experiments in fluids 25, 50–60.

[17] Ferziger, J.H., Perić, M., 2002. Computational methods for fluid dynamics. 3rd, rev. ed., Springer, Berlin ; New York.

[18] George, W., Abrahamson, H., Eriksson, J., Karlson, R., Löfdahl, L., Wosnik, M., 2000. A similarity theory for the turbulent plane wall jet without external stream. Journal of Fluid Mechanics 425, 367–411.

[19] Guerrero, J., 2020. Theory of turbulence modeling by Joel Guerrero. URL: `https://wiki.openfoam.com/Theory_of_turbulence_modeling_by_Joel_Guerrero`.

[20] van Hoff, T., Blocken, B., Defraeye, T., Carmeliet, J., van Heijst, G., 2012. PIV measurements of a plane wall jet in a confined space at transitional slot Reynolds numbers. Experiments in fluids , 499–517.

[21] van Hoff, T., Blocken, B., van Heijst, G., 2013. On the suitability of steady RANS CFD for forced mixing ventilation at transitional slot Reynolds numbers. Indoor air , 236–249.

[22] van Hoff, T., Nielsen, P.V., Li, Y., 2018. Computational fluid dynamics predictions of non isothermal ventilation flow – how can the user factor be minimized? Indoor air 28, 866–880.

[23] van Hooff, T., Blocken, B., 2017. Low-Reynolds number mixing ventilation flows: Impact of physical and numerical diffusion on flow and dispersion. Building simulation 10, 589–606.

[24] van Hooff, T., Blocken, B., Gousseau, P., van Heijst, G., 2014. Counter-gradient diffusion in a slot ventilated enclosure assessed by LES and RANS. Computers and Fluids 96, 63–75.

[25] Ito, K., Inthavong, K., Kurabuchi, T., Ueda, T., Endo, T., Omori, T., Ono, H., Kato, S., Sakai, K., Suwa, Y., Matsumoto, H., Yoshino, H., Zhang, W., Tu, J., 2015. CFD Benchmark Tests for Indoor Environmental Problems: Part 1 Isothermal/Non-Isothermal Flow in 2D and 3D Room Model. International Journal of Architectural Engineering Technology 2, 1–22.

[26] Jones, W., Launder, B., 1973. The Calculation of Low-Reynolds-Number Phenomena With a Two-Equation Model of Turbulence. International Journal of Heat and Mass Transfer 16, 1119–1130.

[27] Joubert, P., Sandu, A., Beghein, C., Allard, F., 1996. Numerical study of the influence of inlet boundary conditions on the air movement in a ventilated enclosure. Proceedings of 5th International Conference on Air Distribution in Rooms , 235–242.

[28] Karimipanah, T., 1996. Turbulent jets in confined spaces. Phd.. Royal Institute of Technology. Gävle Sweden.

[29] Kosutova, K., van Hooff, T., Blocken, B., 2018. CFD simulation of non-isothermal mixing ventilation in a generic enclosure: Impact of computational and physical parameters. International Journal of Thermal Sciences 129, 343–357.

[30] Launder, B.E., Rodi, W., 1979. The turbulent wall jet. Progress in Aerospace Sciences 19, 81–128.

[31] Limane, A., Fellouah, H., Galanis, N., 2014. Thermo-ventilation study by OpenFOAM of the airflow in a cavity with heated floor. Building simulation 8, 271–283.

[32] Müller, D., Kandzi, C., Kosonen, R., Melikov, A.V., Nielsen, P.V., 2013. Mixing ventilation - Guide on mixing air distribution design. Number 19 in REHVA Guidebooks, REHVA.

[33] Nielsen, P., Zhang, C., Kjær, C., Leiria, D., Nørholm, H., Ramstad, T., Rovithakis, A., Jensen, R., 2019. A benchmark test for room air distribution: the backward facing step flow. IOP Conference Series: Materials Science and Engineering 609, 1–6.

[34] Nielsen, P.V., 1974. Flow in air conditioned rooms: Model experiments and numerical solution of the flow equations. PhD. Technical University of Denmark.

[35] Nielsen, P.V., 1990. Specification of a two-dimensional test case. International Energy Agency, Annex 20: Air Flow Pattern Within Buildings .

[36] Nielsen, P.V., 2015. Fifty years of CFD for room air distribution. Building and Environment 91, 78–90.

[37] Nielsen, P.V., Allard, F., Awbi, H.B., Davidson, L., Schälin, A., 2007. Computational Fluid Dynamics in ventilation design. Number 10 in Guidebook, Rehva.

[38] Olmedo, I., Nielsen, P.V., 2010. Analysis of the IEA 2D test. 2D, 3D, steady or unsteady airflow? Technical report 106. Department of Civil Engineering. Aalborg University.

[39] Peng, L., Nielsen, P., Wang, X., 2016. Possible user-dependent CFD predicions of transitional flow in building ventilation. Building and Environment , 130–141.

[40] Ramponi, R., Blocken, B., 2012. CFD simulation of cross-ventilation for a generic isolated building: Impact of computational parameters. Building and Environment 53, 34–48.

[41] Rong, L., Nielsen, P.V., 2008. Simulation with different turbulence models in an annex 20 room benchmark test using Ansys CFX 11.0. Technical report 46. Department of Civil Engineering. Aalborg University.

[42] Susin, R.M., Lindner, G.A., Mariani, V.C., Mendonça, K.C., 2009. Evaluating the influence of the width of inlet slot on the prediction of indoor airflow: Comparison with experimental data. Building and Environment 44, 971–986.

[43] Taghinia, J., Rahman, M., Tse, T.K., 2016. Assessment of zero-equation SGS models for simulating indoor environment. Heat and Mass Transfer 52, 2781–2794.

[44] Versteeg, H., Malalasekera, W., 2007. Introduction to computational fluid dynamics. 2nd ed., Pearson.

[45] Wolfshtein, M., 1969. The velocity and temperature distribution in one-dimensional flow with turbulence augmentation and pressure gradient. International Journal of Heat and Mass Transfer 12, 301–318.

[46] Yan, Z., Zhong, Y., Lin, W.E., Savory, E., You, Y., 2018. Evaluation of RANS and LES turbulence models for simulating a steady 2D plane wall jet. Engineering Computations 35, 211–234.

Appendix:

A   Mesh figures

Benchmark 2
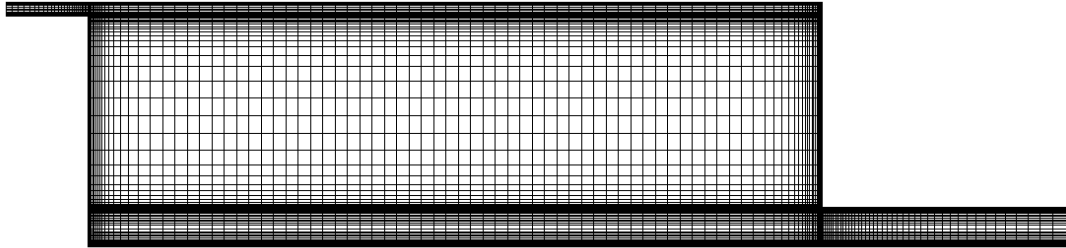
Figure A.1: B2 mesh with 342 thousand cells

Benchmark 3
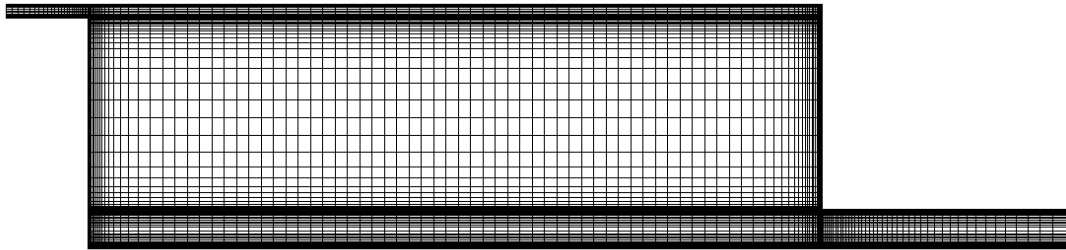
Figure A.2: B3 mesh with 1.7 million cells

Benchmark 4
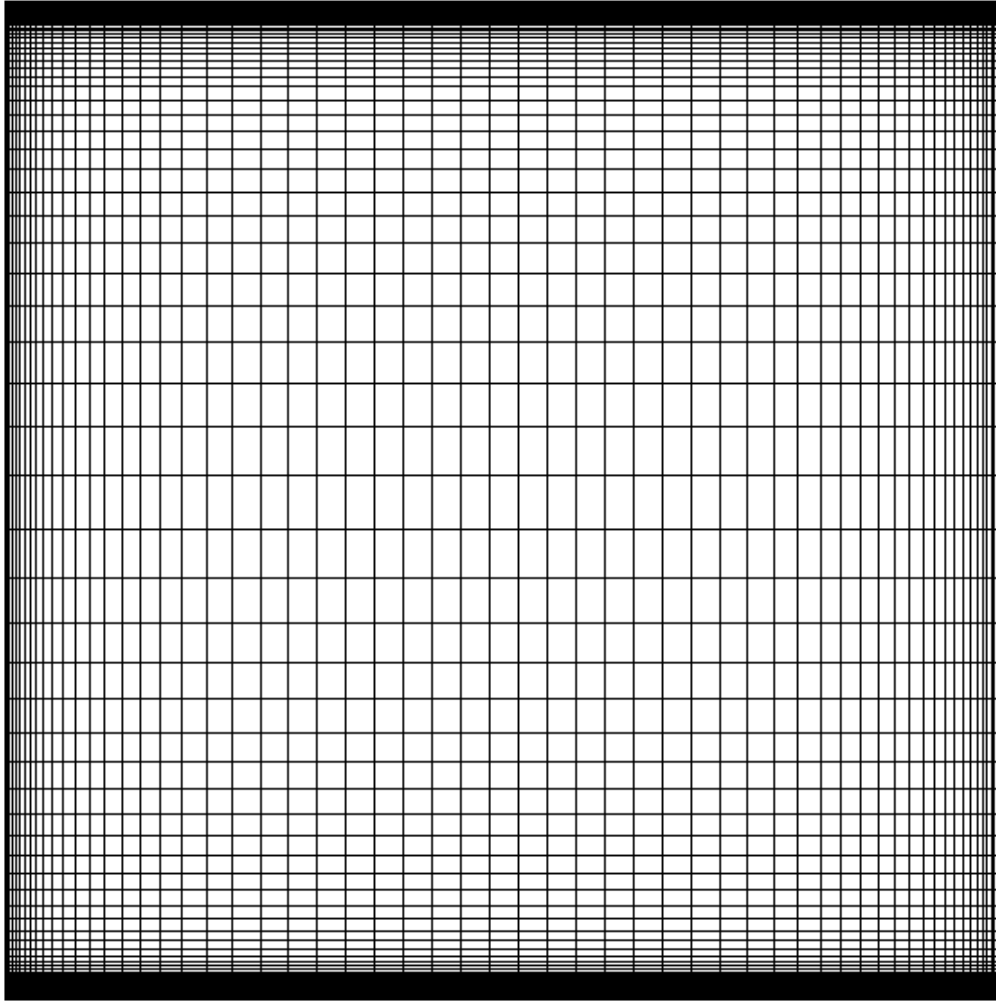
Figure A.3: B4 2D mesh with 7 thousand cells, and 3D mesh with 126 thousand cells

Benchmark 5
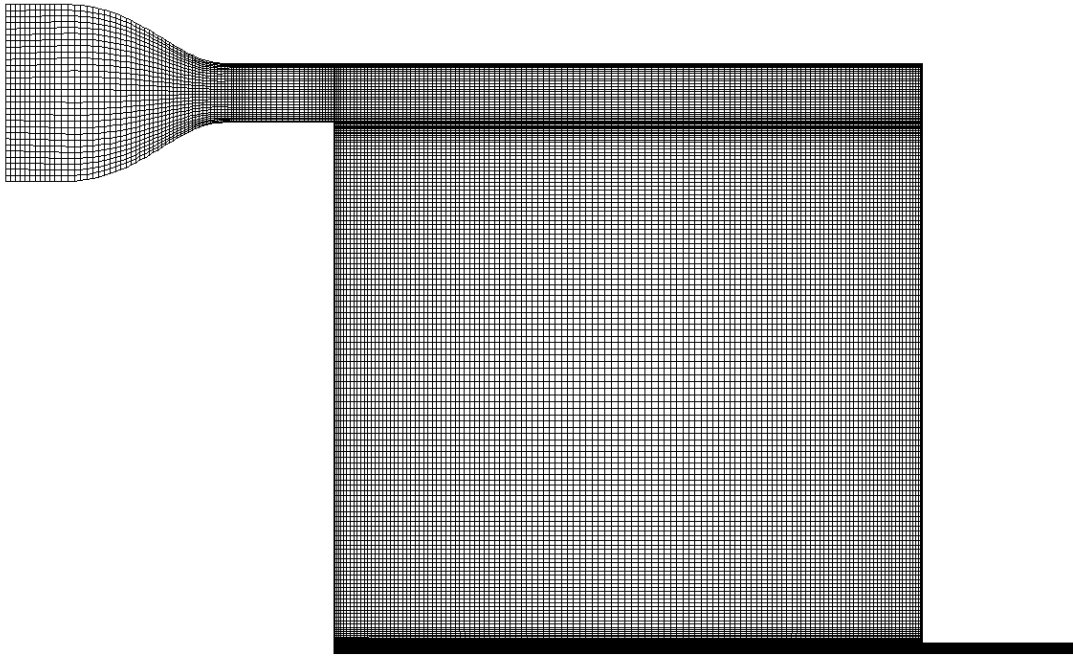
Figure A.4: B5 mesh with 1.2 million cells cells

Benchmark 6
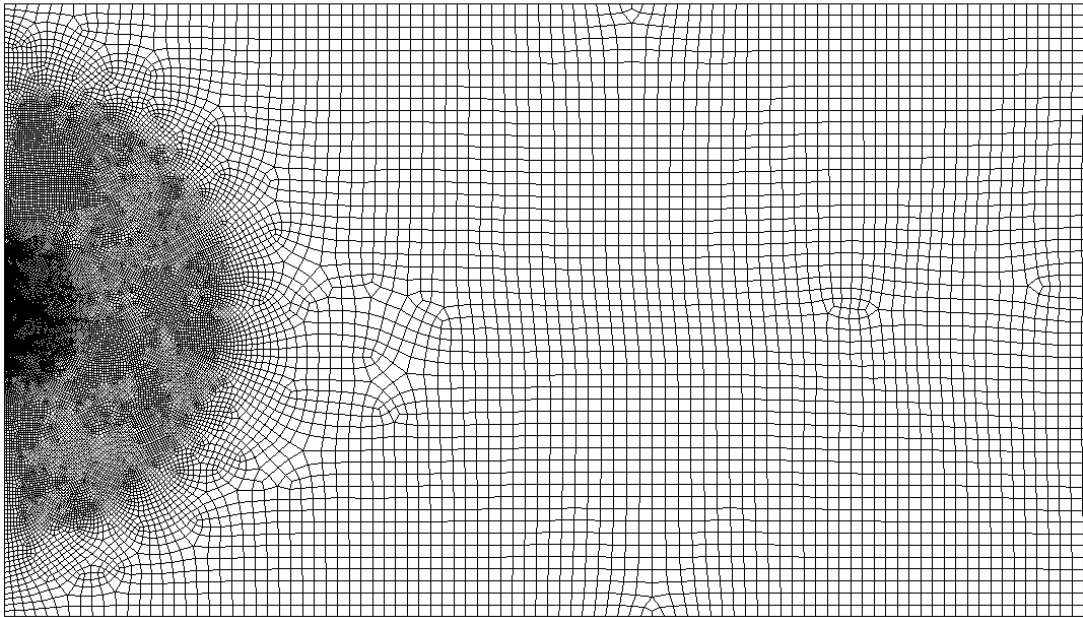
Figure A.5: B6 mesh with 3.7 million cells cells
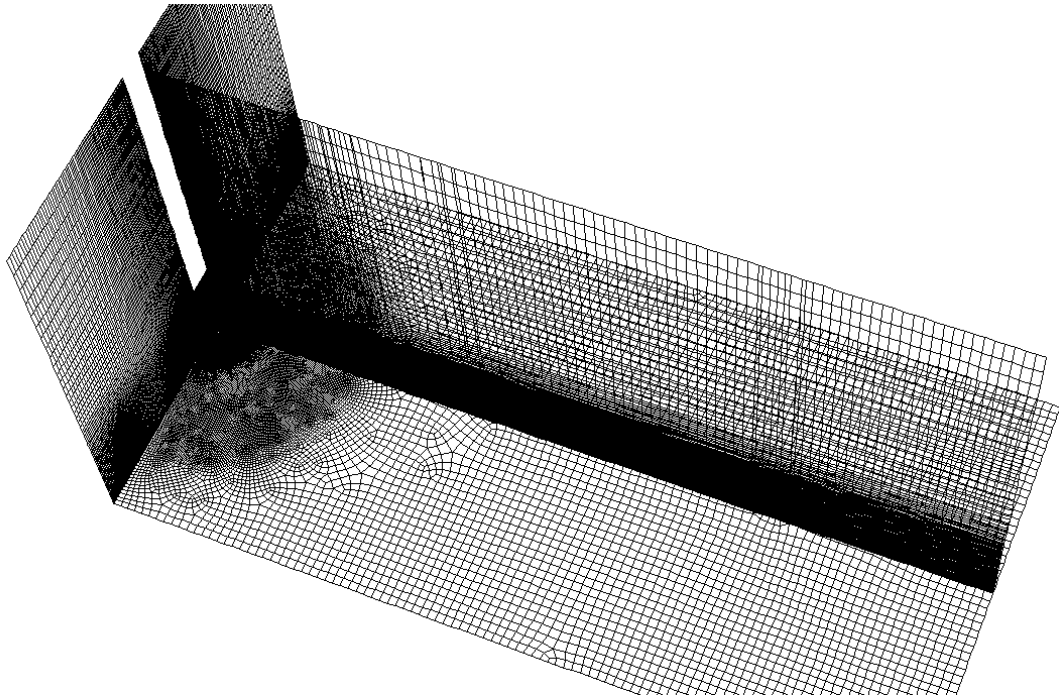
Figure A.6: B6 mesh with 3.7 million cells cells

Benchmark 7
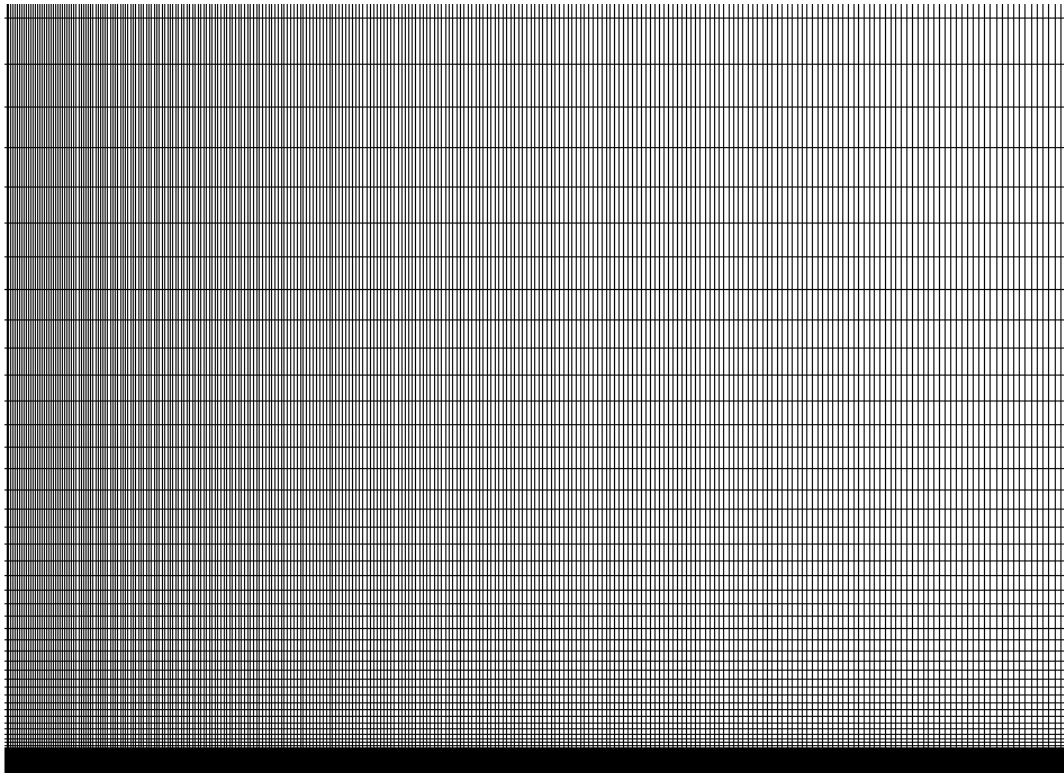
Figure A.7: B7 mesh with 41 thousand cells. Inlet in the bottom left corner. The right and top boundaries are modelled as pressure outlets while the left and bottom boundaries are no slip walls.
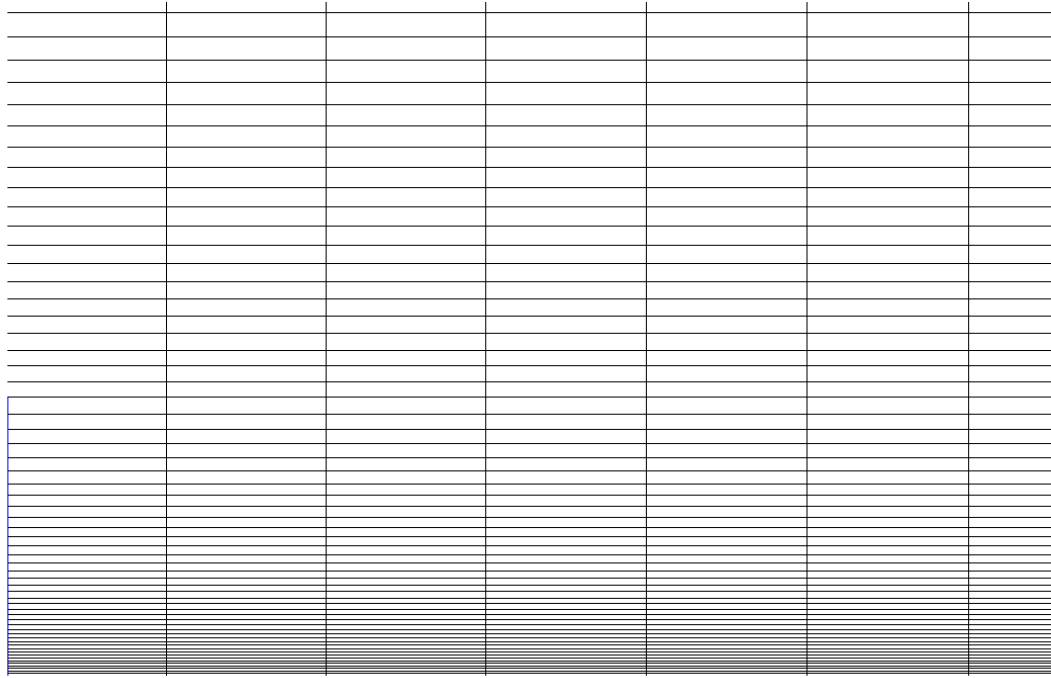
Figure A.8: B7 mesh with 41 thousand cells. Closeup of inlet.

B Additional result figures

Here velocity contours for the four turbulence models that have been tested on all the benchmarks are shown. That is the Standard k-ϵ, RNG k-ϵ, realizable k-ϵ and SST k-ω models. Additionally, there are some extra comparisons with experiments.

Benchmark 2
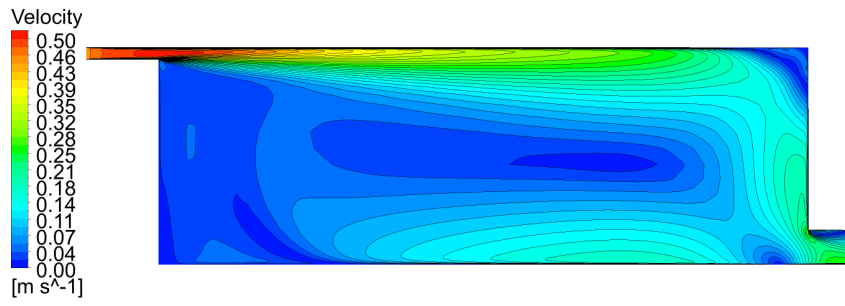
(a) stdke
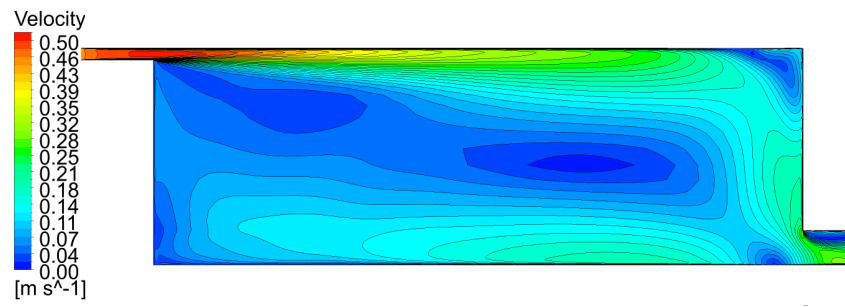
(b) realizable
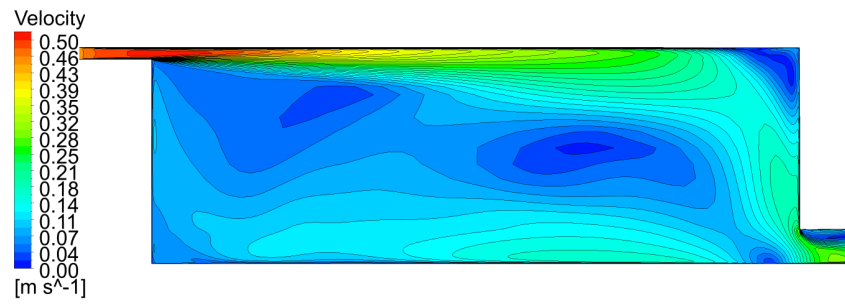
(c) RNG
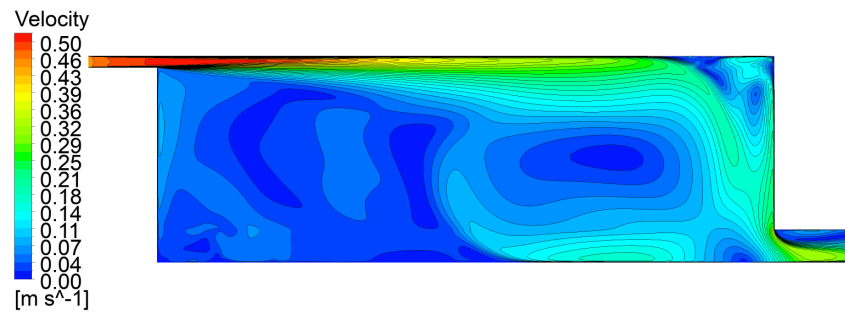
(d) SST

Figure B.1: B2 mid-plane velocity contours for various turbulence models.
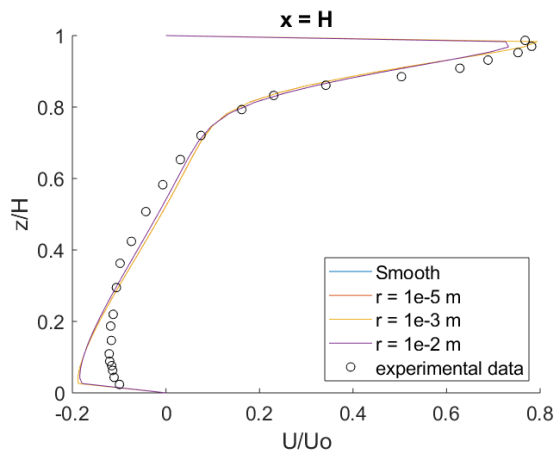
(a) Vertical line: x = H
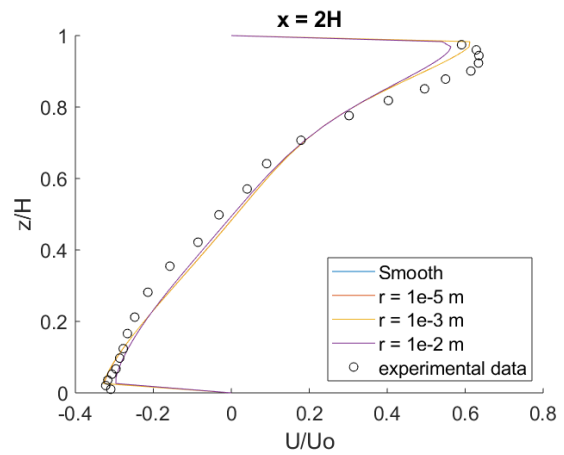
(b) Vertical line: x = 2H
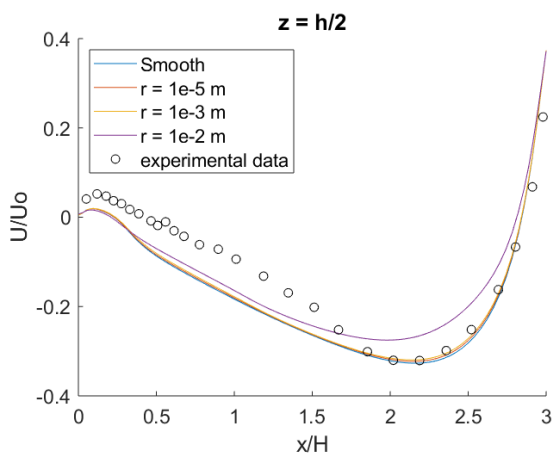
(c) Horizontal line: z = h/2
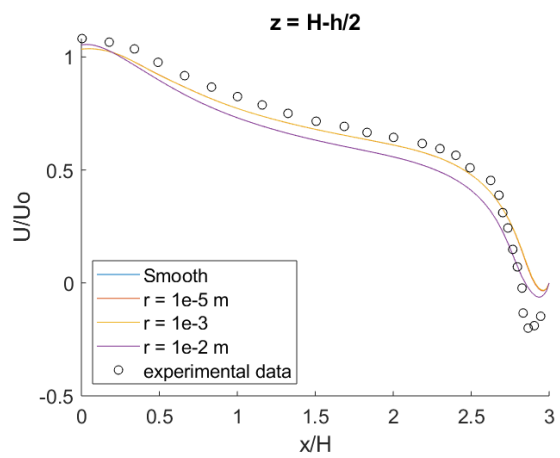
(d) Horizontal line: z = H - h/2

Figure B.2: Impact on roughness on B2 simulation using standard k-ϵ. Roughness height is shown in legend, roughness type is sand-grain roughness. Model scale for the simulation is H = 3m.

Benchmark 3
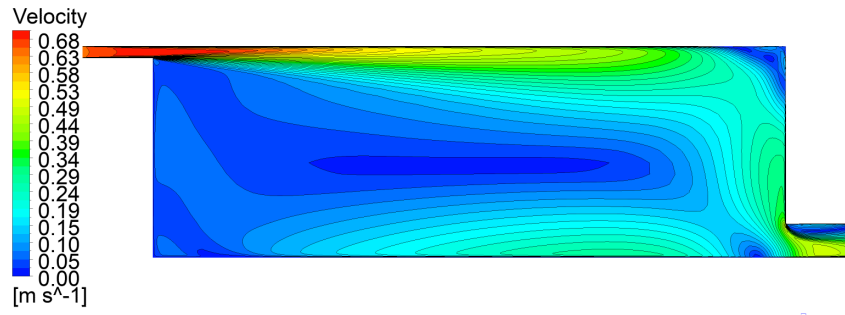
(a) stdke
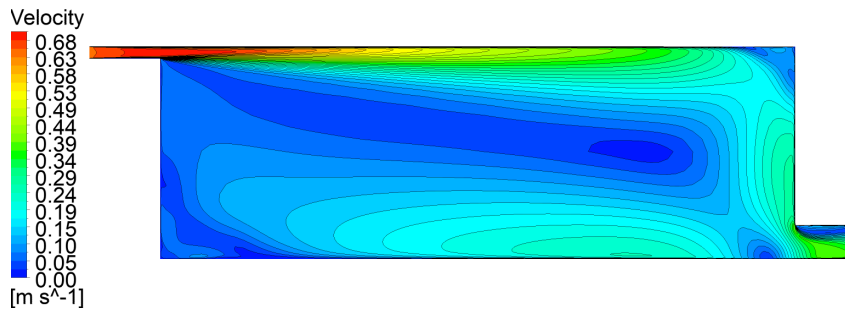
(b) realizable
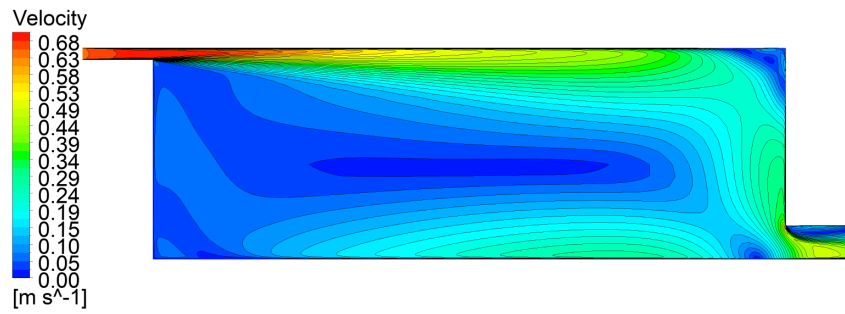
(c) RNG
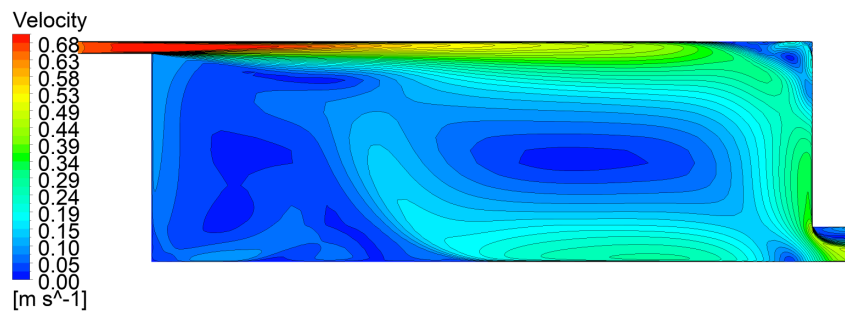
(d) SST

Figure B.3: B3 mid-plane velocity contours for various turbulence models.

(a) stdke

(b) realizable

(c) RNG

(d) SST
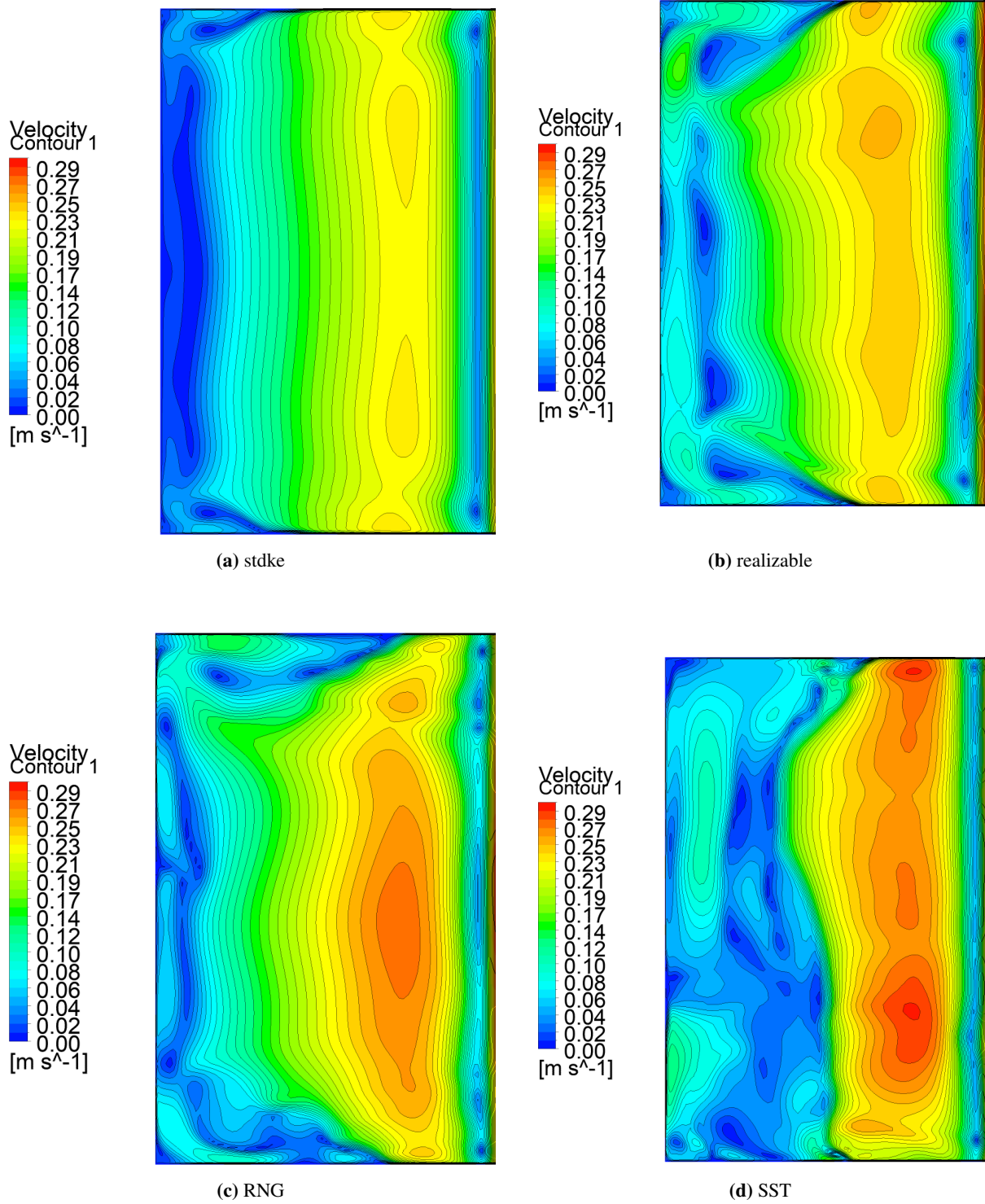
Figure B.4: B3 velocity contours at an isosurface z = h/2 for various turbulence models.

Benchmark 4

(a) stdke

(b) realizable

(c) RNG

(d) SST
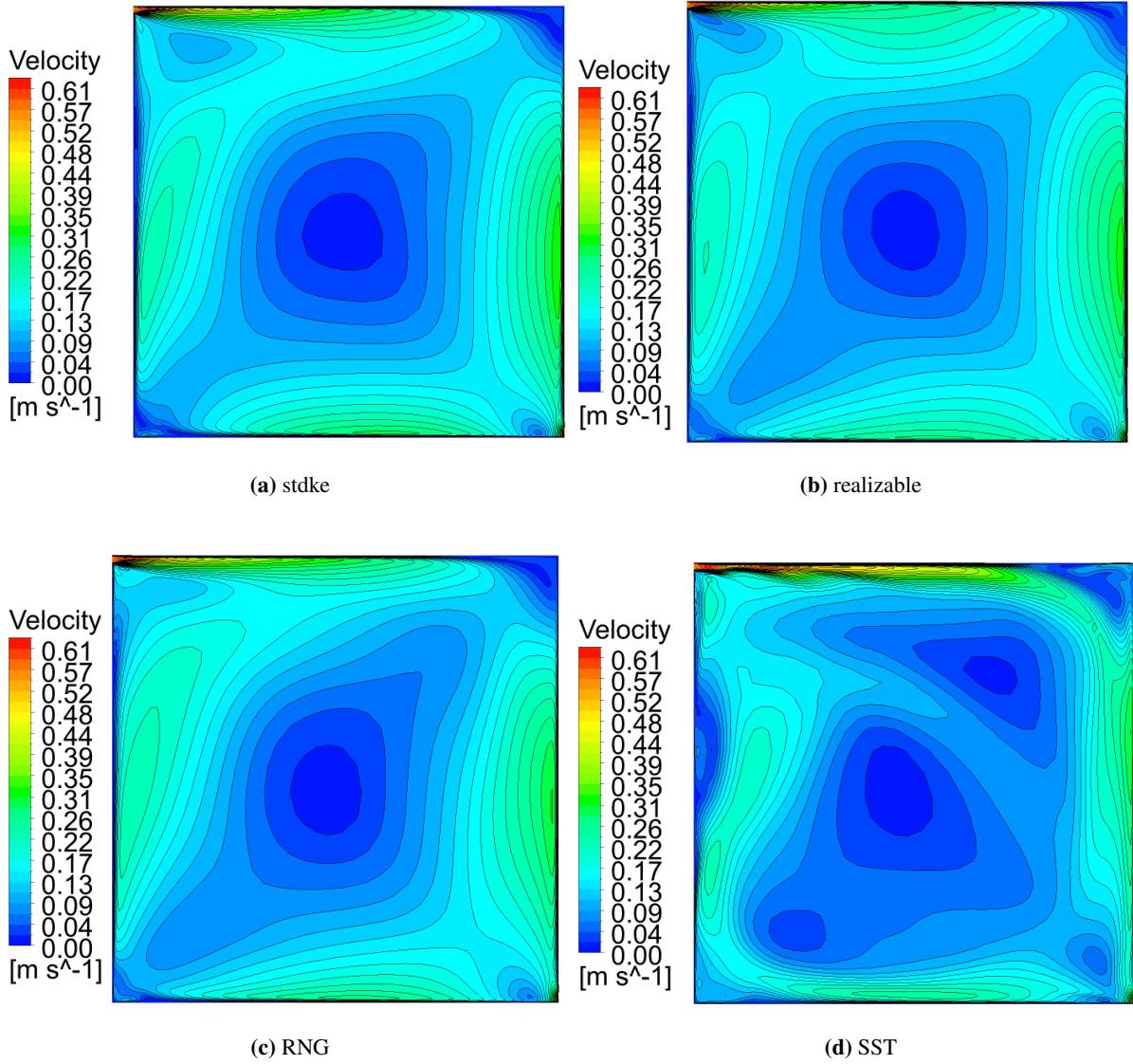
Figure B.5: B4 mid-plane velocity contours for various turbulence models.

Benchmark 5

(a) stdke

(b) realizable

(c) RNG

(d) SST
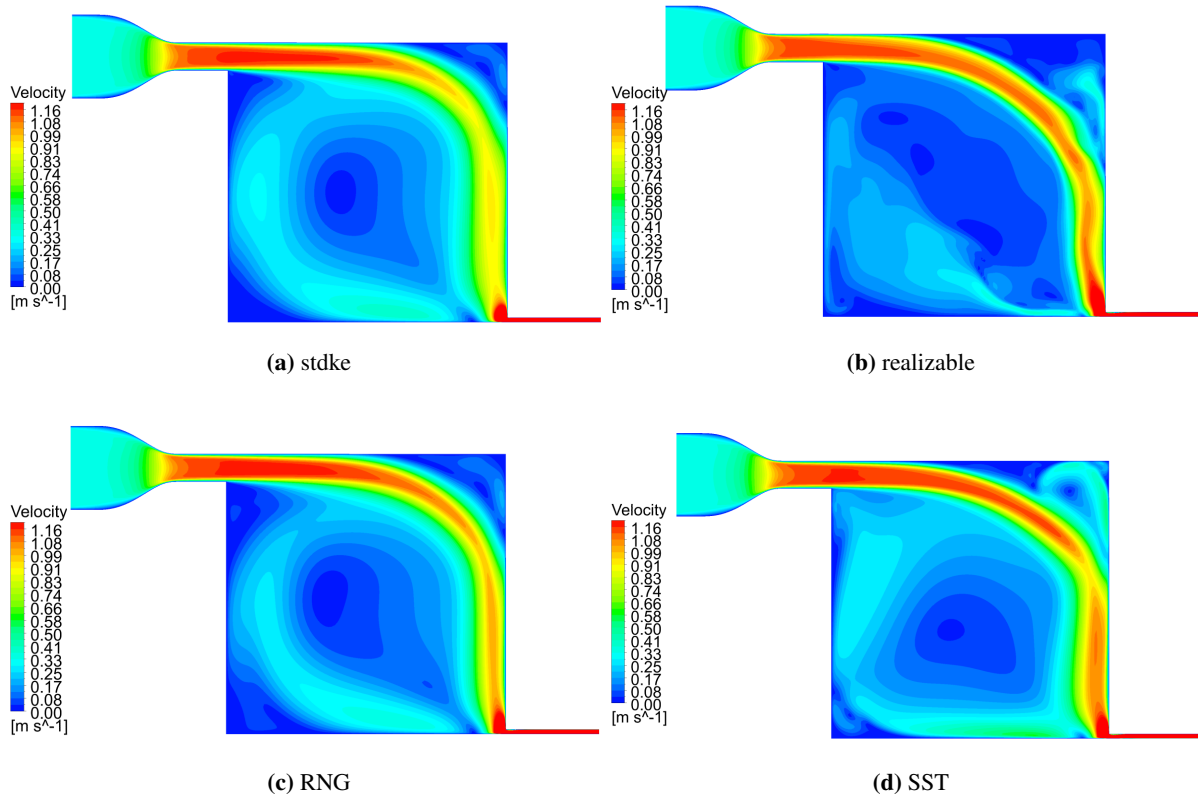
Figure B.6: B5 mid-plane velocity contours for various turbulence models.

Benchmark 6

(a) stdke

(b) realizable

(c) RNG

(d) SST
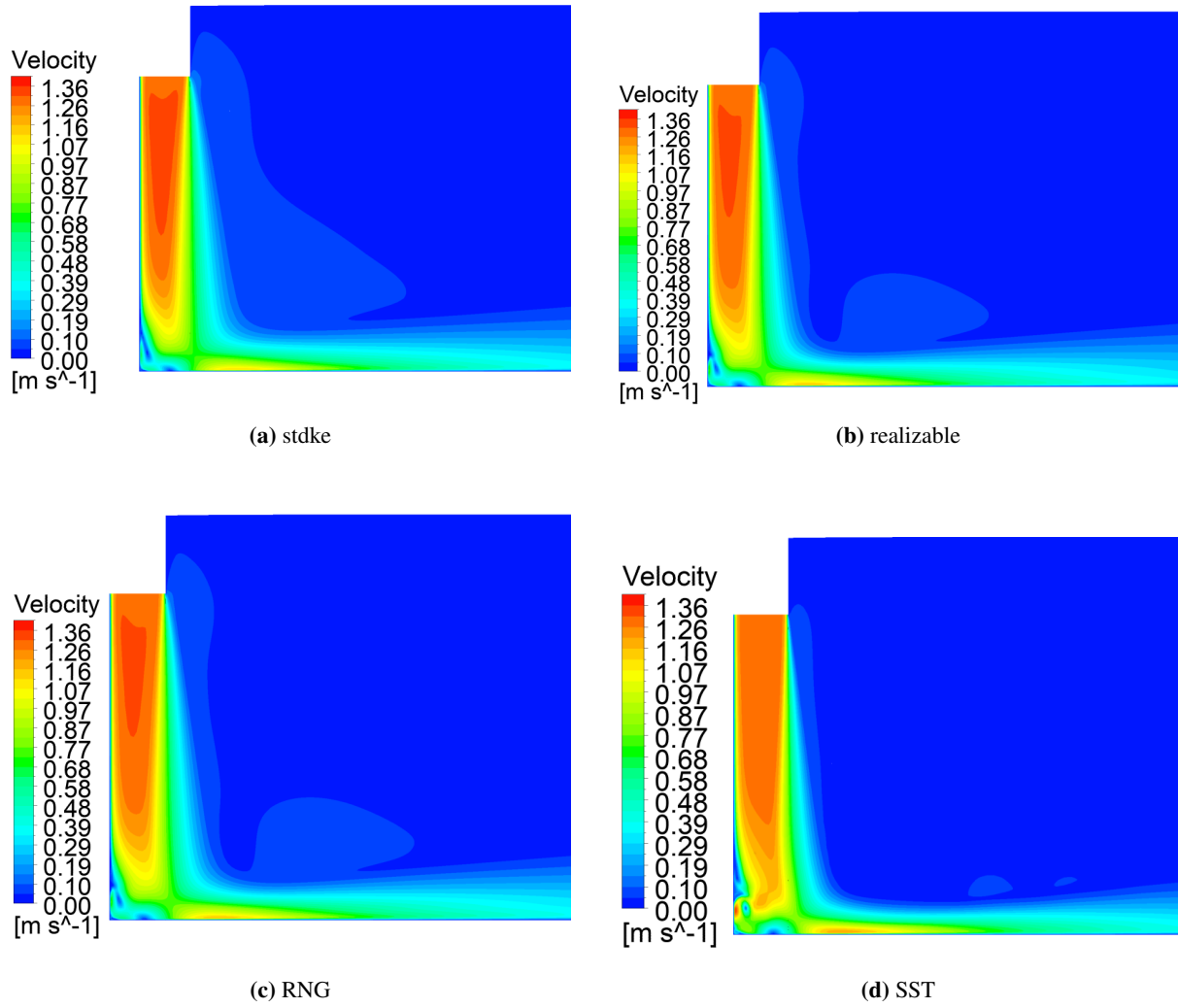
Figure B.7: B6 mid-plane velocity contours in impingement region for various turbulence models.

Benchmark 7

(a) x/h = 70   **(b)** x/h = 150
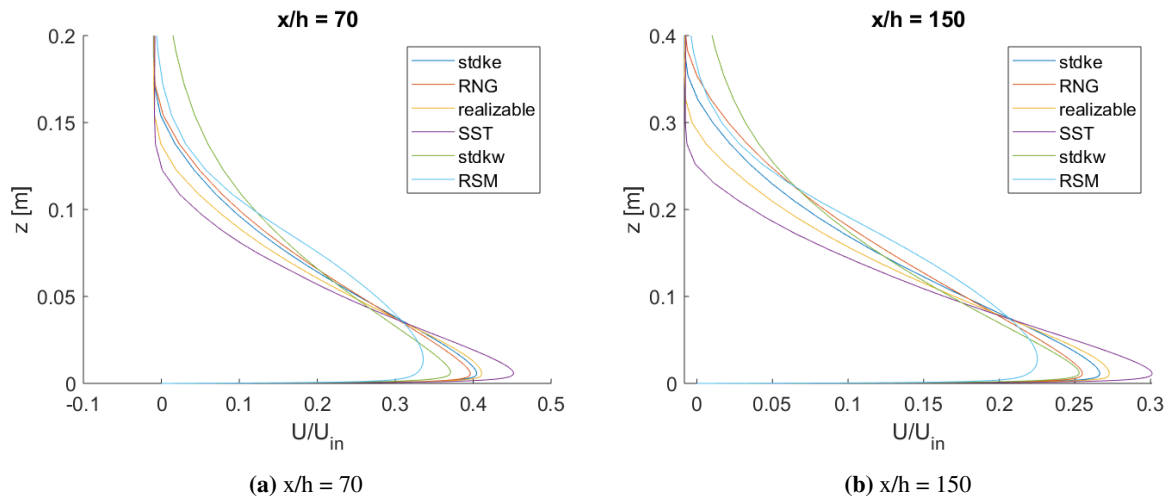
Figure B.8: Comparison of six turbulence models for Benchmark 7 on 41k mesh. Standard k-ω model with Ti = 10% at inlet. Other models with 1%.

C Openfoam case files

0 files

```
/*--------------------------------*- C++ -*----------------------------------*\
  =========                 |
  \\      /  F ield         | OpenFOAM: The Open Source CFD Toolbox
   \\    /   O peration     | Website:  https://openfoam.org
    \\  /    A nd           | Version:  7
     \\/     M anipulation  |
\*---------------------------------------------------------------------------*/
FoamFile
{
    version     2.0;
    format      ascii;
    class       volVectorField;
    object      U;
}
// * * * * * * * * * * * * * * * * * * * * * * * * * * * * * * * * * * * * * //

dimensions      [0 1 -1 0 0 0 0];

internalField   uniform (0 0 0);

boundaryField
{
    inlet
    {
        type            fixedValue;
        value           uniform (0.3333 0 0);
    }

    outlet
    {
        type            inletOutlet;
        inletValue      uniform (0 0 0);
        value           uniform (0 0 0);
```

```
    }

    contraction
    {
        type            noSlip;
    }

    top_wall
    {
        type            noSlip;
    }

    right_wall
    {
        type            noSlip;
    }

    left_wall
    {
        type            noSlip;
    }

    floor
    {
        type            noSlip;
    }

    front
    {
        type            noSlip;
    }

    back
    {
        type            noSlip;
    }

    wall_top_out
    {
        type            noSlip;
    }
    wall_in_lower
    {
        type            noSlip;
    }

}

// ********************************************************************* //
```

```
        \\/        M anipulation    |
\*————————————————————————————————————————————————*/
FoamFile
{
    version     2.0;
    format      ascii;
    class       volScalarField;
    object      p;
}
// * * * * * * * * * * * * * * * * * * * * * * * * * * * * * * * * * //

dimensions      [0 2 −2 0 0 0 0];

internalField   uniform 0;

boundaryField
{
    inlet
    {
        type            fixedFluxPressure;
        value           uniform 0;
    }

    outlet
    {
        type            fixedValue;
        value           uniform 0;
    }

    contraction
    {
        type            fixedFluxPressure;
        value           uniform 0;
    }

    top_wall
    {
        type            fixedFluxPressure;
        value           uniform 0;
    }

    right_wall
    {
        type            fixedFluxPressure;
        value           uniform 0;
    }

    left_wall
    {
        type            fixedFluxPressure;
        value           uniform 0;
    }

    floor
    {
        type            fixedFluxPressure;
        value           uniform 0;
    }
```

```
        }

        front
        {
            type                fixedFluxPressure;
            value               uniform 0;
        }

        back
        {
            type                fixedFluxPressure;
            value               uniform 0;
        }

        wall_top_out
        {
            type                fixedFluxPressure;
            value               uniform 0;
        }
        wall_in_lower
        {
            type                fixedFluxPressure;
            value               uniform 0;
        }
}


// *************************************************************************** //



/*--------------------------------*- C++ -*----------------------------------*\
  =========                 |
  \\      /  F ield          | OpenFOAM: The Open Source CFD Toolbox
   \\    /   O peration      | Website:  https://openfoam.org
    \\  /    A nd            | Version:  7
     \\/     M anipulation   |
\*---------------------------------------------------------------------------*/
FoamFile
{
    version     2.0;
    format      ascii;
    class       volScalarField;
    location    "0";
    object      epsilon;
}
// * * * * * * * * * * * * * * * * * * * * * * * * * * * * * * * * * * * * * * //

dimensions      [0 2 -3 0 0 0 0];

internalField   uniform 0.001714;

boundaryField
{
    inlet
    {
```

```
    type            fixedValue;
    value           uniform    0.027037;
}
outlet
{
    type            zeroGradient;
}

contraction
{
    type            epsilonWallFunction;
    value           uniform 0.000108;
}

top_wall
{
    type            epsilonWallFunction;
    value           uniform 0.000108;
}

right_wall
{
    type            epsilonWallFunction;
    value           uniform 0.000108;
}

left_wall
{
    type            epsilonWallFunction;
    value           uniform 0.000108;
}

floor
{
    type            epsilonWallFunction;
    value           uniform 0.000108;
}

front
{
    type            epsilonWallFunction;
    value           uniform 0.000108;
}

back
{
    type            epsilonWallFunction;
    value           uniform 0.000108;
}

wall_top_out
{
    type            epsilonWallFunction;
    value           uniform 0.000108;
}
wall_in_lower
{
```

```
            type            epsilonWallFunction;
            value           uniform 0.000108;
        }
}


// ************************************************************************* //




/*--------------------------------*- C++ -*----------------------------------*\
  =========                 |
  \\      /  F ield         | OpenFOAM: The Open Source CFD Toolbox
   \\    /   O peration     | Website:  https://openfoam.org
    \\  /    A nd           | Version:  7
     \\/     M anipulation  |
\*---------------------------------------------------------------------------*/
FoamFile
{
    version     2.0;
    format      ascii;
    class       volScalarField;
    location    "0";
    object      k;
}
// * * * * * * * * * * * * * * * * * * * * * * * * * * * * * * * * * * * * * //

dimensions      [0 2 -2 0 0 0 0];

internalField   uniform 0.000497;

boundaryField
{
    inlet
    {
        type            fixedValue;
        value           uniform   0.000599;
    }
    outlet
    {
        type            zeroGradient;
    }

    contraction
    {
        type            kLowReWallFunction;
        value           uniform 0.000497;
    }

    top_wall
    {
        type            kLowReWallFunction;
        value           uniform 0.000497;
    }

    right_wall
    {
```

```
        type            kLowReWallFunction;
        value           uniform 0.000497;
    }

    left_wall
    {
        type            kLowReWallFunction;
        value           uniform 0.000497;
    }
    floor
    {
        type            kLowReWallFunction;
        value           uniform 0.000497;
    }

    front
    {
        type            kLowReWallFunction;
        value           uniform 0.000497;
    }

    back
    {
        type            kLowReWallFunction;
        value           uniform 0.000497;
    }

    wall_top_out
    {
        type            kLowReWallFunction;
        value           uniform 0.000497;
    }
    wall_in_lower
    {
        type            kLowReWallFunction;
        value           uniform 0.000497;
    }


}


// ************************************************************************* //




/*--------------------------------*- C++ -*----------------------------------*\
  =========                 |
  \\      /  F ield         | OpenFOAM: The Open Source CFD Toolbox
   \\    /   O peration     | Website:  https://openfoam.org
    \\  /    A nd           | Version:  7
     \\/     M anipulation  |
\*---------------------------------------------------------------------------*/
FoamFile
{
    version     2.0;
    format      ascii;
```

```
    class           volScalarField;
    location        "0";
    object          omega;
}
// * * * * * * * * * * * * * * * * * * * * * * * * * * * * * * * * * * * * * //

dimensions      [0 0 −1 0 0 0 0];

internalField   uniform 2.42;

boundaryField
{
    inlet
    {
        type                fixedValue;
        value               uniform 11.7;
    }
    outlet
    {
        type                zeroGradient;
    }

    contraction
    {
        type                omegaWallFunction;
        value               uniform 100;
    }

    top_wall
    {
        type                omegaWallFunction;
        value               uniform 100;
    }

    right_wall
    {
        type                omegaWallFunction;
        value               uniform 100;
    }

    left_wall
    {
        type                omegaWallFunction;
        value               uniform 100;
    }

    floor
    {
        type                omegaWallFunction;
        value               uniform 100;
    }

    front
    {
        type                omegaWallFunction;
        value               uniform 100;
    }
```

```
    back
    {
        type            omegaWallFunction;
        value           uniform 100;
    }

    wall_top_out
    {
        type            omegaWallFunction;
        value           uniform 100;
    }
    wall_in_lower
    {
        type            omegaWallFunction;
        value           uniform 100;
    }

}

// ************************************************************************* //
```

```
/*--------------------------------*- C++ -*----------------------------------*\
  =========                 |
  \\      /  F ield         | OpenFOAM: The Open Source CFD Toolbox
   \\    /   O peration     | Website:  https://openfoam.org
    \\  /    A nd           | Version: 7
     \\/     M anipulation  |
\*---------------------------------------------------------------------------*/
FoamFile
{
    version     2.0;
    format      ascii;
    class       volScalarField;
    location    "0";
    object      nut;
}
// * * * * * * * * * * * * * * * * * * * * * * * * * * * * * * * * * * * * * //

dimensions      [0 2 -1 0 0 0 0];

internalField   uniform 0;

boundaryField
{
    inlet
    {
        type            calculated;
        value           uniform 0;
    }
    outlet
    {
        type            calculated;
        value           uniform 0;
    }
```

```
contraction
{
    type            nutkWallFunction;
    value           uniform 0;
}

top_wall
{
    type            nutkWallFunction;
    value           uniform 0;
}

right_wall
{
    type            nutkWallFunction;
    value           uniform 0;
}

left_wall
{
    type            nutkWallFunction;
    value           uniform 0;
}

floor
{
    type            nutkWallFunction;
    value           uniform 0;
}

front
{
    type            nutkWallFunction;
    value           uniform 0;
}

back
{
    type            nutkWallFunction;
    value           uniform 0;
}

wall_top_out
{
    type            nutkWallFunction;
    value           uniform 0;
}
wall_in_lower
{
    type            nutkWallFunction;
    value           uniform 0;
}

}
```

```
// ************************************************************************* //
```

Constant files

```
/*--------------------------------*- C++ -*----------------------------------*\
  =========                 |
  \\      /  F ield         | OpenFOAM: The Open Source CFD Toolbox
   \\    /   O peration     | Website:  https://openfoam.org
    \\  /    A nd           | Version:  7
     \\/     M anipulation  |
\*---------------------------------------------------------------------------*/
FoamFile
{
    version     2.0;
    format      ascii;
    class       dictionary;
    location    "constant";
    object      transportProperties;
}
// * * * * * * * * * * * * * * * * * * * * * * * * * * * * * * * * * * * * * //

transportModel  Newtonian;

nu              [0 2 -1 0 0 0 0] 3e-05;


// ************************************************************************* //
```

```
/*--------------------------------*- C++ -*----------------------------------*\
  =========                 |
  \\      /  F ield         | OpenFOAM: The Open Source CFD Toolbox
   \\    /   O peration     | Website:  https://openfoam.org
    \\  /    A nd           | Version:  7
     \\/     M anipulation  |
\*---------------------------------------------------------------------------*/
FoamFile
{
    version     2.0;
    format      ascii;
    class       dictionary;
    location    "constant";
    object      turbulenceProperties;
}
// * * * * * * * * * * * * * * * * * * * * * * * * * * * * * * * * * * * * * //

simulationType RAS;

RAS
{
    // Tested with kEpsilon, realizableKE, kOmega, kOmegaSST, v2f,
    // ShihQuadraticKE, LienCubicKE.
    RASModel        kOmegaSST;

    turbulence          on;
```

```
    printCoeffs        on ;
}


// ******************************************************************* //
```

System files

```
/*--------------------------------*- C++ -*----------------------------------*\
  =========                 |
  \\      /  F ield         | OpenFOAM: The Open Source CFD Toolbox
   \\    /   O peration     | Website:  https ://openfoam.org
    \\  /    A nd           | Version:  7
     \\/     M anipulation  |
\*---------------------------------------------------------------------------*/
FoamFile
{
    version     2.0;
    format      ascii ;
    class       dictionary ;
    location    "system";
    object      controlDict ;
}
// * * * * * * * * * * * * * * * * * * * * * * * * * * * * * * * * * * * * * //

application     simpleFoam ;

startFrom       latestTime ;

startTime       0;

stopAt          endTime ;

endTime         9000;

deltaT          1;

writeControl    timeStep ;

writeInterval   1000;

purgeWrite      0;

writeFormat     ascii ;

writePrecision  6;

writeCompression  off ;

timeFormat      general ;

timePrecision   6;

runTimeModifiable true ;
```

```
functions
{
    fieldAverage1
    {
        type            fieldAverage;
        functionObjectLibs ( "libfieldFunctionObjects.so" );

        writeControl    writeTime;

        restartOnRestart    false;
        restartOnOutput     false;
        periodicRestart     false;

        timeStart       7000;
        timeEnd         9000;

        fields
        (
            U
            {
                mean        on;
                prime2Mean  on;
                base        time;
            }

            p
            {
                mean        on;
                prime2Mean  off;
                base        time;
            }
            k
            {
                mean  on;
                prime2Mean  off;
                base  time;
             }
            omega
            {
                mean  on;
                prime2Mean  off;
                base  time;
             }
        );
    }
}


// ************************************************************************* //



/*--------------------------------*- C++ -*----------------------------------*\
  =========                 |
  \\      /  F ield         | OpenFOAM: The Open Source CFD Toolbox
```

```
    \\      /    O peration      | Website:     https://openfoam.org
     \\    /     A nd            | Version:     7
      \\/        M anipulation   |
\*-----------------------------------------------------------------------*/
FoamFile
{
    version     2.0;
    format      ascii;
    class       dictionary;
    location    "system";
    object      fvSchemes;
}
// * * * * * * * * * * * * * * * * * * * * * * * * * * * * * * * * * * * //

ddtSchemes
{
    default         steadyState;
}

gradSchemes
{
    default         Gauss linear;
}

divSchemes
{
    default                 none;
    div(phi,U)              Gauss      linearUpwind Grad(U);
    div(phi,k)              Gauss      limitedLinear 1;
    div(phi,epsilon)        Gauss      limitedLinear 1;
    div(phi,omega)          Gauss      limitedLinear 1;
    div(phi,v2)             Gauss      upwind;
    div((nuEff*dev2(T(grad(U)))))    Gauss linear;
    div(nonlinearStress)             Gauss linear;

}

laplacianSchemes
{
    default         Gauss linear corrected;
}

interpolationSchemes
{
    default         linear;
}

snGradSchemes
{
    default         corrected;
}

wallDist
{
    method meshWave;
}
```

// *** //

```
/*--------------------------------*- C++ -*----------------------------------*\
  =========                 |
  \\      /  F ield         | OpenFOAM: The Open Source CFD Toolbox
   \\    /   O peration     | Website:  https://openfoam.org
    \\  /    A nd           | Version:  7
     \\/     M anipulation  |
\*---------------------------------------------------------------------------*/
FoamFile
{
    version     2.0;
    format      ascii;
    class       dictionary;
    location    "system";
    object      fvSolution;
}
// * * * * * * * * * * * * * * * * * * * * * * * * * * * * * * * * * * * * * //

solvers
{
    p
    {
        solver          GAMG;
        tolerance       1e-07;
        relTol          0.1;
        smoother        GaussSeidel;
    }

    "(U|k|epsilon|omega|f|v2)"
    {
        solver          smoothSolver;
        smoother        symGaussSeidel;
        tolerance       1e-07;
        relTol          0.1;
    }
}

SIMPLE
{
    nNonOrthogonalCorrectors 1;
    consistent          yes;

    residualControl
    {
        p               1e-5;
        U               1e-6;
        "(k|epsilon|omega|f|v2)" 1e-6;
    }
}

relaxationFactors
{
    equations
```

```
    {
        U                   0.7;
        ".*"                0.7;
    }
}


//  ************************************************************** //
```

Vegard M. Bjerkeli

Computational Fluid Dynamics of airflows inside buildings

NTNU
Norwegian University of
Science and Technology